DISS. ETH NO. 18010

Design of Solar Powered Airplanes
for Continuous Flight

A dissertation submitted to

ETH ZÜRICH

for the degree of

Doctor of Technical Sciences

presented by

André NOTH

Ingénieur en Microtechnique
Ecole Polytechnique Fédérale de Lausanne, Suisse

Born February 10, 1980
Citizen of Zumholz, Switzerland

accepted on the recommendation of

Prof. Roland Siegwart, Principal Advisor
Prof. Peter Corke, Member of the Jury
Ing. Dipl. EPFL André Borschberg, Member of the Jury
Prof. Claude Nicollier, Member of the Jury

ETH Zürich
September 2008

Acknowledgments

This thesis is the result of the four years I spent as a research assistant in the Autonomous Systems Lab of Prof. Roland Siegwart, first at EPF Lausanne and then at ETH Zürich which are the two Swiss Federal Institutes of Technology in Switzerland. This period was a very interesting and rewarding time, with many collaborations and it was a pleasure to work in such environment.

First, I would like to thank my supervisor, Prof. Roland Siegwart for the great opportunity he gave me to write this thesis, and also for his advices, support and leadership, that makes our lab feel like a big family. Thanks also to the members of the thesis committee, André Borschberg, Peter Corke and Claude Nicollier for the careful reading of the thesis and for their constructive feedback.

This thesis wouldn't have been possible without the great help of Walter Engel, the builder and pilot of Sky-Sailor. I would like to thank him very much because during the four years of this project, he taught me thousands of things in the domain of model aircraft. It was always a big pleasure to work with him and test our airplane in Einsiedeln.

I also gratefully acknowledge Samir Bouabdallah, with whom I first achieved my diploma thesis before continuing with a PhD thesis, Daniel Burnier, Janosh Nikolic, Stéphane Michaud, Jean-Christophe Zufferey and all the people of Aero Initiative at EPFL/ETHZ for the fruitful discussions we had on flying robots and electronics.

For their help on the control side, I would like to thank Philippe Müllhaupt, Sébastien Gros and Davide Buccieri from the Automatic Laboratory of EPFL.

These four years were also full of collaborations with the model-making world. Far away from the complex mathematical formulas, they have an exceptional technical and practical know-how in the many fields which this thesis approaches. My gratefulness goes to Christoph Bachmann, Marco Cantoni, Emil Hilber, Urs Leodolter, Peter Ott, Dieter and Urs Siebenmann,

i

Abstract

This thesis deals with airplanes using solar energy as their only source of energy for more than 24 hours flight. Using solar panels, they collect it during the day for immediate use but also store the remaining part for the night flight. This work presents a new analytical methodology for the conceptual design of such airplane. Its major advantage lies in the fact that it is simple and versatile, which makes it applicable to a large range of airplanes of different wingspans, from the small MAV to the large manned aircraft.

The design methodology is based on power and mass balances occurring during level flight. An extensive study was done on the mathematical modeling of the subparts, for example concerning electric motors the question being to know how their mass and their efficiency vary with power. Empirical data over a large range were used in this study. Finally, the analytical method contains 5 mission parameters and 25 others linked to the various technologies involved that the user can vary in order to see on a graph the dependencies between the 3 layout variables (aspect ratio, wingspan and total mass) for all the feasible solutions. The final selection can then be easily made.

Sky-Sailor, a 3.2 meters wingspan solar powered airplane, was then designed using this methodology. A prototype, with an ultra lightweight structure covered by silicon solar cells was built in order to validate the process. We also developed in this framework dedicated electronics for the autonomous navigation and the efficient solar power management. The final 2.44 kg airplane was tested with success during several autonomous flights, showing capabilities that were very close to the one calculated in theory. The longest flight achieved lasted more than 27 hours within a circuit length of more than 874 kilometers and proved the feasibility of solar powered continuous flight.

In addition to the first application example on Sky-Sailor, other designs are presented and discussed, like the case of a 70 cm solar UAV but also a 60 m manned solar airplane. It is then very interesting to see how things evolve with scaling. In fact, going in each direction removes and adds its batch of

new problems : the poor efficiencies of aerodynamics and propulsion group prove very unfavorable when down-scaling whereas the weight and fragility of the enormous wing structure become the nightmare of engineers working on large-sized models.

Finally, various additional possibilities to improve or enhance the endurance of a solar airplane are addressed, such as gaining altitude to store energy, taking benefit of ascending thermal winds or using a swiveling solar tracker.

Key words: Solar powered UAV, Solar Energy, Solar Airplane, Sustainable Flight, Sky-Sailor, MPPT, Conceptual Design Methodology

Version abrégée

Cette thèse traite des avions utilisant l'énergie solaire comme unique source d'énergie pour des vols de plus de 24 heures. A l'aide de panneaux solaires, ils collectent cette énergie durant le jour pour les besoins immédiats et stockent le surplus pour le vol de nuit. Ce travail présente une nouvelle méthodologie analytique pour le design de ces avions solaires. Son principal avantage réside dans le fait qu'elle est simple et versatile, pouvant être appliquée à une très large gamme d'avions de différentes envergures, du micro-drone jusqu'à l'avion habité.

La méthodologie de design est basée sur les équilibres de puissance et de poids ayant lieu durant le vol palier. Une importante recherche a été effectuée sur la modélisation mathématique de tous les éléments constituant l'avion, par exemple dans le cas des moteurs électriques, s'agissant de savoir comment leur masse et leur efficacité varient avec leur puissance. Des données empiriques sur une très grande échelle ont été utilisées dans cette optique. Finalement, la méthode analytique contient 5 paramètres de mission et 25 liés à la technologies des différents composants qui peuvent être modifiés afin de visualiser sur un graphique les dépendances entre les 3 variables de configuration (allongement, envergure et masse totale) pour toutes les solutions réalisables. La sélection finale en est ensuite facilitée.

Sky-Sailor, un avion solaire de 3.2 mètres d'envergure, a été conçu avec cette méthodologie. Un prototype, avec une structure ultra-légère recouverte de cellules solaires en silicium, a été réalisé afin de valider le processus. De l'électronique dédiée à la navigation autonome ainsi qu'à la gestion efficace de l'énergie solaire a aussi été développée dans ce cadre. L'avion final de 2.5 kg fut testé avec succès durant plusieurs vols autonomes, démontrant des caractéristiques très proches de celles calculées en théorie. Le plus long vol dura plus de 27 heures sur un parcours de 874 kilomètres ce qui prouva la faisabilité du vol continu solaire.

En plus du premier exemple d'application sur Sky-Sailor, d'autres exemples sont présentés et discutés. C'est le cas d'un drone solaire de 70 cm mais

aussi d'un avion solaire habité de 60 m d'envergure. Il est ainsi très intéressant de voir comment les choses évoluent lors du changement d'échelle. En effet, le fait d'aller dans chaque direction ôte et ajoute son lot de nouveaux problèmes : les faibles efficacités de l'aérodynamique et du groupe propulseur s'avèrent très défavorables à petite échelle alors que le poids et la fragilité de l'énorme structure de l'aile deviennent le cauchemar des ingénieurs travaillant sur des modèles de grandes dimensions.

Finalement, plusieurs possibilités supplémentaires d'améliorer l'endurance des avions solaires sont abordées, comme l'utilisation de panneaux solaires orientables ou la recherche de thermiques ascendantes.

Mots clés : Propulsion solaire, Energie solaire, Avion solaire, Vol continu, Sky-Sailor, MPPT, Méthodologie de design conceptuel

Kurzfassung

Diese Doktorarbeit befasst sich mit Flugzeugen, die Sonnenenergie als ihre einzige Energiequelle für Flüge von mehr als 24 Stunden verwenden. Die Energie wird mittels Solarzellen Tags durch gesammelt und für den unmittelbaren Flugbetrieb eingesetzt, wobei überschüssige Energie für den Nachtbetrieb gespeichert wird. Diese Arbeit stellt eine neue analytische Methode für die konzeptuelle Auslegung solcher Solarflugzeuge vor. Der Hauptvorteil dieser Methode besteht darin, dass sie einfach und vielseitig anwendbar ist, so dass sie einen weiten Bereich von Flugzeugen – vom kleinen, unbemannten bis zum grossen, bemannten Flugzeug – abdecken kann.

Die Auslegungsmethode basiert auf der Abstimmung von Leistung und Gewicht während eines Schwebefluges. Eine umfangreiche Untersuchung zur mathematischen Modellierung aller Elemente eines Flugzeuges wurde durchgeführt. So zum Beispiel wurde untersucht, wie das Gewicht und der Wirkungsgrad von Elektromotoren sich mit der Leistung verändern. Zur Untersuchung wurden empirische Daten von grosser Vielfalt herangezogen. Schlussendlich verwendet die Auslegungsmethode fünf Parameter zur Beschreibung der Flugmanöver und 25 andere, die mit den verwendeten Technologien der verschiedenen Flugzeugkomponenten zusammenhängen. Mittels einer Software können die Parameter durch einen Benutzer verändert werden, so dass der Einfluss auf die drei Auslegungsvariablen (Längenverhältnis, Spannweite und Gesamtgewicht des Flugzeuges) für alle Lösungsmöglichkeiten direkt in einem Diagramm sichtbar wird. Die endgültige Wahl der Parameter ist so einfach zu bewerkstelligen.

Sky-Sailor, ein Solarflugzeug mit 3.2 Meter Spannweite, wurde mit Hilfe dieser Auslegungsmethode entwickelt. Ein Prototyp mit einer extraleichten Flügelstruktur überzogen mit Siliziumsolarzellen wurde gebaut, um die theoretische Auslegungsmethode zu validieren. Ebenfalls wurde die dazugehörige Elektronik zur autonomen Navigation und effizienten Energieverwaltung entwickelt. Das resultierende Solarflugzeug mit einem Gewicht von 2.44 Kilogramm wurde mit Erfolg getestet. Es vollzog mehrere autonome Flüge, wobei

die gemessenen Parameter sehr gut mit den berechneten übereinstimmten. Der längste Flug dauerte mehr als 27 Stunden auf einer Strecke von mehr als 874 Kilometern, womit die Durchführbarkeit von solargetriebenen Schwebeflügen bestätigt wurde.

Zusätzlich zum Sky-Sailor werden in dieser Arbeit andere Entwürfe vorgestellt und diskutiert, so zum Beispiel ein unbemanntes Solarflugzeug mit 70 cm, aber auch ein bemanntes Solarflugzeug mit 60 m Spannweite. Dabei ist die Entwicklung der Parameter in Funktion der Baugrösse sehr interessant. Beide Grössenrichtungen bieten dabei ihre eigenen Probleme : der schlechte Wirkungsgrad der Aerodynamik und der Antriebsgruppe machen sich bei der Skalierung nach unten bemerkbar, hingegen bereiten Gewicht und Zerbrechlichkeit von grossen Flügelstrukturen bei der Skalierung nach oben den Ingenieuren Kopf zerbrechen.

Am Schluss der Arbeit werden verschiedene zusätzliche Möglichkeiten behandelt, die die Reichweite von Solarflugzeuge verbessern können, wie zum Beispiel eine gesteigerte Flughöhe um Energie zu speichern, das Ausnützen von Thermik oder das Verwenden von ausrichtbaren Solarzellen.

Schlüsselwörter: Solarangetriebene Flugzeuge, Solarenergie, Solarflugzeug, Ununterbrochener Flug, Sky-Sailor, MPPT, Konzeptuelle Auslegungsmethode

List of symbols

AR	aspect ratio [-]
b	wingspan [m]
c	wing chord [m]
C_D	drag coefficient [-]
C_{D0}	drag coefficient at zero lift [-]
C_L	lift coefficient [-]
C_{Lmax}	maximum lift coefficient [-]
C_M	pitching moment coefficient [-]
d	diameter [m]
D	drag force [N]
e	Oswald efficiency factor [-]
g	gravitational acceleration [m/s^2]
I	current [A]
I_A	motor stall current [A]
I_0	motor no load current [A]
I_{max}	maximum sun irradiance [W/m^2]
I_{MP}	maximum power current [A]
I_{SC}	short circuit current [A]
J	propeller advance ratio [-]
k_m	motor torque constant [Nm/A]
k_u	motor voltage constant [Vs/rad]
L	lift force [N]
M	pitching moment [Nm]
M_{em}	motor electromagnetic moment [Nm]
M_H	motor stall moment [Nm]
M_{mot}	motor output moment [Nm]
M_R	motor friction moment [Nm]
m	mass [kg]
n	number of blades [-]
n	number of tail booms [-]

P	power [W]
r	gearbox reduction ratio [-]
r_a	motor terminal resistance [Ohm]
Re	Reynolds number [-]
S	wing area or wing surface [m^2]
T	thrust [N]
T	time period [s]
U	voltage [V]
v	flight speed [m/s]
V	voltage [V]
V_{MP}	maximum power voltage [V]
V_{OC}	open circuit voltage [V]
W	weight [N]
α	angle of attack [-]
η	efficiency [-]
μ	fluid dynamic viscosity [Ns/m^2]
ν	fluid kinematic viscosity [m^2/s]
ρ	air density [kg/m^3]
θ	sun elevation angle [rad]
ω	rotational speed [rad/s]

Subscripts

af	airframe
av	avionics
bat	battery
bec	battery eliminator circuit
cbr	camber
$chrg$	charge
$ctrl$	motor controller
$dchrg$	discharge
enc	solar cells encapsulation
grb	gearbox
lev	level flight
mot	motor
pld	payload
plr	propeller
$prop$	propulsion group
sc	solar cells
$wthr$	weather

Acronyms

AGL Above Ground Level

ASL Autonomous Systems Laboratory

BLDC Brushless Direct Current

BEC Battery Eliminator Circuit

BET Blade Element Theory

CFD Computed Fluid Dynamics

DC Direct Current

EPFL Ecole Polytechnique Fédérale de Lausanne

ESA European Space Agency

ETHZ Eidgenössische Technische Hochschule Zürich

FAI Fédération Aéronautique Internationale

GCS Ground Control Station

GUI Graphical User Interface

HALE High Altitude Long Endurance

IMU Inertial Measurement Unit

MAV Micro Aerial Vehicle

MPPT Maximum Power Point Tracker

NASA National Aeronautics and Space Administration

PWM Pulse Width Modulation

RC Radio Command

UAV Unmanned Aerial Vehicle

Simplicity is the final achievement. After one has played a vast quantity of notes and more notes, it is simplicity that emerges as the crowning reward of art.

Chopin

Contents

List of Tables

List of Figures

Chapter 1

Introduction

1.1 Motivations and Objectives

The ability for an aircraft to fly during a much extended period of time
has become a key issue and a target of research, both in the domain of
civilian aviation and unmanned aerial vehicles. This latter domain takes an
increasingly important place in our society, for civilian and unfortunately
military applications. The required endurance is in the range of a couple of
hours in the case of law enforcement, border surveillance, forest fire fighting or
power line inspection. However, other applications at high altitudes, such as
communication platform for mobile devices, weather research and forecast,
environmental monitoring, would require remaining airborne during days,
weeks or even months.

   For the moment, it is only possible to reach such ambitious goals using
electric solar powered platforms. Photovoltaic modules may be used to collect
the energy of the sun during the day, one part being used directly to power
the propulsion unit and onboard instruments, the other part being stored for
the night time.

   In order to reach the target endurance, the design of the airplane has to
be thought carefully and globally, as a system composed of many subsystems
that are continuously exchanging energy. Due to these relationships, each
part has to be sized accordingly to all the others. Here, the design method
is to engineering what the recipe is to cooking. A good chef can cook an
exceptional meal with standard products, whereas his apprentice can miss
it completely even using expensive high quality products. Simply because a
crucial part lies in the combination of all the elements, and not only in their
quality. This is especially true for multidisciplinary projects, the case of a

solar airplane being an ideal example as it requires knowledge in the fields of aerodynamics, actuators, sensors, electronics, energy storage, photovoltaic, etc.

In 2004, the Autonomous Systems Lab of EPFL/ETHZ started the Sky-Sailor project, under a contract with the European Space Agency. ESA had the vision to send to Mars an airplane that could achieve various scientific missions. Compared to other airplane concepts for planetary missions, like AME (Airplane for Mars Exploration) [63] or ARES (Aerial Regional-scale Environmental Survey) [67] that would be capable of embedding several kilograms for missions limited to a few hours, the goal was here to embed a payload of less than half a kilogram but for missions of weeks, even months, using solar energy. So the target was to study the feasibility of a solar powered airplane aimed at flying continuously in the atmosphere of Mars. As a first step, the feasibility of continuous flight on Earth was to be studied, with the idea to fly an Earth prototype at altitudes where similarities occur with the red planet.

Figure 1.1: The fully functional solar airplane prototype, named Sky-Sailor, developed within the framework of this thesis during an autonomous flight

The present thesis lies within the scope of this project. Its objective is not only to study a fixed design for a well determined mission, but rather to develop a versatile design methodology, that can be used for other projects, with different wingspans or payloads, and rapidly adapted to new technology improvements. It is not intended to focus on aerodynamics only, as this domain was already often covered [43, 128], but aims rather at studying the sizing relationships between the elements and especially at developing accurate weight prediction models for all of them. Laws of scaling make then clear what becomes problematic or easier when decreasing or increasing the airplane wingspan.

In order to locate clearly where the contributions lie, we should first recall that the design process of an airplane is composed of three main phases [103]:

- **Conceptual Design** : it is in this phase that the basic questions of configurations arrangement, size, weight and performance are answered. The design requirements are used to guide and evaluate the development of the overall aircraft configuration. The level of detail is not deep but a good understanding of the interactions among all the different components is crucial.
- **Preliminary Design** : during this phase, the specialists in areas such as structures, control systems, propulsion, etc. will design and analyze their portion of the aircraft. The design evolves with ever-increasing level of understanding and confidence that it will work.
- **Detail Design** : assuming a favorable decision for entering full-scale development, the detail design phase begins in which the actual pieces to be fabricated are designed. The many little pieces not considered during the two first phases must be designed and it has also to be decided how everything will be produced and assembled.

Hence, this thesis concentrates mostly on the conceptual design phase. However, in order to validate the theory through experiments, a full prototype of solar powered airplane was realized, for which the two last design phases are also described. Finally, the prototype that was built has the ability to fly more than 24 h on solar power and completely autonomously in terms of navigation and control.

1.2 History of Solar Powered Flight

1.2.1 The Conjunction of two Pioneer Fields, Electric Flight and Solar Cells

The use of electric power for flight vehicles propulsion is not new. The first one was the hydrogen-filled dirigible France in year 1884 that won a 10 km race around Villacoulbay and Medon. At this time, the electric system was superior to its only rival, the steam engine, but then with the arrival of gasoline engines, work on electrical propulsion for air vehicles was abandoned and the field lay dormant for almost a century [33].

On the 30th of June 1957, Colonel H. J. Taplin of the United Kingdom made the first officially recorded electric powered radio controlled flight with his model "Radio Queen", which used a permanent-magnet motor and a silver-zinc battery. Unfortunately, he didn't carry on these experiments. Further developments in the field came from the great German pioneer, Fred Militky,

who first achieved a successful flight with an uncontrolled model in October 1957. Since then, electric flight continuously evolved with constant improvements in the fields of motors and batteries [4].

Three years before Taplin and Militky's experiments, in 1954, photovoltaic technology was born at Bell Telephone Laboratories. Daryl Chapin, Calvin Fuller, and Gerald Pearson developed the first silicon photovoltaic cell capable of converting enough of the sun's energy into power to run everyday electrical equipment. First at 4 %, the efficiency improved rapidly to 11 % [5]. Two more decades will be necessary to see the solar technology used for the propulsion of electric model airplanes.

1.2.2 Early Stages of Solar Aviation with Model Airplane

On the 4th of November 1974, the first flight of a solar powered aircraft took place on the dry lake at Camp Irwin, California. Sunrise I, designed by R.J. Boucher from Astro Flight Inc. under a contract with ARPA, flew 20 minutes at an altitude of around 100 m during its inaugural flight. It had a wingspan of 9.76 m, weighed 12.25 kg and the power output of the 4096 solar cells was 450 W [33]. Scores of flight for three to four hours were made during the winter, but Sunrise I was seriously damaged when caught flying in a sand storm. Thus, an improved version, Sunrise II, was built and tested on the 12th of September 1975. With the same wingspan, its weight was reduced to 10.21 kg and the 4480 solar cells were able this time to deliver 600 W thanks to their 14 % efficiency. After many weeks of testing, this second version was also damaged due to a failure in the command and control system. Despite all, the history of solar flight was engaged and its first demonstration was done.

Figure 1.2: Sunrise I (1974) and Solaris (1976)

On the other side of the Atlantic, Helmut Bruss was working in Germany on a solar model airplane in summer 1975 without having heard anything about Boucher's project. Unluckily, due to overheating of the solar cells on his model, he didn't achieve level flight and finally the first one in Europe was his friend Fred Militky, one year later, with Solaris. On the 16th of August 1976, it completed three flights of 150 seconds reaching the altitude of 50 m [38]. Since this early time, many model airplane builders tried to fly with solar energy, this passion becoming more and more affordable. Of course, at the beginning, the autonomy was limited to a few seconds, but it rapidly became minutes and then hours.

Some people distinguished themselves like Dave Beck from Wisconsin, USA, who set two records in the model airplane solar category F5 open SOL of the FAI [21]. In August 1996, his Solar Solitude flew a distance of 38.84 km in straight line and two years later, it reached the altitude of 1283 m [18, 21]. The master of the category is still Wolfgang Schaeper who holds now all the official records : duration (11 h 34 mn 18 s), distance in a straight line (48.31 km), gain in altitude (2065 m), speed (80.63 km/h), distance in a closed circuit (190 km) and speed in a closed circuit (62.15 km/h). He achieved these performances with Solar Excel from 1990 to 1999 in Germany [15].
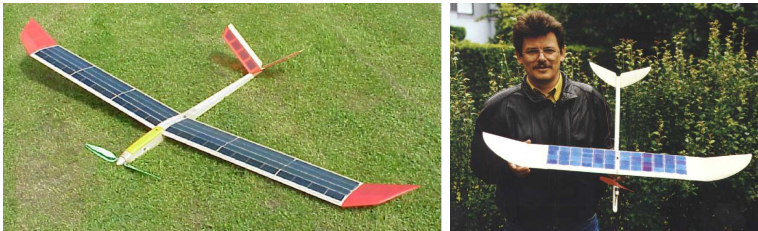
Figure 1.3: Solar Excel (1990) and PicoSol (1998)

We can mention as well the miniature models MikroSol, PicoSol and NanoSol of Dr. Sieghard Dienlin [22]. PicoSol, the smallest one, weighs only 159.5 g for a wingspan of 1.11 m and its solar panels can provide 8.64 W.

1.2.3   The Dream of Manned Solar Flight

After having flown solar model airplanes and proved it was feasible with sufficient illumination conditions, the new challenge that fascinated the pioneers at the end of the 70's was manned flights powered solely by the sun.

On the 19th of December 1978, Britons David Williams and Fred To launched Solar One on its maiden flight at Lasham Airfield, Hampshire [33,

121]. First intended to be human powered in order to attempt the Channel crossing, this conventional shoulder wing monoplane proved too heavy and thus was converted to solar power. The concept was to use nickel-cadmium battery to store enough energy for short duration flights. Its builder was convinced that with high-efficiency solar cells like the one used on Sunrise, he could fly without need of batteries, but their exorbitant price was the only limit.

On April 29, 1979, Larry Mauro flew for the first time the Solar Riser, a solar version of his Easy Riser hang glider, at Flabob Airport, California. The 350 W solar panel didn't have sufficient power to drive the motor directly and was here again rather used as a solar battery charger. After a three hours charge the nickel-cadmium pack was able to power the motor for about ten minutes. His longest flight covered about 800 m at altitudes varying between 1.5 m and 5 m [33].

This crucial stage consisting in flying with the sole energy of the sun without any storage was reached by Dr. Paul B. McCready and AeroVironment Inc, the company he founded in 1971 in Pasadena, California. After having demonstrated, on August 23, 1977, sustained and maneuverable human-powered flight with the Gossamer Condor, they completed on June 12, 1979 a crossing of the English Channel with the human-powered Gossamer Albatross. After these successes, Dupont sponsored Dr. MacCready in an attempt to modify a smaller version of the Gossamer Albatross, called Gossamer Penguin, into a man carrying solar plane. R.J. Boucher, designer of Sunrise I and II, served as a key consultant on the project. He provided the motor and the solar cells that were taken from the two damaged versions of Sunrise. On the 18th of May 1980, the Gossamer Penguin, with 13 years old MacCready's son Marshall on board, realized what can be considered as the world's first piloted, solar powered flight.

Figure 1.4: Gossamer Penguin (1980) and its successor, Solar Challenger (1981)

However, the Gossamer Penguin was not safe for a pilot flying at more than a few feet above ground. The Dupont Company, encouraged by the results of the Gossamer Penguin, sponsored MacCready for building a new solar airplane that would cross the English Channel. The Solar Challenger was a 14.2 m wingspan high-wing monoplane with 16 128 solar cells offering 2500 W at sea level. On July 7, 1981, it flew from Puntoise-Cormeilles near Paris to Manston RAF Base near London in 5 hours 23 minutes covering 262.3 km, with solar energy as its sole power source and no onboard energy storage system.

Figure 1.5: Solair I (1981) and Sunseeker (1990)

As they were in England, the members of the Solar Challenger team were surprised to hear for the first time about a German competitor who was trying to realize exactly the same performance at the same time from Biggin Hill airport. Günter Rochelt was the designer and builder of Solair I, a 16 m wingspan solar airplane based on the Canard 2FL from AviaFiber that he slightly modified and covered with 2499 solar cells providing 1800 W. He invited members of the Solar Challenger team to visit him and R.J. Boucher, who accepted the invitation, was very impressed by the quality of the airplane [33]. However, with a little more than half the wing area of solar cells, Solair I didn't have enough energy to climb and thus incorporated a 22.7 kg nickel-cadmium battery. Rochelt didn't realize the Channel crossing this year but on the 21st of August 1983 he flew in Solair I, mostly on solar energy and also thermals, rising currents of warm air, during 5 hours 41 minutes.

In 1986, Eric Raymond started the design of the Sunseeker in the United States. The Solar Riser in 1979, Solar Challenger two years later and a meeting with Günter Rochelt in Germany had convinced him to build his own manned solar powered aircraft. At the end of 1989, the Sunseeker was test flown as a glider and during August 1990, it crossed the USA in 21 solar powered flights with 121 hours in the air [20].

Figure 1.6: Icaré 2 (1996) and Solair II (1998)

In Germany, the town of Ulm organized regularly aeronautical competitions in the memory of Albrecht Berblinger, a pioneer in flying machines 200 years ago. For the 1996 event, they offered attractive prizes to develop a real, practically usable solar aircraft that should be able to stay up with at least half the solar energy a good summer day with clear sky can give [6]. This competition started activities round the Earth and more than 30 announced projects, but just some arrived and only one was ready to fly for the final competition. On the 7th of July, the motorglider Icaré 2 of Prof. Rudolf Voit-Nitschmann from Stuttgart University won the 100,000 DM price [8,126]. Two other interesting competitors were O Sole Mio from the Italian team of Dr. Antonio Bubbico and Solair II of the team of Prof. Günter Rochelt who took profit of the experiences gained with the Solair I. Both projects were presented in an advanced stage of development, but were not airworthy at the time of the competition. The first flight of Solair II took place two years later in May 1998.

1.2.4 On the Way to High Altitude Long Endurance Platforms and Eternal Flight

After the success of Solar Challenger, the US government gave funding to AeroVironment Inc. to study the feasibility of long duration, solar electric flight above 19 812 km (65 000 ft). The first prototype HALSOL proved the aerodynamics and structures for the approach, but it suffered from its subsystem technologies, mainly for energy storage, that were inadequate for this type of mission. Thus, the project took the direction of solar propulsion with the Pathfinder that achieved its first flight at Dryden in 1993. When funding for this program ended, the 30 m wingspan and 254 kg aircraft became a part of NASA's Environmental Research Aircraft Sensor Technology (ERAST) program that started in 1994. In 1995, it exceeded Solar Challenger's altitude record for solar powered aircraft when it reached 15 392 m

(50 500 ft) and two years later he set the record to 21 802 m (71 530 ft). In 1998, Pathfinder was modified into a new version, Pathfinder Plus, which had a larger wingspan and new solar, aerodynamic, propulsion and system technologies. The main objective was to validate these new elements before building its successor, the Centurion.

Centurion was considered to be a prototype technology demonstrator for a future fleet of solar powered aircrafts that could stay airborne for weeks or months achieving scientific sampling and imaging missions or serving as telecommunications relay platforms [17]. With a double wingspan compared to Pathfinder, it was capable to carry 45 kg of remote sensing and data collection instruments for use in scientific studies of the Earth's environment and also 270 kg of sensors, telecommunications and imaging equipment up to 24 400 m (80 000 ft) altitude. A lithium battery provided enough energy to the airplane for two to five hours flight after sunset, but it was insufficient to fly during the entire night.

Figure 1.7: Centurion (1997-1999) and Helios (1999-2003)

The last prototype of the series designated as Helios was intended to be the ultimate "eternal airplane", incorporating energy storage for night-time flight. For NASA, the two primary goals were to demonstrate sustained flight at an altitude near 30 480 m (100 000 ft) and flying non-stop for at least 24 hours, including at least 14 hours above 15 240 m (50 000 ft). In 2001, Helios achieved the first goal near Hawaii with an unofficial world-record altitude of 29 524 m (96 863 ft) and a 40 minutes flight above 29 261 m (96 000 ft). Unfortunately, it never reached the second objective as it was destroyed when it fell into the Pacific Ocean on June 26, 2003 due to structural failures.

In Europe, many projects were also conducted on high altitude, long endurance (HALE) platforms. At the DLR Institute of Flight Systems, Solitair was developed within the scope of a study from 1994 to 1998 [19,124]. The solar aircraft demonstrator was designed for year-around operations in northern

European latitude by satisfying its entire onboard energy needs by its solar panels. So far, a 5.2 m wingspan proof-of-concept model aircraft was built with adjustable solar panels for optimum solar radiation absorption. Flight tests were achieved and various projects are still carried out on this scaled version [71].

The Helinet project, funded by a European Program, ran between January 2000 and March 2003 with the target to study the feasibility of a solar powered high altitude platform of 73 m wingspan and 750 kg named Heliplat. It was intended to be used for broadband communications and Earth observation. The project involved ten European partners and led to the construction of a 24 m wingspan scale prototype of the structure. Politecnico di Torino, the overall coordinator, is still leading research on Heliplat and also on a new platform named Shampo [113, 124].
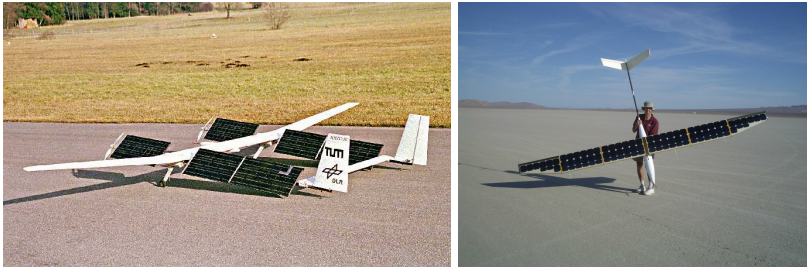
Figure 1.8: Solitair (1998) and Solong (2005)

The objective of Helios to prove the feasibility of eternal flight for an unmanned airplane was reached on the 22nd of April 2005. Alan Cocconi, president and founder of AcPropulsion, flew his Solong during 24 hours and 11 minutes using only solar energy coming from its solar panels and also thermals. The 4.75 m wingspan and 11.5 kg airplane confirmed its capabilities two months later, on the 3rd of June, with a flight lasting 48 hours and 16 minutes taking place in California's Colorado Desert.

QinetiQ, a British company, is also very active in the field of solar HALE platforms. Two Zephyr aircrafts were first tested in New Mexico in December 2005, achieving a maximum duration of 6 hours and reaching an altitude of 7 925 m (26 000 ft). After an 18 hours flight in July 2006, one Zephyr exceeded the official world record time for the longest duration unmanned flight with a 54 hours flight in New Mexico on the 10th of September 2007, reaching a maximum altitude of 17 786 m (58 355 ft). Weighing only 30 kg for 18 m wingspan, the aircraft used solar power for the ascent, reverting to lithium-

sulphur battery power as dusk fell. QinetiQ expects in the future flight duration of some months at an altitude above 15 240 m (50 000 ft) [23].

Zephyr has recently been selected as the base platform for the Flemish HALE UAV remote sensing system Mercator in the framework of the Pegasus project [13]. The targeted platform should be able to carry a 100 kg payload in order to fulfill its missions that are forest fire monitoring, urban mapping, coastal monitoring, oil spill detection and many others.

Figure 1.9: Zephyr (2005) and the future Solar Impulse

The next dream to prove continuous flight with a pilot on board will perhaps come true with Solar-Impulse [16], a project officially announced in Switzerland in 2003. A nucleus of twenty-five specialists, surrounded by some forty scientific advisors from various universities like EPFL, is working on the 80 m wingspan, 2000 kg lightweight solar airplane. After the manufacturing of a 60 m prototype in 2007-2008 and the final airplane in 2009-2010, a round-the-world flight should take place in May 2011 with a stopover on each continent.

Of course History is still going on. In early 2007, the DARPA announced the launch of a new solar HALE project [10]. The Vulture air vehicle program aims at developing the capability to deliver and maintain a single 453 kg (1000 lb), 5 kW airborne payload on station for an uninterrupted period of at least 5 years.

1.3   State of the Art

Establishing the state of the art of solar airplane design methodologies is complex because of a flagrant contradiction : the history of solar aviation has seen the realization of exceptional airplanes, manned or unmanned, that showed outstanding capacities and broke records but for which the design process is never explained or even kept secret. On the other side, there is a

literature of more than thirty papers covering the subject of solar powered airplane design. However, the majority of them always stayed at a theoretical level and do not include the realization of a prototype that could validate and add far more credibility to the theory. Also, many studies are very local, only taking into account a precise wingspan and being thus not applicable to different sizes.

In the first category, R. J. Boucher published in 1979 a nice description of the performances and hardware of the first solar powered airplane Sunrise, unfortunately without explanation about the design process [32]. This lack of design guidelines is also present in the publication of P. B. MacCready about the Gossamer Penguin and Solar Challenger in 1983 [77] and N.J Colella about Pathfinder in 1994 [46].

Some experienced authors discussed the different technologies involved in solar powered airplane design, without describing a global design method, but sharing useful practical knowledge on separate aspects. In 1978, J. Gedeon was already presenting "Some Thoughts on the Feasibility of a Solar-Powered Plane" that are still valid today [62]. E. Schoeberl published very interesting articles, especially about propulsion group elements efficiencies and aerodynamics [115, 116], and A. J. Colozza discussed in details the solar cells and their integration [51]. Finally, two books, the first one on solar model airplane building [38] and the second one on the 1996 Berblinger Contest in Ulm [119], concentrate an impressive amount of practical knowledge. In model-making magazines as well, many of them from Germany like *Aufwind*, *Flug- und Modelltechnik* or *Modellflug international*, there are also some interesting descriptions of solar powered airplane executions, but here again the design, if explained, is local and not applicable to different dimensions.

In the category of papers describing the design process, the first scientific publication is from F. G. Irving. In September 1974, he presented a manned airplane design [70] using weight prediction models for the airframe, the propulsion group and the solar cells, making their weight vary parametrically with the wingspan or the power. To estimate the airframe weight he used Stender's equation based on statistical data for sailplanes with twin boom tails [120]. This model was very widely used in the literature for solar airplane design and very often misused. As will be shown in section 3.4.2, it is only valid for a very limited range in the region of large aircrafts, but proves to be wrong elsewhere. It was used by J. W. Youngblood for a long-endurance unmanned airplane design in 1982 [130, 131], by M. D. Bailey in 1992 who introduces also separate weight models for the motor, its controller, the gearbox, the propeller and also the fuel cell [27]. It was also utilized by the group of Politecnico di Torino working mainly on aerodynamic analysis

and structural concepts [113].

David and Stan Hall developed in 1984 a new method to predict the airframe weight of a solar aircraft, taking into account all the parts (ribs, spar, tail booms, etc.). It proved to be very accurate, but also complex and was said to be valid for an airplane weight of 1000 to 3000 lbs (453 to 1360 kg) [69]. This model is also used by Colozza in 1993 [50] and inspired Keidel who determined separately the weight of the airframe parts [71]. In 2005, Rizzo developed a nice methodology with weight models and a study of the wing configuration, but limited to big airplanes. The structural weight prediction model from the interpolation of only four NASA airplanes makes it also valid in a very narrow design space, as shown in section 3.4.2 [110].

In fact, the main problem of the publications listed above is that they don't validate the design method and models with a real prototype and real flight experiments. This point is important to be mentioned, because using far too optimistic efficiencies or weight prediction models, especially outside their domain of validity, ends with solutions that are not realistic. Boucher presented a very optimistic study about a high altitude solar airplane, the Starduster, based on Sunrise II [34]. The result is a 10 m wingspan airplane that weighs 8.5 kg and consumes only 18 W whereas the maximum solar power is 2300 W. Some papers present plots and sensitivity analysis, but unfortunately without presenting the weight prediction models and the equations behind [28, 107].

Concerning the weight models, some authors consider the weight of all the elements as proportional to the wing surface, such as Brandt in 1995 using an iterative design approach [36]. Guglieri in 1996 simplifies the problem too much saying that the wing structural weight is linear to the surface but also fixing directly the weight of the pilot, the mass of the motor, gearbox, propeller and fuselage without any parametric relationship [66]. Rehmet also considers a wing weight proportional to its surface in [105], which is only locally correct but gives wrong results if used outside a certain range. However, after the Berblinger contest in 1996, he revised it and used a polynomial formula with surface and wingspan. It is still valid for 15 to 40 m wingspan only, but values are very good and the results coherent, as it gave rise to the Icaré 2, a project that is well summarized in [126]. The publications of Rehmet are of especially very high quality because the theory is linked to and validated with real experiments and data, for example concerning the different efficiencies.

In 2006, Moffitt uses a discrete design method where 20 motors, 2 gear ratios, 53 propellers, etc. are tested before selecting the best combination [87]. The drawback is that this kind of method requires a lot of different parts to

be tested, necessitates then as he said a high computational time to test all these possible combinations but also doesn't lead to a model that would show tendencies and general principles extracted from sensitivity analysis.

The design of solar powered airplane was also studied by many students during bachelor or master projects. Compared to the publications cited above, the design process is often poorer, selecting the elements one after the other without taking the design as a whole, which leads to more or less success concerning the final performances [25, 31, 99]. Their great advantage is that they very often lead to a prototype and flight experiments, giving a feedback on the design. Even if in some cases this feedback leads to the calculation of efficiencies above 100 % [55], it allows reconsidering the validity of the models used. Additionally, some of them are proposing very inventive ideas. This is the case of Tegeder who implemented a sun tracking system that orients the solar panels and discusses the energy benefit compared to the additional weight [122]. Some students are focusing more on the aerodynamic optimization, neglecting the design of the other components, which leads to low performances [43, 128]. Others tried to really down scale the solar airplane to the MAV size [111]. The best solar airplane design comes from a student team from Israël who built SunSailor in 2006 [127].

A few studies were also conducted to evaluate the feasibility of solar flight on other planets. Colozza [49] tackled the problem for Mars where the low atmosphere density problems dominate the low gravity benefit. Landis evaluated the feasibility on Venus [74] where flight conditions are more favorable if one considers the gravity that is close to Earth's and the air density that is very high.

1.4 Contributions

This thesis focuses on the design of solar powered airplanes. We propose a new design methodology and want to address the problems that were highlighted in the last section. The contributions concerning this methodology lie on four pillars :

- **simplicity** : the first objective is to develop a method that is clear, complete and still very simple, which is not contradictory. For this purpose, it is completely analytical and uses mathematical models that are not discrete but continuous. It shows the real tendency of physics and does not for example interpolate physical effects using a polynomial without any physical significance. Hence, the reader can very easily output a valid conceptual design in only minutes with the help of the short Matlab® program given in the appendix.

- **large design space** : the methodology is not only valid for a limited range of wingspan or weight, but remains applicable to a large scale of solar airplanes, from the tiny MAV to the manned aircraft. To reach this goal, the mathematical models of the subparts, for example the weight or the efficiency of electric motors according to their power, was not only studied in a limited domain, but over a very large scale, for some models with up to 7 orders of magnitude, showing on the same graphics a tendency that encompasses motors from 1 mW to 10 kW. Combining this very large final design space with the analytical character of the methodology, it allows achieving sensitivity analysis on certain parameters and for example point out what are the emerging problems when up or down-scaling.
- **concrete and experienced based** : The mathematical models and the various technological parameters used in the methodology are based on real and practical cases. Large sets of empirical data that we then interpolated were preferred to theoretical estimation that proved to be sometimes far too optimistic leading to unrealistic design, as we will see in section 3.4.2.
- **flexibility and versatility** : the method contains exactly 30 parameters, either linked to mission or technology, that can be easily modified to evaluate the sensitivity of a solution with a change in mission or with a technology improvement. As well, the method can be used to design not only an airplane that achieves 24 hours continuous flight, but also for many other scenarios; one that stores its electrical energy into potential energy gaining altitude or another one that would have an endurance of a few hours, flying only during the day time. We will even present the design of such an airplane flying not only on Earth, but in the atmosphere of our neighbor planet, Mars.

Another contribution of this thesis is the realization of a fully functional unmanned solar airplane. In fact, the design methodology was not limited to a theoretical study only verified with simulations, but we wanted to validate it through the realization of a real prototype and flight experiments. The airplane, named Sky-Sailor, was designed on paper to fly more than 24 h at the beginning of the project. Four years later, in June 2008, it successfully reached its objective with a flight of more than 27 h, confirming the effectiveness of the method. For its building, the idea was to combine the theoretical knowledge available in a university with the impressive practical experience of model-making experts.

Finally, this thesis has the modest ambition to draw up a state of the art on solar aviation from its beginning until now, referencing the major scientific

papers on the subject and trying to summarize the history of solar flight and its major contributors in section 1.2. An exhaustive list of all solar airplanes flown to date for which it was possible to obtain technical information is also given in appendix. As well, we will in the conclusion try to anticipate the future and predict the evolution of solar aviation in the next decades.

1.5   Structure of this Work

After this brief introduction, explaining our motivations and the state of the art, the chapter 2 will explain the theoretical principles behind a solar airplane. Chapter 3 will then expose the development of the conceptual design methodology, introducing the models that were used for irradiance and weight prediction of all the elements, without limiting the design to a given mission or dimension. It is only in chapter 4 that we will see how it was concretely applied to design the Sky-Sailor, a 3.2 m wingspan solar airplane and how it was then validated using a real-time simulation environment that shows the evolution of energy flows on the airplane, second after second, during a day. The first prototype that was entirely built and tested is then presented in chapter 5. This part will be very practical with the detailed description of the aircraft's hardware and experiments validating the conceptual design. The objective of chapter 6 will be then to push the limits of our design methodology to extreme cases like a solar MAV of some grams or a manned solar airplane weighing nearly a ton. The analytical character of our methodology will enhance interesting concepts that occur when scaling up or down, showing clearly where the difficulties lay. Having discussed the actual limitations and estimating future technological improvements in the next years, we will then try to predict how solar aviation will evolve and conclude this report.

This work is arranged so that the student who is new to the topic will start from the beginning, the scientist familiar with the field will skip chapter 2 and the model-maker interested mostly by the hardware and the experiments with the Sky-Sailor prototype will directly jump to chapter 5.

Chapter 2

Basic Concepts

2.1   Introduction

In this chapter, we briefly explain the basic principles that make a solar airplane fly and especially the technologies that are involved. Only the theory that is needed to understand the design in the next chapter is discussed. References allow the reader who wants to dig deeper in a subject to do so.

Like all other airplanes, a solar airplane has wings that constitute the lifting part. During steady flight, the airflow due to its relative speed creates two forces : the lift that maintains the airplane airborne compensating the weight and the drag that is compensated by the thrust of the propeller.
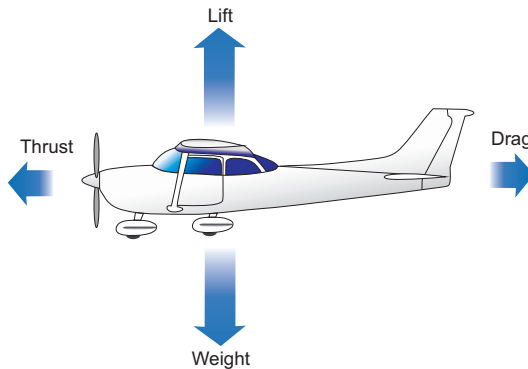
Figure 2.1: Forces acting on an airplane at level flight

The solar panels, composed by solar cells connected in a defined config-

uration, cover a given surface of the wing or potentially other parts of the airplane like the tail or the fuselage. During the day, depending on the sun irradiance and elevation in the sky, they convert light into electrical energy. A converter ensures that the solar panels are working at their maximum power point. That is the reason why this device is called a Maximum Power Point Tracker, that we will abbreviate MPPT. This power obtained is used firstly to supply the propulsion group and the onboard electronics, and secondly to charge the battery with the surplus of energy.
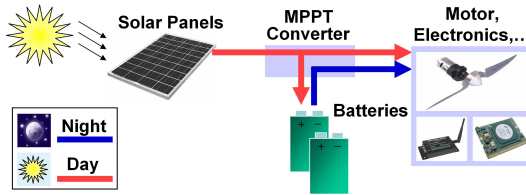
Figure 2.2: Solar airplane basic principle

During the night, as no more power comes from the solar panels, the various elements consuming energy are supplied by the battery that has to last until the next morning where a new cycle starts. After the description of this general concept, we will approach the theory of the different parts separately in the next sections.

2.2   Aerodynamics of a Wing

Figure 2.3 shows the cross section of a wing in a laminar airflow with a constant speed v. The circulation of this airflow creates a different pressure distribution on the upper and lower side of this section that once integrated can be represented as two forces, the lift and the drag. These forces can be calculated using the following equations :
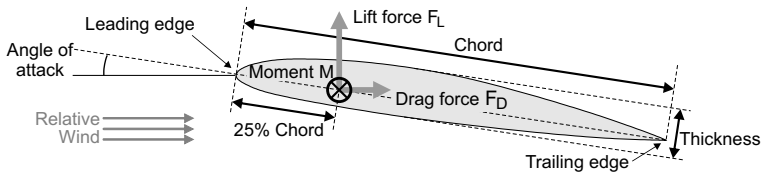
Figure 2.3: Section of an airfoil

$$F_L = C_L \frac{\rho}{2} S v^2 \tag{2.1}$$

$$F_D = C_D \frac{\rho}{2} S v^2 \tag{2.2}$$

Where C_L and C_D are respectively the lift and drag coefficients, ρ is the air density, S the wing area and v the relative airspeed. The C_L and C_D heavily depend on the airfoil, the angle of attack and the Reynolds number Re which is representative of the air flow viscosity.

$$Re = \frac{\rho v c}{\mu} = \frac{v c}{\nu} \tag{2.3}$$

Here, μ is the dynamic viscosity that once divided by the air density gives the kinematic viscosity ν and c represents the chord. The dependency on the angle of attack is depicted in figure 2.4. Increasing it makes the C_L increase, but progressively the flow separates from the airfoil starting at the trailing edge and this lets place to a turbulent zone that makes the C_D increase. At stall, the lift is maximum but the drag is high too. After this point, the behavior is more difficult to predict or simulate, but basically the drag still increases but without being followed by the lift that drops. Thus, the interesting and safe zone for an airplane is before the stall point, for glider especially at the point where the glide ratio C_L/C_D is maximum.
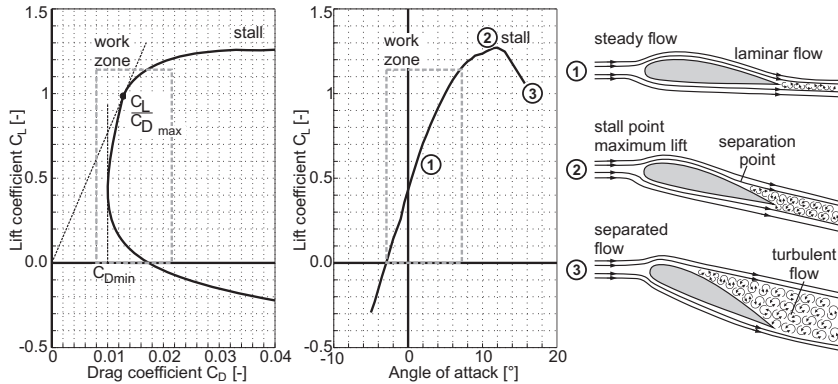
Figure 2.4: Lift and drag coefficients depending on the angle of attack

What was depicted so far is the case of an infinite length wing, but for a real wing, vortices are produced at the wing tips, which induce an additional drag called the induced drag. It represents the energy spent for producing the wake behind the wing and follows :

$$C_{D\,ind} = \frac{C_L^2}{e\pi AR} \tag{2.4}$$

AR is the aspect ratio, i.e. the ratio between the wingspan b and the chord length c that can also be expressed with the wing area using $AR = b/c = b^2/(bc) = b^2/S$. The variable e is the Oswald efficiency factor that has a value between 0 and 1, 1 being the ideal case where the load distribution on the wing is elliptical. In many cases, its value is between 0.75 and 0.85. This induced drag has to be taken into account especially for small aspect ratios airplane as it becomes more important. Finally, there is the parasitic drag coming from non-lifting parts, like the fuselage or the tail. The final drag coefficient is thus the sum of them.

$$C_D = C_{D\,afl} + C_{D\,ind} + C_{D\,par} \tag{2.5}$$

2.3   Solar Cell

A solar cell or photovoltaic cell is a device that converts solar energy into electricity by the photovoltaic effect. It is very widely used in space application because it allows a clean and long-duration source of energy requiring almost no maintenance. Solar cells are composed of various semiconducting materials, constituting one or more layers. Silicon is very often used as it is the second most abundant element in Earth's crust and thus inexpensive. For this reason, this material will be considered in the further explanations that are also valid for other types of semiconductors.

2.3.1   Working Principles

In figure 2.5, a simple silicon solar cell is represented with two doped semiconductors layers, p-type and n-type. When the sunlight strikes the solar cell surface the cell creates charge carriers as electrons and holes. The internal field produced by junction separates some of the positive charges (holes) from the negative charges (electrons). The holes are swept into the positive or p-layer and the electrons are swept into the negative or n-layer. When a circuit is made, the free electrons have to pass through the load to recombine with the positive holes, current can be produced from the cells under illumination.

2.3.2   Solar Irradiance

The energy coming from the sun depends on the wavelength, leading to the solar spectrum represented in figure 2.6. The reference solar spectral irradi-
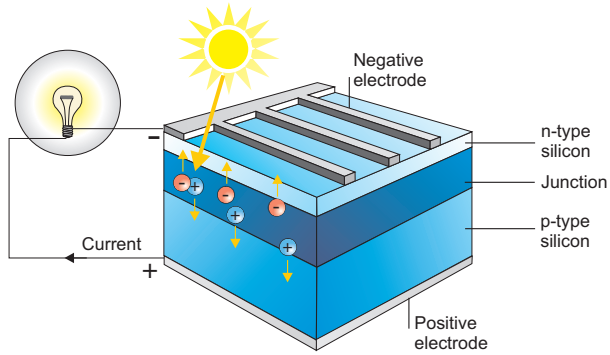
Figure 2.5: Working principle of a solar cell (Source : http://www.renewables-made-in-germany.com/en/photovoltaik/)

ance AM0 (Air Mass 0) represents the irradiance at the top of the atmosphere with a total energy of $1353\,\mathrm{W/m^2}$. At sea level, it is referred as AM1.5 and the total energy equals $1000\,\mathrm{W/m^2}$.
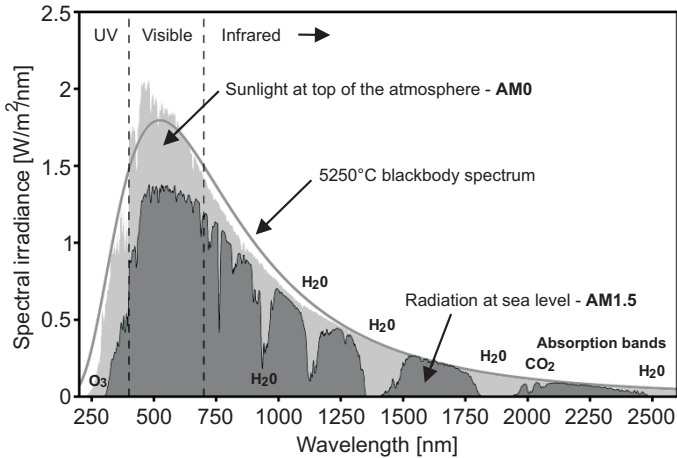
Figure 2.6: Solar radiation spectrum (Source : http://www.physforum.com)

An ideal and perfect solar cell that would cover the entire spectrum and convert all this energy into electricity would have an efficiency of $100\,\%$. In reality, depending on the semiconductors used, only a part of this spectrum is covered.

In addition to the direct irradiance, we also have to consider the diffuse irradiance, which is predominant on a cloudy day, and the reflected irradiance. Reflected irradiance is dependent on the albedo, which is a measure of the reflectivity of the Earth's surface. Fresh snow has an albedo of around 80 %, desert sand 40 % and grass between 5 % and 30 %.
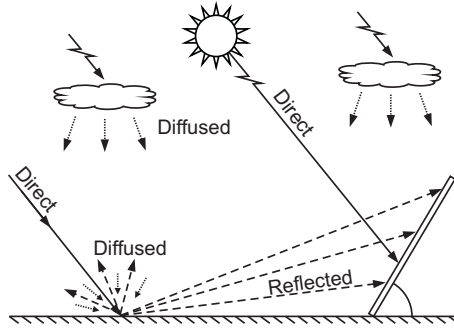
Figure 2.7: Direct, diffuse and reflected irradiance [71]

2.3.3   Types of Solar Cells

There exist various types of photovoltaic cells that can be sorted according to the type of material, the fabrication process, substrate, etc. The objective here is only to give a short and non-exhaustive overview of the existing types. The reader can refer to [82] for deeper information.

The most widely used type of material is silicon, because of its abundance and low cost. We can distinguish three types of ***silicon solar cells*** according to the type of crystal :

- monocrystalline, for which absolutely pure semiconducting material is used which gives a high level of efficiency but at a high cost.
- polycrystalline, composed of crystal structures of varying sizes. The manufacturing process is more cost efficient but leads to less efficient solar cells.
- amorphous, or thin-layer cell, where a silicon film is deposited on glass or another substrate material, even flexible. The thickness of this layer is less than $1\,\mu$m, thus the production costs are very low, but the efficiency is poor as well.

However, other materials can be used as well like elements from groups three to five of the periodic table of the elements to produce ***compound solar***

cells. These include gallium arsenide, copper indium diselenide, cadmium telluride, etc. These cells are more expensive to produce, but lead to higher efficiency.

We can also mention the **polymer solar cells** made of organic material and the **dye sensitized solar cells** that are very promising technologies because they are inexpensive to fabricate. However, these technologies suffer from unstable efficiency problems that still must be solved and are not yet viable for industry.

In fact, the most efficient solar cells are of a stack of individual single-junction cells in descending order of bandgap. The top cell captures high-energy photons and passes the rest on to lower-bandgap cells. These multi-junction cells can then convert a wider part of the solar spectrum of figure 2.6 leading to a high efficiency that goes up to 40 %. Figure 2.8 shows the best efficiencies obtained for various solar cell technologies.
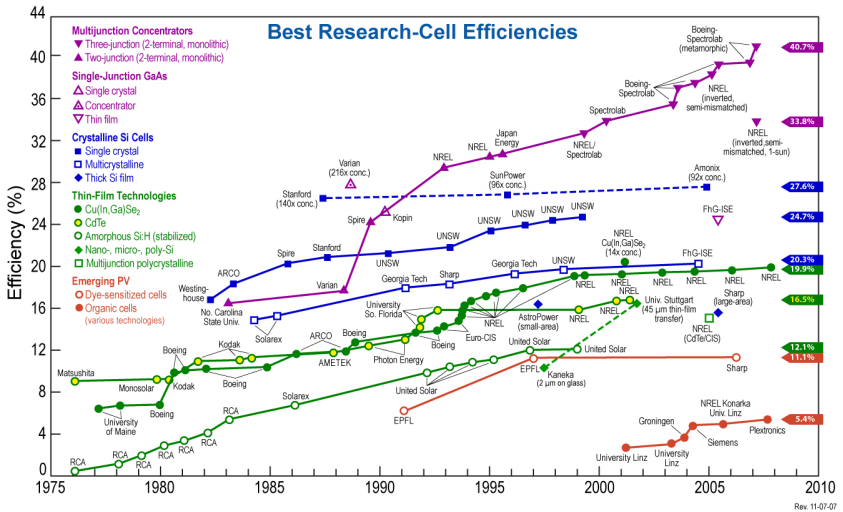
Figure 2.8: Best research - cell efficiencies (Courtesy of L.L. Kazmerski, NREL)

2.3.4   Current and Voltage of a Solar Cell

The current to voltage curve of a solar cell has a very characteristic shape and can be described by the mathematical models of an ideal or real photovoltaic generator that will not be developed here but can be found in [78]. As depicted in figure 2.9, when the cell pads are not connected, no current is

produced and the voltage equals V_{OC}, the open circuit voltage. When it is
short circuited, the voltage is zero but the current equals I_{SC}. In between
these two points where in both cases the power retrieved is zero, there is a
working point, called the maximum power point, where the power one can
retrieve is the highest and equals $P_{max} = V_{MPP} I_{MPP}$. It is precisely at
this point that the cells should be used and the ratio between P_{max} and the
light intensity represents precisely the efficiency of the solar cell. However,
the curve, and thus this point, is not fixed and varies depending on many
parameters.
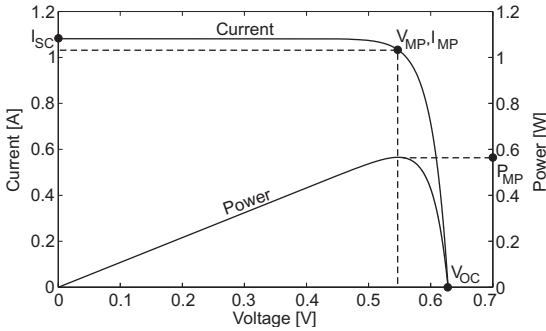
Figure 2.9: Current to voltage curve of a solar cell (Silicon RWE-S-32)

The current of a solar cell is proportional to its area and varies almost
linearly with the light intensity (Figure 2.10). The voltage varies only a little
bit when the light intensity changes and is independent of the cell surface, but
depends on the semiconductor material. For a single layer silicon cell, V_{MPP}
is around 0.5 V, but for a triple junction gallium arsenide cell, it increases up
to 2.27 V. The important values of V_{OC}, I_{SC}, V_{MPP}, I_{MPP} are given in solar
cells datasheets under standard spectrum conditions, either AM0 or AM1.5,
that were presented previously.

Temperature also affects the characteristics of solar cells. When it in-
creases, the voltage decreases slightly whereas the current increases insignif-
icantly. Globally, the power that a solar cell can give is higher for lower
temperature, considering the same irradiance conditions (Figure 2.10).

An assembly of solar cells connected electrically in parallel, which in-
creases the current, or in series, increasing then the voltage, is referred to as
a solar module or solar panel. The I-V curve of a solar module has a scaled
but similar shape to that of the single cell curve.
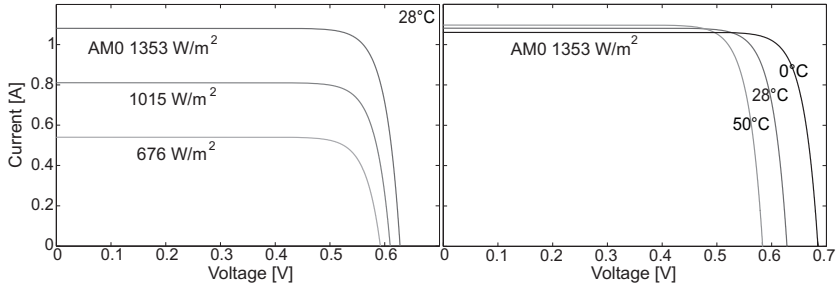
Figure 2.10: Variation of the current to voltage curve of a solar cells with irradiance and temperature (Silicon RWE-S-32)

2.4 Energy Storage

When the energy production is not constant and continuous, a good energy storage method is necessary. We can list many different ways to store energy [11] :

- Chemical (hydrogen, biofuels)
- Electrochemical (batteries, fuel cells)
- Electrical (capacitor, supercapacitor, superconducting magnetic energy storage or SMES)
- Mechanical (compressed air, flywheel)
- Thermal

These different technologies coexist because their characteristics make them attractive to different applications. From a user point of view, the main selection criteria are the energy and power density, the response time, the lifetime, the efficiency and of course the costs.

In the case of a solar airplane, the gravimetric energy density in Wh/kg, also called specific energy, and the peak power are the most crucial parameters that determine the choice of the energy storage method. The volumetric energy density will of course also have an influence on the fuselage size, but this volume plays a minor role on the power required compared to the weight. A look at figure 2.11 shows that in the present case, electrochemical batteries and fuel cells are the two best candidates. In fact, they have the highest gravimetric energy density from all the solutions that are reversible.
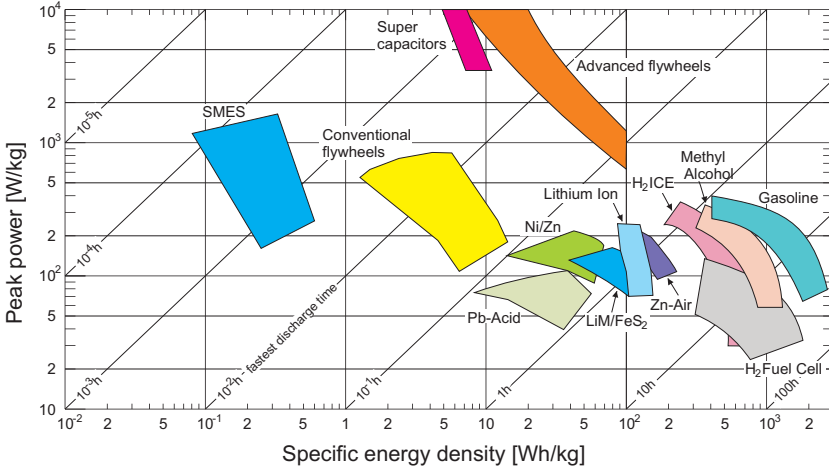
Figure 2.11: The Ragone Plot - Peak power and specific energy density of various energy storage methods (Source : Forschungsverbund Energie Niedersachsen with data from Lawrence Livermore Labs)

2.4.1   Electrochemical Batteries

Working Principles

Electrochemical batteries are energy storage devices, which are able to convert chemically stored energy into electrical energy during discharging. They are composed of a cathode and an anode, made of two dissimilar metals, that are in contact with an electrolyte. When all elements are in contact with each other, a flow of electron is produced. If the process is reversible so that they can be recharged, they are referred to as secondary batteries, in the other case they are primary batteries [97]. Concerning a solar airplane, rechargeable batteries will of course be used.

Several technologies are available and currently, the lithium-ion (or lithium-ion-polymer where the electrolyte is a gel and not a liquid) technology is the best concerning gravimetric energy density, compared to lead-acid, nickel-cadmium (NiCd) or nickel-metal-hydride (NiMH). The nominal voltage of a lithium-ion cell is $3.7\,\text{V}$ compared to $1.2\,\text{V}$ for NiCd and NiMH and its capacity, in Ah depends on its size.

Charge and Discharge Process of a Lithium-Ion Battery

The charging process of lithium-ion batteries is quite simple, but has to be done very carefully because of safety reasons. During a first phase, a constant current charges the battery while the voltage increases as depicted in figure 2.12. Once 4.2 V is reached, the second phase starts during which the voltage is kept constant while the current accepted by the cell slowly decreases. When this current is below 5 % of the maximum current, the battery is charged.
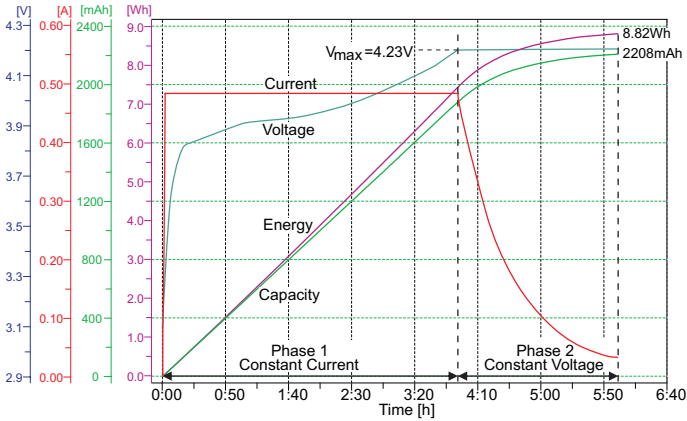
Figure 2.12: Charge process of a lithium-ion battery

The maximum charge rate, depending on the manufacturer, is always lower than 1 C, where C stands for the capacity of the battery. Considering a cell with a capacity of 800 mAh, 1 C represents a current of 800 mA during one hour, 0.5 C gives 400 mA during 2 hours, etc. For this reason, lithium-ion cells always need a minimum of one hour to be charged. Concerning the charging voltage, it should never exceed 4.2 V. Using a charge rate higher than 1 C or overcharging above the maximum voltage damages the cell and potentially results in explosion and/or fire.

Concerning the discharge process, the maximum discharge current is specific to each model. Batteries with high discharge rates of around 20 C are available, but the models that offer a high gravimetric energy density are always rated to less than 1 C. At the end of the discharge, the voltage drops very fast below 3 V, as seen in figure 2.13. At this moment, the load has to be removed as soon as the voltage reaches approximately 2.7 V per cell, or else the battery will subsequently no longer accept a full charge and may experience problems holding voltage under load.
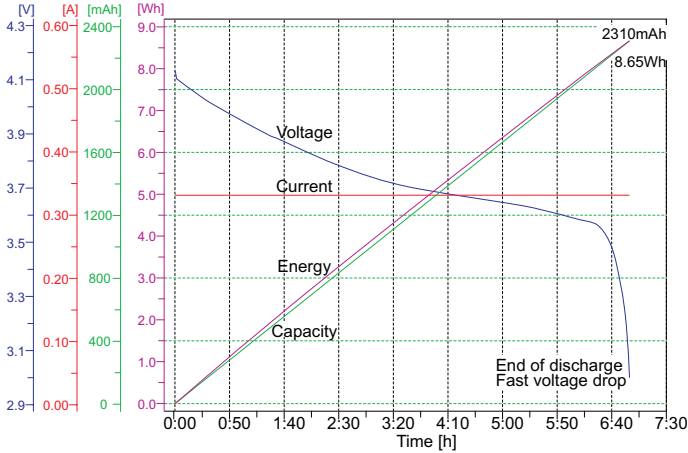
Figure 2.13: Discharge process of a lithium-ion battery. The energy and capacity curve have to be seen here as supplied to the load.

Energy Density and Efficiency

A professional lithium-ion battery charger allows measuring the energy stored and retrieved from the battery during the charging and discharging process very precisely, as shown in figures 2.12 and 2.13. These measured energies should be preferred for estimating available energy, because the values are always slightly different from the product of the capacity and the nominal voltage. The ratio between them allows computing the efficiency of a charge cycle that is between 95 % and 99 %, and knowing the cell weight, we can also compute the gravimetric energy density. The ideal operating temperature varies between the manufacturers but is in general between 0 °C and 50 °C, the discharge being a little bit more tolerant than the charge. Outside this range, the characteristics of the battery, especially the capacity and maximal discharge current, decrease. At low temperature for example, the gravimetric energy density drops very rapidly.

Figure 2.14 shows the evolution of gravimetric energy density and price since 1991. Over the 14 years represented, the energy density increased by 6.6 %/year while the price was reduced by 17 %/year. In 2008, as this thesis is written, the best energy density for commercially available lithium-ion cells is 240 Wh/kg which confirms the trend. This strong improvement and cost reduction in battery technology has been driven by the growing market of portable computers and mobile devices (phones, mp3 players, etc.). This

progression will certainly continue in the next years leading to more efficient, lighter and cheaper battery technologies.

	1991	1992	1993	1994	1995	1996	1997	1998	1999	2000	2001	2002	2003	2004	2005
[Wh/l]	204	208	250	260	271	281	292	321	343	386	428	471	471	514	514
[Wh/kg]	88	90	108	113	114	119	123	135	143	159	172	189	189	202	202
[US$/Wh]	3.17	2.63	2.09	1.75	1.71	1.24	0.95	0.59	0.51	0.42	0.35	0.35	0.33	0.31	0.28
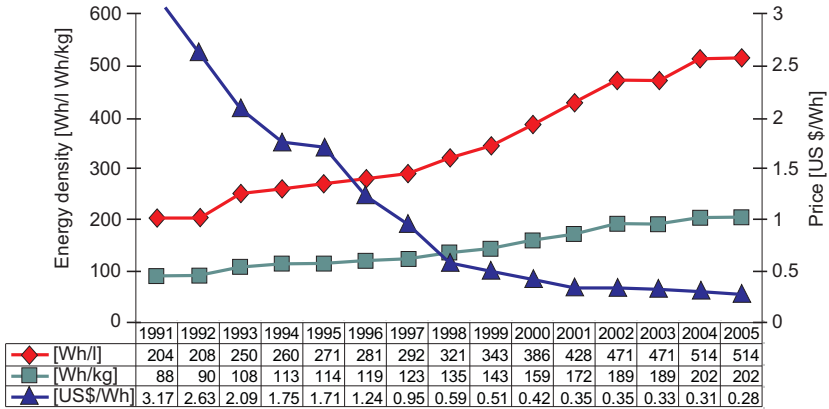
Figure 2.14: Lithium-ion batteries evolution over the last years [1]

2.4.2 Fuel Cells

A fuel cell is a system where the chemical energy of reactants, often a gaseous fuel and the oxygen in the atmosphere, is converted directly into electrical energy and heat. It is the equivalent of burning the fuel; however, as the energy is directly converted to electricity, it is more efficient. What is called the fuel cell is only the part where the reaction and the conversion occurs. It doesn't include the reactants that are stored in separated tanks.

Thank to its high gravimetric energy density, hydrogen is the most favored and common fuel used, that is the reason why we will consider it for the following explanation. The fuel cell consists of two electrodes, known as the anode and cathode that are separated by an electrolyte (Figure 2.15). Oxygen is passed over the cathode and hydrogen over the anode. Hydrogen ions are formed together with electrons at the anode. The hydrogen ions migrate to the cathode through the electrolyte and the electrons produced at the anode flow through an external circuit to the cathode. At the anode they combine with oxygen to form water. The flow of electrons through the external circuit provides the current of the cell.

The great advantage is that the combustion of hydrogen with oxygen produces only water, which is not a pollutant, and that hydrogen has also a very high gravimetric energy density when compared to other fuels. Table
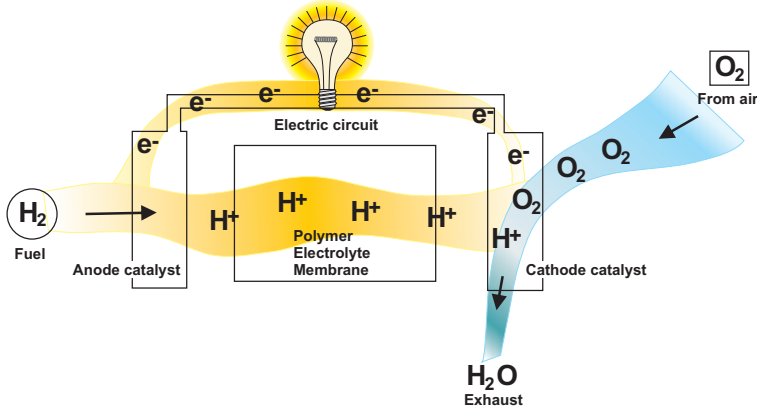
Figure 2.15: Working principle of a fuel cell (Source : www.fuelcells.org)

2.1 establishes a list of commonly used fuels with their energy density, sugar being given just as an interesting comparison point. Of course, we have to keep in mind that the problem of hydrogen is that it is not present in nature but can be obtained through the electrolysis of water, and that at atmospheric pressure, its volumetric energy density is very low.

Table 2.1: Energy density of some reactants (LHV Lower heating value [118])

Reactant	[MJ/kg]	[kWh/kg]
Hydrogen	120	33.3
Methane	50	13.9
Propane	46.3	12.9
Gasoline	44	12.2
Diesel	42	11.7
Ethanol	27	7.5
Methanol	20	5.6
Sugar (glucose)	15.9	4.4

At a first glance, the 33.3 kWh/kg of hydrogen makes the 0.2 kWh/kg of lithium-ion batteries seen above look ridiculous, but this is a wrong comparison. In fact the whole system that converts this chemical energy into electricity is constituted by the hydrogen compressed in a tank, the fuel cell stack, pumps, filters, valves, pressure transducers, etc. All these elements

mean additional weight compared to the hydrogen only and losses, taking into account that all the pumps, valves and control electronics require power.

There are different types of fuel cells, varying with the type of electrolyte and fuel, but the more suitable for solar powered airplane are the PEM (Proton Exchange Membrane or Polymer Electrolyte Membrane) fuel cells, because they have a fast start and response time, are compact and operate at low temperature (80 °C). Their disadvantages are that they are still very expensive because of the platinum they use, have a poor efficiency and their lifetime and reliability are still to be improved [118].

However, if we want to use a fuel cell on a solar airplane to store the energy during the day and reuse it during the night, not only the generation of electricity from hydrogen and oxygen has to be realized on the plane, but also the reverse reaction where the cell act as an electrolyzer, electricity and water being combined to create oxygen and hydrogen. This dual-function system is known as a reversible or unitized regenerative fuel cell (URFC).

Since the beginning of the 90's, the Lawrence Livermore National Laboratory is a world leader in this field, especially under the lead of Fred Mitlitsky [84]. The collaboration with the NASA on the Pathfinder, Pathfinder Plus and Helios solar airplanes oriented the research efforts not only in the direction of efficiency but also towards very low weight [86]. Militsky achieved a packaged specific energy of 400 to 1000 Wh/kg for an URFC with lightweight pressure vessels [85]. A lot of work has to be done on the round trip efficiency, which is the product of the charge and discharge efficiencies. While the theoretical round-trip efficiency of regenerative $H_2/0_2$ fuel cells is about 80 %, practically achievable efficiencies hardly reached 50 % [29, 61]. The hydrogen-bromine regenerative fuel cells offer an efficiency of up to 80 % [76] and research is still going on. So, there will certainly be many improvements in the gravimetric energy density, efficiency and hopefully miniaturization of fuel cells in the future decades.

2.5   Maximum Power Point Tracker

As described in section 2.3, a solar cell has a working point on its current to voltage curve where the power retrieved is maximal. In order to work at this point, which is continuously moving because of the constantly changing irradiance conditions, and thus get the highest amount of energy, a so called Maximum Power Point Tracker (MPPT) is required. An MPPT is basically a DC/DC converter with variable and adjustable gain between the input and the output voltage, the input being the solar panels and the output the battery. It contains electronics that monitor both the current and the voltage

on each side, which allows a determination for how the gain has to be changed to ensure the best use of the solar panels.

There are different algorithms to track this maximum power point. One very well known is called the "Hill Climbing" method; considering a constant battery voltage, which is valid at short term, increasing/decreasing the voltage gain makes the working point, on the power curve of figure 2.9, move respectively to the left/right. The current and voltage are measured to compute the actual power. If it is higher than the previous power, the direction of movement is kept as one is getting more energy, if not, direction is changed. A consequence is that the working point is never at the MPP, but oscillating around it, giving thus an average power slightly below the maximum power. This tracking function operates only during the first phase of the battery charge, when the voltage is below the maximal value that would destruct the lithium-ion cells ($4.23\,V$/cell). In the second phase, i.e. constant voltage, decreasing current, the power has to be reduced below MPP. That means that the tracking is still executed, but with an additional condition that if the voltage approaches the maximum, the direction is automatically changed, reducing the power.

As part of the energy chain, the MPPT has to be as efficient as possible. Thus, not only the hardware design has to be optimized to minimize the losses in diodes, transistors and inductors, but also the algorithm has to be tuned to have a fast adaptation to irradiance variations and a good tracking precision. A well designed MPPT should have an efficiency above $95\,\%$, but the best products reach $99\,\%$.

2.6   Electric Motor

An electric motor uses electrical energy to produce mechanical energy. This definition is very general and in fact there exist a very large variety of electric motors that coexist because of the different supply sources, sizes, torques and speeds depending on the application.

In the present case, DC (Direct Current or Continuous Current) motors will be used as they are designed to run on DC electric power supplied by a battery. By far the most common types are the brushed and brushless types, which use mechanical and electronic commutation respectively to create a rotating magnetic field vector that pulls an electromagnet or a permanent magnet.

In a classic DC motor, the inner part is the rotor, which consists of a wound coil generating a rotating magnetic field, and the outer part is either an electromagnet or permanent magnet stator, which creates a fixed magnetic

field. The electrical connection between the rotor and the external power supply are ensured by brushes. Hence, the rotation will continuously change the coil polarity, thus generating an oscillating current. This current is at the origin of the rotating magnetic field and the turning moment. The limitations of DC motors are due to the need for brushes to press against the commutator what creates friction, sparks and electrical noise, especially as currents and speeds get higher. Also, the windings induce a high inertia to rotate and as they are placed in the center of the motor, they have trouble getting rid of the heat due to the Joule effect. In order to have high efficiency, a precision assembly and good components are required. Anyway, their speed control is easily achieved by varying the constant voltage or the duty cycle of a Pulse Width Modulated signal (PWM).

In a brushless DC motor, often abbreviated BLDC, the coils do not move. Instead, the permanent magnets rotate and the armature remains static. This gets around the problem of how to transfer current to a moving armature. In order to do this, the brush-system/commutator assembly is replaced by an electronic controller that performs the same power distribution found in a brushed DC motor. The drive electronics is more complex that for brushed motors because it has to activate the coils one phase after the other, what has to be synchronized to the rotor's position. In order to sense the position, either Hall Effect sensors or Back Electro Magnetic Force (BEMF) are used. When configured with the magnets on the outside, they are referred to as outrunner motors, else they are called inrunner. The advantages of BLDC motors are numerous : very precise speed control, high efficiency, reliability, reduced noise, longer lifetime (no brush abrasion), no ionizing sparks. Additionally, they run much cooler than brushed motors which allows the use of higher currents. For this reason, their power to weight ratio is exceptionally high, as it will be showed in figure 3.11.

2.6.1 Motor Dynamics

The behavior of a DC motor will be shortly described here, as it will be used later on to optimize the propulsion group selection (Section 5.4.2). It follows two well known equations [9] :

$$\begin{cases} U = r_a\ i + k_u\ \omega_{mot} \\ M_{em} = k_m\ i \end{cases} \tag{2.6}$$

where U and i are the terminal voltage and the current, r_a is the terminal resistance, k_m the torque constant, ω_{mot} the rotational speed and M_{em} the electromagnetic moment. The voltage constant k_u expressed in [Vs/rad] is

the inverse of the speed constant k_n expressed in [rad/Vs]. We can isolate the rotational speed :

$$\omega_{mot} = \frac{U - r_a\,i}{k_u} \tag{2.7}$$

The electromagnetic moment is proportional to the current. Once the friction moment of the motor is subtracted, it gives the effective moment given to the load.

$$M_{mot} = M_{em} - M_R = k_m\,i - k_m\,i_0 = k_m(i - i_0) \tag{2.8}$$

With a fixed voltage, we can see that the speed and the torque are linearly dependant. For different voltages, the lines of figure 2.16 a are always parallel. This means that only the load will fix the working point. In fact, this working point is the intersection of the speed/torque characteristic of the motor and the speed/torque characteristic of the load. Combining equations (2.6) and (2.8), we obtain :

$$U = r_a\left(i_0 + \frac{M_{mot}}{k_m}\right) + k_u\omega_{mot} \tag{2.9}$$

For DC motors, $k_u = k_m$ when expressed with the same SI units. We can now isolate the speed and the torque to highlight their linear dependance.

$$\omega_{mot} = -\frac{r_a}{k_m^2}M_{mot} + \left(\frac{U - r_a i_0}{k_m}\right) \tag{2.10}$$

$$M_{mot} = -\frac{k_m^2}{r_a}\omega_{mot} + k_m\left(\frac{U}{r_a} - i_0\right) \tag{2.11}$$

2.7   Propeller

The propeller is a device consisting of a set of two or more twisted, airfoil-shaped blades mounted around a shaft and spun to provide propulsion of a vehicle through a fluid. It accelerates incoming air particles creating a reaction force called thrust. If we consider a stream tube around it, as the mass of air passing through the stream tube must be constant, the increased velocity leads to a contraction of the stream tube passing through the propeller disk, neglecting compressibility.

In order to better understand how it works, we will present the Blade Element Theory (BET) that gives basic insight into the rotor performance
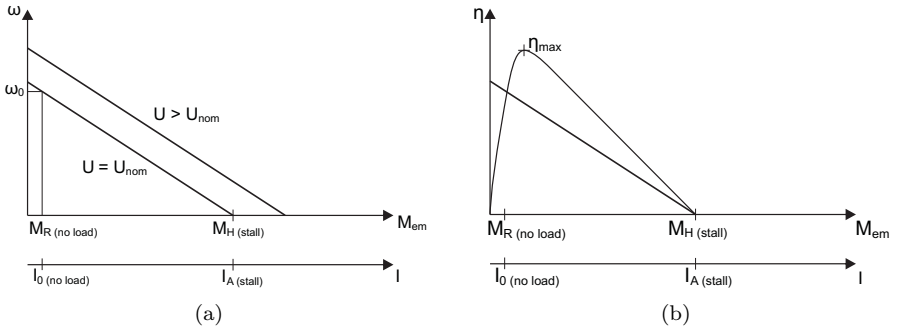
Figure 2.16: (a) Speed vs torque linear characteristic (b) Efficiency vs torque [9]

as well as other characteristics. In this theory the blade is assumed to be composed of numerous, infinitesimal strips with width 'dr' that are connected from tip to tip. The lift and drag are estimated at the strip using the 2-D airfoil characteristics of the section. Also, the local flow characteristics are accounted for in terms of climb speed, inflow velocity, and angular velocity. The section lift and drag may be calculated and integrated over the blade span. The propeller efficiency η_{plr} is defined as the ratio between the propeller thrust T times the propeller axial speed v and the resistance moment M_{plr} times the rotational speed ω.

$$\eta_{plr} = \frac{T\,v}{M_{plr}\,\omega} \tag{2.12}$$

So designing an efficient propeller comes to the same challenges as for an airplane wing : find the best airfoil, chord and incidence angle that minimize the resistance torque and maximize the thrust for a given axial speed. This optimum varies along the blade, from the hub to the tip, due to the increasing radius and thus airspeed, explaining the twisting shape of propellers. A good propeller designed for a specific flight domain should have an efficiency of at least 80 %, 85 % being an excellent value that is difficult to surpass. Unfortunately, it is not constant and varies with air speed and rotational speed, or more precisely with the dimensionless propeller advance ratio $J = v/nd$ where n is the number of blades and d their diameter (Figure 2.18) . As the propeller rotates through one circle the airplane advances a distance v/n. J is then the ratio of this value and the diameter.

For airplanes flying in changing conditions, in terms of speed and altitude for example, a variable pitch propeller can be used at the expense of weight.
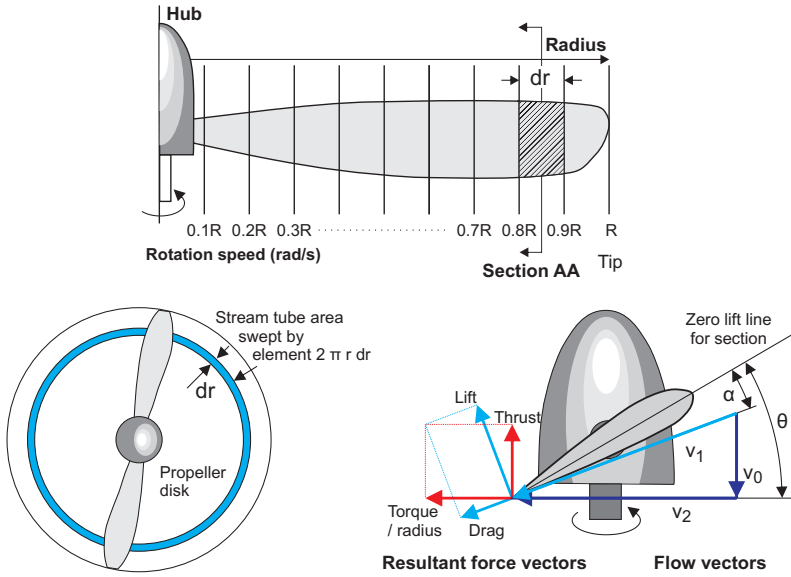
Figure 2.17: Concept of the blade element theory (Source : http://classes.cecs.ucf.edu/eas5157/lin/Ch3-1.ppt)
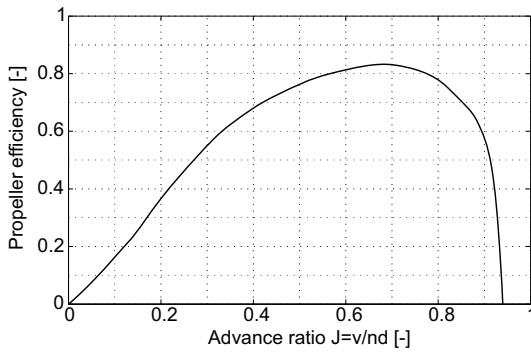
Figure 2.18: Propeller efficiency versus advance (Source : http://www.mh-aerotools.de/airfoils/propuls3.htm)

Chapter 3

Conceptual Design Methodology

3.1   Introduction

This chapter is the theoretical heart of this thesis as it describes in detail the conceptual design methodology. Whether it is intended to achieve surveillance at low altitude or serve as a high altitude communication platform, a solar aircraft capable of continuous flight needs to fly at constant altitude. In fact, the first one would be useless for ground surveillance at high altitude and the second one wouldn't cover a sufficient area at low altitude. For this reason, we concentrate the following study on straight level flight only, storing the surplus of solar energy in the battery. Other scenarios, such as storing energy through potential energy in altitude or using ascending thermals, will also be treated but later on in chapter 6.

Our methodology is based on two simple balances, which are represented in figure 3.1.

- weight balance : the lift force has to be equal to the weight of all the elements constituting the airplane
- energy balance : the energy that is collected during a day from the solar panels has to be equal to or higher than the electrical energy needed by the airplane.

From here on, and considering the type of mission and the payload to embed, there are two different methods to achieve the airplane conceptual design :
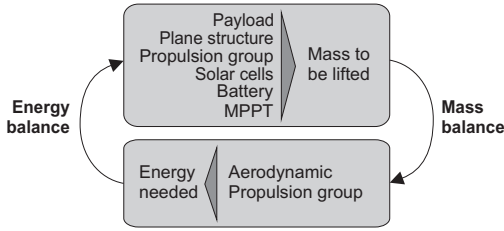
Figure 3.1: Energy and mass balances

1. The ***discrete and iterative approach*** consists in selecting a first
   set of components (motor, solar panels, battery, etc.) based on pure
   estimation of the final required power or on previous designs. Then,
   having their total mass, the wing surface and propulsion group can
   be sized. Having chosen a precise motor, gearbox and propeller, we
   can calculate the power needed for level flight. This value is then
   compared with the power available from the previously selected solar
   generator, and so on. An iterative process takes place, refining selec-
   tions, improving the design at each step and ending hopefully with a
   converging solution.
2. The other approach developed in this thesis is an ***analytical and
   continuous approach*** that consists in establishing all the relations
   between the components with analytical equations using models de-
   scribing the characteristics of each of them. This method has the ben-
   efit of directly providing a unique and optimized design, but requires
   very good mathematical models. In the present case, an important
   effort will be made to have these models as accurate as possible on
   a very wide range, so that the methodology can be applied for solar
   MAVs as well as for manned solar airplanes.

   In the following sections, we will first establish the expression of the power
needed for an aircraft at level flight and then present the irradiance model
that will lead to the daily solar energy available. After that, we will develop
the weight prediction models for all the airplane elements, which will close
the loop before presenting the analytical resolution and the solution of the
problem.

   In order to lighten the equations, substitution variables a_i will be used
instead of long formulas. The reader can easily go through the design process
keeping an eye on figure 3.17 that summarizes in a very simple graphical way
all the calculations and models hereafter.

3.2 Daily Electrical Energy Required

3.2.1 Power for Level Flight

At steady level flight, the lift force generated by the wing exactly compensates for the weight and the propeller thrust compensates for the drag force. Using equations (2.1) and (2.2) we can write :

$$mg = C_L \frac{\rho}{2} S v^2 \tag{3.1}$$

$$T = C_D \frac{\rho}{2} S v^2 \tag{3.2}$$

We can isolate the speed v from equation (3.1) :

$$v = \sqrt{\frac{2\,m\,g}{C_L\,\rho\,S}} \tag{3.3}$$

and then substitute it in equation (3.2) in order to calculate the power for level flight :

$$P_{lev} = T\,v = \frac{C_D}{C_L^{3/2}} \sqrt{\frac{(mg)^3}{S}} \sqrt{\frac{2}{\rho}} \tag{3.4}$$

Using the definition of aspect ratio $AR = b^2/S$, where b is the wingspan and S the wing area, we rewrite the previous equation :

$$P_{lev} = \underbrace{\frac{C_D}{C_L^{3/2}} \sqrt{\frac{2ARg^3}{\rho}}}_{a_0} \frac{m^{3/2}}{b} \tag{3.5}$$

3.2.2 Calculation of the Daily Required Energy

To obtain the total electrical power consumption $P_{elec\,tot}$, efficiencies of the motor, its electronic controller, the gearbox and the propeller have to be taken into account, as well as the power consumption of the avionic system P_{av} and the payload instruments P_{pld}. If the voltage of these two last elements has to be reduced, the efficiency of the step-down, also named in this case the BEC, has to be considered. This leads finally to a total electrical power consumption of :

$$P_{elec\ tot} = \underbrace{\frac{1}{\eta_{ctrl}\ \eta_{mot}\ \eta_{grb}\ \eta_{plr}}}_{a_1} P_{lev} + \underbrace{\frac{1}{\eta_{bec}}\left(P_{av} + P_{pld}\right)}_{a_2} \qquad (3.6)$$

The calculation of this daily energy consumption uses the total power consumption (Equation 3.6) and takes into account the charge and discharge efficiency of the battery for the night period.

$$E_{elec\ tot} = P_{elec\ tot}\ \left(T_{day} + \frac{T_{night}}{\eta_{chrg}\eta_{dchrg}}\right) \qquad (3.7)$$

At dusk and dawn, when the solar power is below the total required power, it is clear that both sources, i.e. the solar generator and the battery, are used and that the switch from one source to the other is progressive. In order to simplify the calculation, we will consider it as instantaneous, introducing the day period T_{day} during which we charge the battery and the night period T_{night} during which we use it. This assumption is valid because firstly the transition period is relatively small. Secondly, the impact of considering that the power comes from the battery and not from the solar panels is a division by the efficiency of the charge cycle that is very close to $100\,\%$.

3.3 Daily Solar Energy Obtained

3.3.1 Irradiance Model

The irradiance depends on a lot of variables such as geographic location, time, plane orientation, weather conditions and albedo that represents the reflection on the ground surface. A good model was developed based on [54]. For the present need, this model was simplified for flat surfaces and replaced with the positive part of a sinusoid, as shown in figure 3.2.

In the literature, Baldock uses a 4th order polynomial formula as simplification [28]. This latter solution has the drawback that it is not logical or intuitive at all. Adapting the profile of irradiance to a different date or geographic location, a completely new polynomial has to be interpolated. Here we will use a simple trigonometric model with only two parameters, the maximum irradiance I_{max} and the duration of the day T_{day}, that can be easily interpreted. The daily solar energy per square meter is the surface below the curve and can be easily calculated in equation (3.8). In order to take into account cloudy days, a constant η_{wthr} is added with a value between 1 (clear sky) and 0 (dark). This constitutes a margin for the calculation.
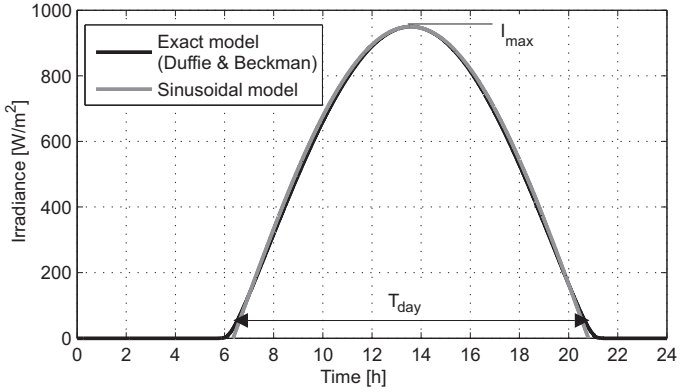
Figure 3.2: Approximation of irradiance as a sinusoid

$$E_{day\ density} = \frac{I_{max}T_{day}}{\pi/2}\eta_{wthr} \tag{3.8}$$

The two parameters I_{max} and T_{day} are depending on the location and the date. Figure 3.3 shows the evolution of these parameters throughout the year for Lausanne, Switzerland.
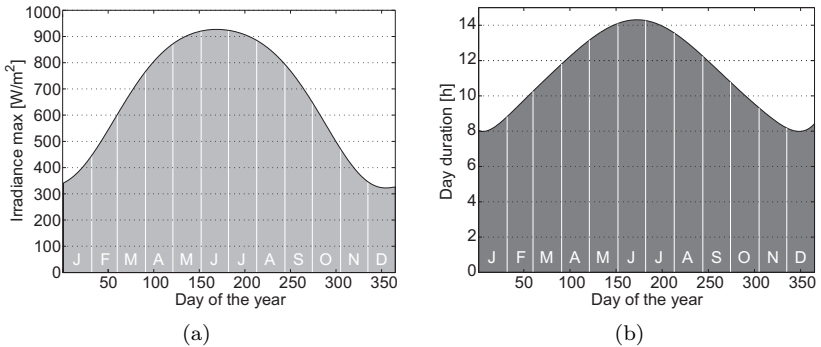
Figure 3.3: Maximum irradiance and day duration throughout a year in Lausanne, Switzerland

We can observe that in winter, the duration of the day but also the maximum irradiance decrease due to the very low sun elevation. For these reasons it is easier to achieve 24 hours continuous flight in summer than in

winter in central Europe, the day lasting longer than the night. Concerning the influence of the location on Earth, of course near the equator, the sun elevation becomes more favorable, but the night and day duration are then equivalent. Going in the opposite direction at higher latitude in the North, we can take benefit of the sun the entire 24 hours, but the elevation being very low, the maximum power is also reduced. Anyway the total amount of energy along the day is higher than on the equator.

3.3.2   Calculation of the Daily Solar Energy

The total electric energy is obtained by multiplying the result of equation (3.8) with the surface of solar cells, their efficiency and the efficiency of the MPPT. Additionally, we have to take into account the fact that the cells are not disposed on a horizontal surface but follow the cambered airfoil. In a series of interconnected cells, the one with the lowest irradiance limits the current for all the others. This problem occurs mainly at sunrise or sunset, when the sun elevation is low, and depends also on the airplane orientation. This situation is represented in figure 3.4 where the first cell, near the border of attack, has the smallest elevation angle θ_1 and will then penalize the other cells.
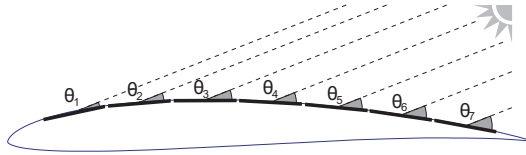
Figure 3.4: Variation of incidence angle on the solar cells for a cambered wing at sunrise or sunset

For this reason it is important to take care about the wiring configuration and preferably dispose the cells connected in series along the wing, so that they have the same orientation. Simulations have been realized in order to study this impact and the results show that compared to a flat disposition, the camber decreases the energy by almost 10 % during a whole day in central Europe. In order to take this effect into account in our methodology, we will consider a new efficiency η_{cbr} that is above 90 %. Thus, the daily electrical energy is :

$$E_{elec\,tot} = \frac{I_{\max}\,T_{day}}{\pi/2}\,A_{sc}\,\eta_{wthr}\,\eta_{sc}\,\eta_{cbr}\,\eta_{mppt} \qquad (3.9)$$

3.4 Mass Prediction Models

For each part on the airplane, a good mass model is necessary in order to calculate the total mass m and use it in equation (3.5). In this section, we will go through all the parts constituting the airplane and establish their mass models.

3.4.1 Fixed Masses

First of all, there are some fixed masses that will not depend on the sizing of other parts. In this category, we include the payload that is a mission requirement defined at the beginning. To some extent, we can also include the autopilot system if defined at the beginning also.

$$m_{fixed} = \underbrace{m_{av} + m_{pld}}_{a_3} \qquad (3.10)$$

3.4.2 Airplane Structure

The mass of the airplane structure is certainly the most difficult part to model and the two main approaches widely used in the literature for solar airplanes appeared inadequate at a scale of a couple of meters. That is the reason why we will study this part more in details and propose a new model valid for sizes on three orders of magnitude.

The first approach from D.W. Hall [69] consists in calculating separately the mass of all the elements constituting the airframe, i.e. the spar, the leading and trailing edges, covering, ribs, control surfaces, fuselage and tail as functions of the total mass, aspect ratio and wing area. The method is very detailed and precise. However, their authors clearly limit its validity for airplanes with a weight between 1000 to 3000 lbs, which corresponds to a mass of 453 to 1360 kg. It was applied by Colozza [50] on a solar airplane with more than 60 m wingspan but is inapplicable in the range of UAVs or MAVs. The second approach, proposed by W. Stender in 1969 [120], is based on statistical data for sailplanes with twin boom tails. The entire airframe weight W_{af} is estimated in a parametrical way as a function of wingspan b, surface S and number of boom tails n, A and B being constants.

$$W_{af} = A \left(n\,S\,b^3 \right)^B \qquad (3.11)$$

Data and calculated estimates of airframe weight, ultimate loads, and airplane geometry of MacCready's Solar Challenger and another high-altitude

solar powered airplane design concept were used in a regression analysis to define $A = 0.310$ and $B = 0.311$ (Imperial Units lbs/ft) for a class of ultralight, cantilever wing airplanes with twin boom tails [131]. Once converted in the Standard International Unit System (Metric Units), and using the aspect ratio definition $AR = b^2/S$, we can rewrite :

$$W_{af} = 8.763\,n^{0.311}\,S^{0.778}\,AR^{0.467} \tag{3.12}$$

This model was widely adopted by Bailey [27], Colozza [49], Irving [70], Romeo [113], Youngblood [131] and also Rizzo [110] who additionally proposed his own model obtained by interpolating NASA prototypes data and that is said to be preferred for UAVs.

$$W_{af} = 15.19\,S^{0.656}\,AR^{0.651} \tag{3.13}$$

Another model used is to consider the airframe weight proportional to its surface. Guglieri makes this same assumption using $2.5\,\text{kg/m}^2$ [66, p.50] for a manned version, as well as Brandt who considers a ratio of $0.97\,\text{kg/m}^2$ [36, p.706] for his $61\,\text{m}$ HALE. For their $38\,\text{cm}$ solar powered MAV "SunBeam", Roberts et al. [111] used a value of $0.2\,\text{kg/m}^2$. Rehmet [105, p.5] considers the formula $M_{af} = 0.103\,[kg/m^2]\,b^2 + 1.157\,[kg/m^2]\,S$ which can be rewritten as $M_{af} = (0.103/AR + 1.157)\,S$ leading here again to a linear model between airframe mass and wing surface.

Validation of the Model

In order to verify these models, a database containing the parameters of 415 sailplanes of various dimensions was created. They are divided into 92 radio-controlled unmanned models and 323 manned sailplanes. For each of them, the following values are available : wingspan, wing area, aspect ratio, structure weight and gross weight. Figure 3.5 presents the structure weight of these 415 sailplanes with respect to the wing area, the color representing the aspect ratio. On both axes, a logarithmic scale is used to have good global view of the tendency, from the radio-controlled models in the lower-left corner to the manned sailplanes in the upper-right part.

The objective now is to see if the equations mentioned above, which are extensively used in solar airplane designs, follow this tendency. For this purpose, the Stender and the Rizzo models are plotted on the same graph, using two different aspect ratios of 15 and 30. The result is that Rizzo's equation approaches the best sailplane models, which is normal as it was derivated from unmanned solar airplanes data, but it is not convenient for small scale models where it is too pessimistic. In fact, for an airplane with
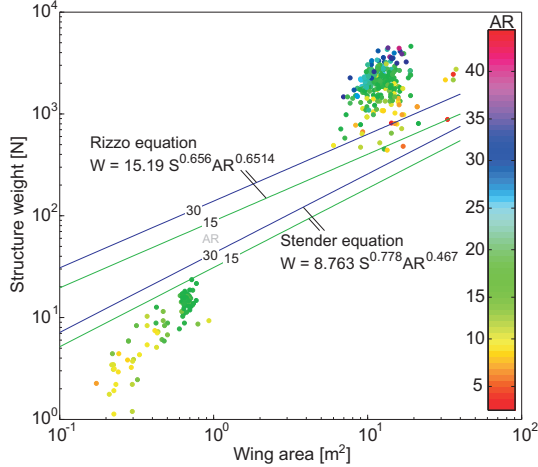
Figure 3.5: Evaluation of Stender and Rizzo airframe weight equations with real manned and radio piloted sailplanes data

$0.3\,\mathrm{m}^2$ wing area, it would predict a weight 10 times bigger than in reality. Concerning Stender's equation, we can see that it is far too optimistic for manned airplanes and also too pessimistic for small scale models.

New Model

We propose here a new empirical model based on the created sailplanes database, and following equation :

$$W_{af} = g\, M_{af} = g\, k_{af}\, S^{x_1} AR^{x_2} \tag{3.14}$$

where g is the gravity constant and k_{af}, x_1 and x_2 are going to be found using a least square fitting method that minimizes the sum of square errors :

$$\sum_{i=1}^{n} \frac{1}{\widehat{W}_i^{\,2}} \left(W_i - \widehat{W} \right)^2 \tag{3.15}$$

For the 415 samples, the following equation minimizes the above criteria:

$$W_{af} = 5.58\, S^{1.59}\, AR^{0.71} \tag{3.16}$$

However, this equation, represented in figure 3.6 with aspect ratio of $10, 20, 30$ and 40, only gives the mean tendency of all the 415 records, in
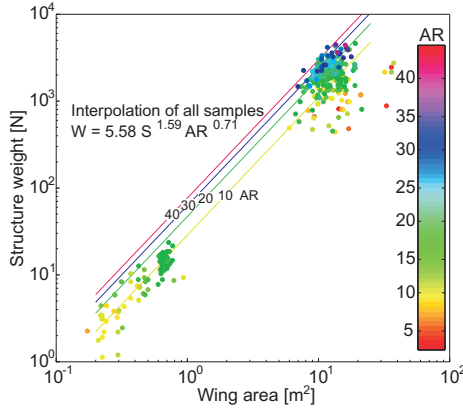
Figure 3.6: Newly proposed structural weight model

which the construction quality of airplane varies. It would be interesting to
have a model of the highest quality sailplanes only. In order to achieve this,
the records can be separated in two groups : the one that are lighter and
the one that are heavier than the mean weight model. The condition to be
member of the first group is :

$$W_{af,i} < 5.58 \ S_i^{1.59} \ AR_i^{0.71} \tag{3.17}$$

The new set of data contains now 260 airframes that are lighter than the
mean model, so we could state that their construction quality, in terms of
weight, is better than the other half. Anyway with this new set of data,
a second iteration can be executed with the least square fitting method in
order to find new constants k_{af}, x_1 and x_2 matching this best data set.
Using this second model, we can divide again the airframes in two groups,
etc. This process was repeated five times successively and for each iteration,
the number of data and the equation of the model is reported in table 3.1.
The equations are written in three different manners, that are all equivalents,
passing easily from one to the other using $S = b^2/AR$. On the last line, we
have the best model in terms of weight that was interpolated using the 19
best sailplanes, what represents $5\,\%$ of the 415 initial airframes. We will
hereafter call this model the top $5\,\%$ airframe weight prediction model.

It is interesting to see the evolution of the constants k_{af}, x_1 and x_2 when
the quality of the construction increases. The wing area is always related to
the weight with a power of around 1.55 to 1.59, this exponent doesn't change
significantly. Concerning the wingspan, it has a clear cubic relation to the

Table 3.1: Airframe weight prediction models for lightweight sailplanes. At each row, the construction quality is improved by interpolating only the best sailplanes from the previous data set. The three columns correspond to three different ways to write the model, the third one being the wing loading

Samples	$W_{af} = f(S, AR)$	$W_{af} = f(b, AR)$	$W_{af}/S = f(W_{af}, AR)$
415	$5.58\ S^{1.59}\ AR^{0.71}$	$5.58\ b^{3.18}\ AR^{-0.88}$	$2.94\ W_{af}^{0.37}\ AR^{0.45}$
260	$2.31\ S^{1.58}\ AR^{0.94}$	$2.31\ b^{3.16}\ AR^{-0.64}$	$1.70\ W_{af}^{0.37}\ AR^{0.59}$
143	$1.15\ S^{1.57}\ AR^{1.13}$	$1.15\ b^{3.14}\ AR^{-0.44}$	$1.09\ W_{af}^{0.36}\ AR^{0.72}$
73	$0.78\ S^{1.55}\ AR^{1.21}$	$0.78\ b^{3.10}\ AR^{-0.34}$	$0.85\ W_{af}^{0.35}\ AR^{0.78}$
40	$0.56\ S^{1.55}\ AR^{1.27}$	$0.56\ b^{3.10}\ AR^{-0.28}$	$0.69\ W_{af}^{0.35}\ AR^{0.82}$
19	$0.44\ S^{1.55}\ AR^{1.30}$	$0.44\ b^{3.10}\ AR^{-0.25}$	$0.59\ W_{af}^{0.35}\ AR^{0.84}$

weight. At the opposite, we can see that the influence of the aspect ratio is increasing rapidly with the quality. In fact, the exponent x_2 which is 0.71 when we consider all the records increased constantly and reaches 1.3 when only the top 5 % are taken into account.

The Great Flight Diagram

A couple of scientists studied the correlations between weight, wingspan, wing area and speed more generally, not only from the hang glider to the big airliners, but even in the animal kingdom, from the flies to the albatross. An excellent and concise review of all these correlations can be found in [117].

One of the best contributors in this field is Henk Tennekes who presented, in his book "The Simple Science of Flight" [123] very interesting correlations including insects, birds and airplanes. He summarized the relations in a log-log diagram named "The Great Flight Diagram" where, following his own words, everything that can fly is represented. The result is impressive : 12 orders of magnitude in weight, 2 orders of magnitude in cruising speed and 4 orders of magnitude in wing loading, defined as the ratio between the weight and the wing area. From the common fruit fly, Drosophilia Melanogaster, to the Boeing 747, the wing loading of all these flying objects follows quite well:

$$W/S = 47\ W^{1/3} \tag{3.18}$$

The concept of geometric similarity is the base of this equation. In fact, as explained in [117], if we assume geometric similarity among birds, the weight W, lift L and mass m, for unaccelerated level flight, can be expressed with respect to a characteristic length b as :

$$W = L = mg \approx b^3 \tag{3.19}$$

The wing area S can be expressed as :

$$S \approx b^2 \tag{3.20}$$

and the wing loading :

$$W/S \approx b \tag{3.21}$$

which can further be developed to :

$$W/S = k_1 \, W^{\frac{1}{3}} \tag{3.22}$$

where k_1 is a constant that was determined empirically to be 47.

It is interesting to notice that the model proposed for lightweight airplane airframes links the weight to the wing loading with an exponent of 0.35, which is almost identical to the 1/3 proposed by Tennekes. Figure 3.7 shows the position of the 415 sailplanes of the database on the great flight diagram. The RC sailplanes were separated in two categories according to their construction techniques, either balsa ribs or molded. The mean and the top 5 % model developed above are also plotted. They are parallel to Tennekes curve and thus show very well the same cubic tendency. In his book "Aerodynamics, Aeronautics and Flight Mechanics" [80], McCormick proposed his own model, also based on a cubic scaling law, for the estimation of the wing loading of manned airplanes. He identified an upper and a lower boundary defined as :

$$\begin{cases} W/S = 85.5 \, W^{1/3} - 9.9 & \textit{Upper boundary} \\ W/S = 44.8 \, W^{1/3} - 9.9 & \textit{Lower boundary} \end{cases} \tag{3.23}$$

When represented in the Great Flight Diagram, his model proves to be excellent. One remarkable point is its asymptote at a weight of 1000 N which corresponds to the weight of a single human person in an incredibly lightweight airplane. The airplane that approaches this asymptote the most is the Gossamer Albatross, a human powered aircraft built by Dr. Paul B. MacCready, that crossed the English Channel on June 12, 1979. Its empty weight was only 32 kg and the gross weight during the record around 100 kg.

We can also plot all the major solar airplanes flown to date on the Great Flight Diagram. 86 of them, from a 1 g MAV to the impressive Helios, the last solar prototype of NASA weighing more than 900 kg, are represented in figure 3.8.

We can see that the small scale solar airplanes are located on the graph in the same region as the non-solar radio-controlled sailplanes of figure 3.7.
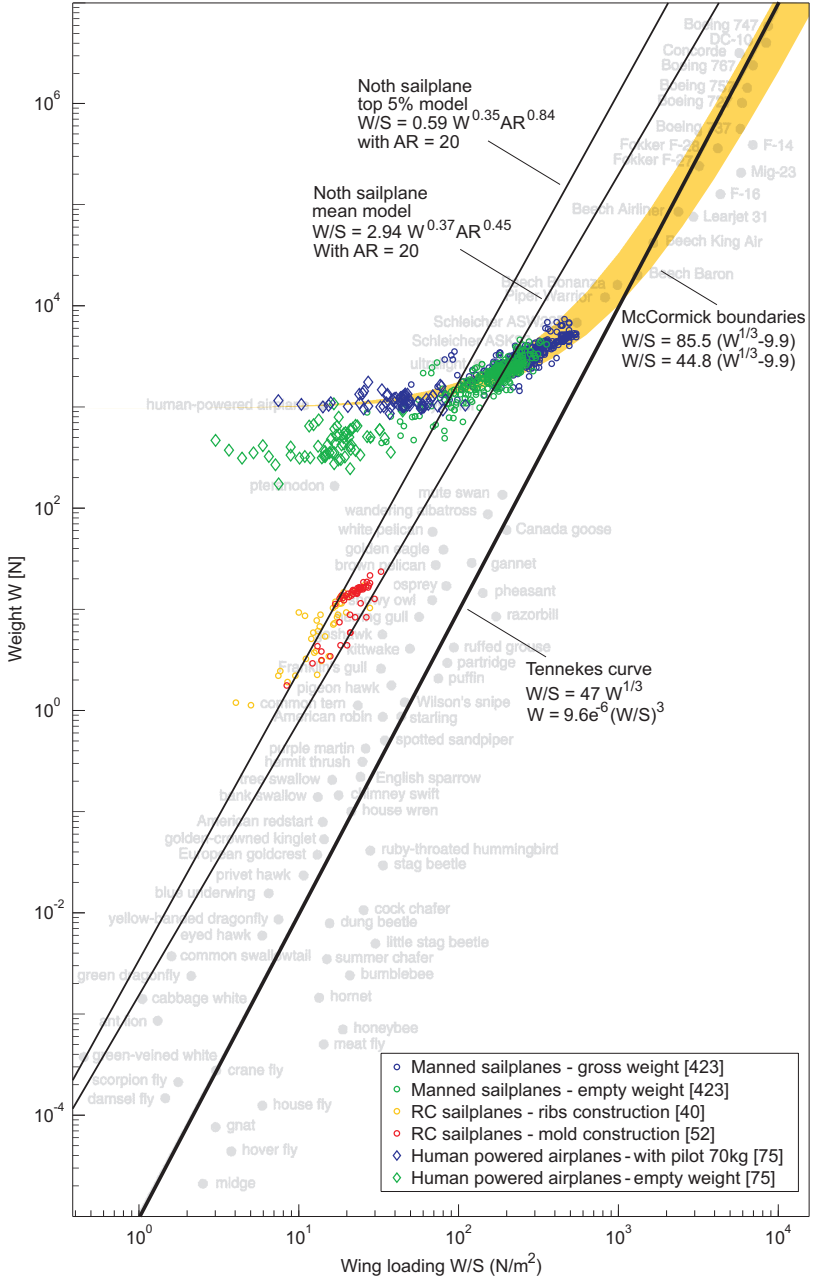
Figure 3.7: The Great Flight Diagram from Henk Tennekes [123], augmented with 515 RC and manned sailplanes and 75 human powered airplanes
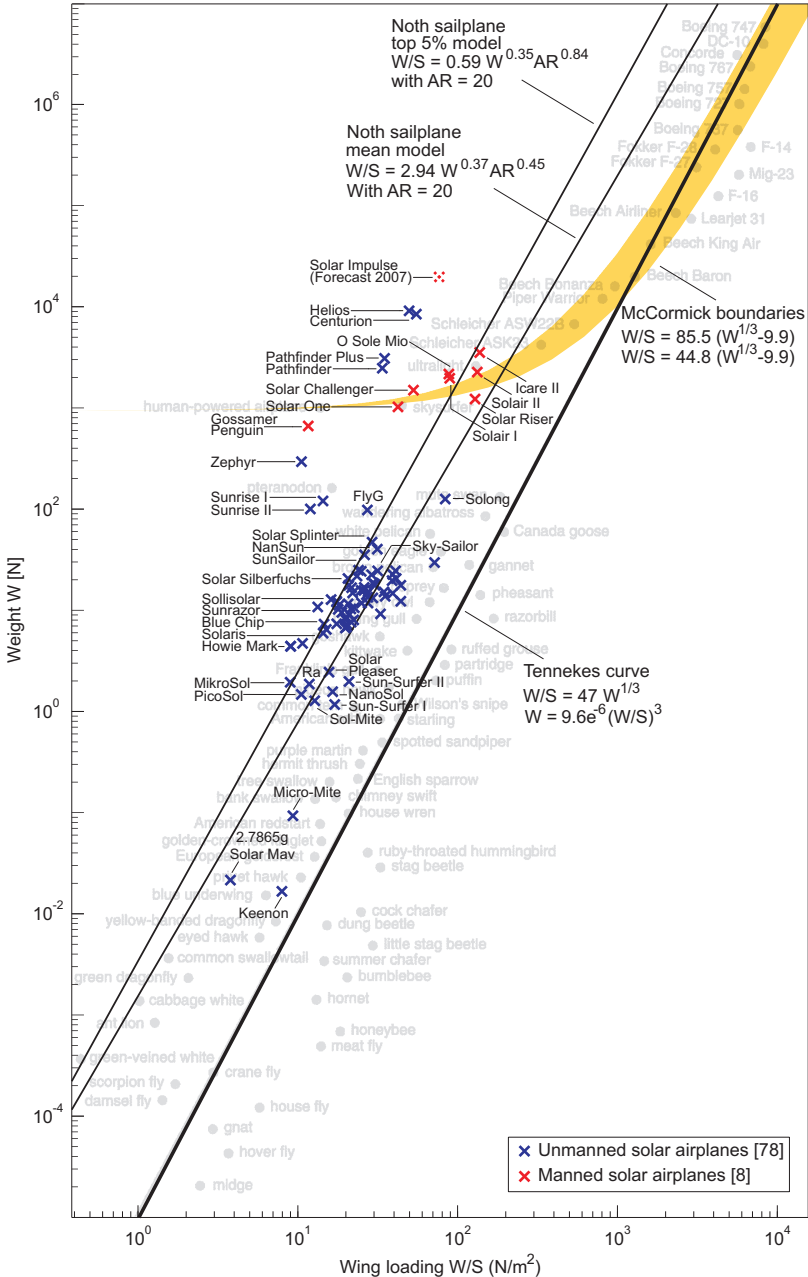
Figure 3.8: The Great Solar Flight Diagram, augmented version of Tennekes Great Flight Diagram with 86 solar airplanes flown from 1974 to 2008

At the opposite, many large solar airplanes are far away from the model we developed in this document. The line parallel to Tennekes' curve, which means that we assume a similar exponent, that contains the Helios, with its 30.85 aspect ratio, has the equation :

$$
\begin{aligned}
W_{af} &= 0.022\ b^{3.1}\ AR^{-0.25} \\
W_{af} &= 0.022\ S^{1.55}\ AR^{1.3} \\
W_{af}/S &= 0.09\ W_{af}^{0.35}\ AR^{0.84}
\end{aligned}
\tag{3.24}
$$

This means that its weight is around 20 times lower than it would have been estimated with the top 5 % model. However, we have to be careful about the fact that Helios, Centurion, Pathfinder Plus, Pathfinder and Zephyr have a major difference in their configuration compared to all other models. In fact, in the case of NASA prototypes and Zephyr, the wing extremities are supported by several wheels, when not in flight. For all other airplanes, the weight of the entire wing, from the center to the extremities, is supported at the center. This means that in the first category, the flexion constraints on the wing are not very high and quite homogeneous, which allows a lighter construction method. These big models have impressive low weight but the direct consequence is their incredible fragility. The cause of Helios' crash in 2003 was precisely a structural failure. For the second category, as all the weight of the wing is concentrated at the center, constraints at this location are high and that explains the need of stronger spar which as a consequence increases the weight.

We can try to plot, into the great flight diagram, Rizzo's and Stender model, which has been widely used in solar airplane design papers since thirty years without having being questioned. Their equations putting the weight, the surface and the aspect ratio in relation can be written as before following two different notations that are anyway equivalent (Table 3.2). The result is quite interesting : the weight varies with around $b^{1.5}$ instead of b^3 as in our case. In the case of Rizzo's equation, the exponent of aspect ratio approaches zero, which would mean that for a defined wingspan, the chord has no influence on the weight. Using the third notation that relates the empty airframe wing loading to its weight (no payload so far), there is clear contradiction because these two models, due to the negative weight exponent, consider that the wing loading decreases when the weight increases. This appears to be contradictory with everything that was flying so far on Earth, human inventions as well as insects and birds. This is represented graphically in figure 3.9 where the curves tendencies are very different from what was presented before, even if they could be valid in the domain where the NASA prototypes are located.
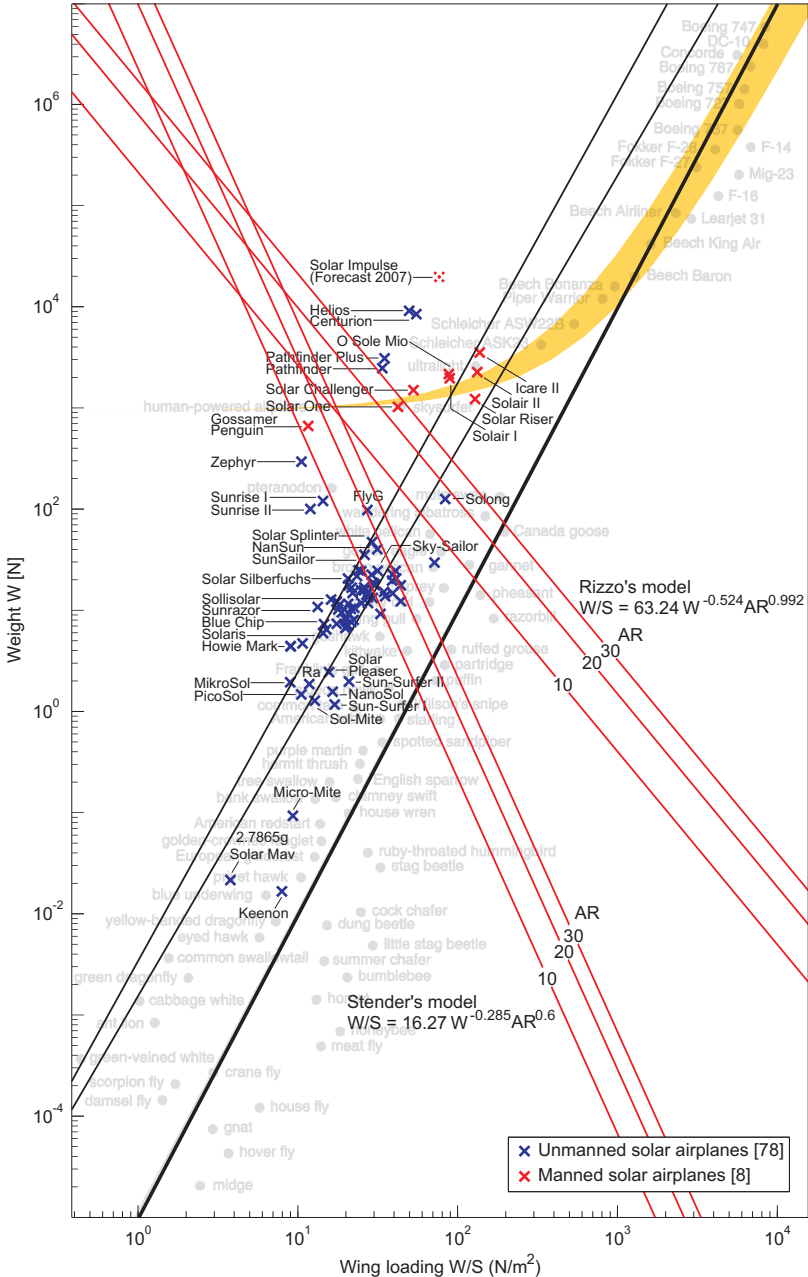
Figure 3.9: The Great Solar Flight Diagram with the weight prediction models of Stender and Rizzo

Table 3.2: Comparison of the airframe weight prediction models

Model	$W_{af} = f(S, AR)$	$W_{af} = f(b, AR)$	$W_{af}/S = f(W_{af}, AR)$
Noth	$0.44\ S^{1.55}\ AR^{1.30}$	$0.44\ b^{3.10}\ AR^{-0.25}$	$0.59\ W_{af}^{0.35}\ AR^{0.84}$
Stender	$8.763\ S^{0.778}AR^{0.467}$	$8.763\ b^{1.556}AR^{-0.311}$	$16.27\ W_{af}^{-0.285}AR^{0.600}$
Rizzo	$15.19\ S^{0.656}AR^{0.651}$	$15.19\ b^{1.312}AR^{-0.005}$	$63.24\ W_{af}^{-0.524}AR^{0.992}$

The airframe weight prediction model that will be used hereafter will thus be based on our top 5 % model. Considering the same construction technique, we should always consider a cubic relation between the wingspan and the airframe mass, as it was demonstrated here above. We will then model the mass of the airframe using :

$$m_{af} = \underbrace{k_{af}\ AR^{x_2}}_{a_4}\ b^{x_1} \tag{3.25}$$

By varying k_{af} keeping the two exponents constant, we create a curve that is parallel to our 5 % model and to Tennekes curve. Decreasing this value, thus making the construction method lighter, lets this parallel move upward, to where the NASA prototypes are located. Increasing it, the parallel goes down to heavier flying objects and birds. It is interesting to realize that the more it goes down, the more acrobatic and agile the elements that are on the parallel become. As an example, it is below Tennekes curve that we find the combat aircrafts like the F-16 and the house fly.

3.4.3 Solar Cells

Compared to other approaches where a fixed percentage of the wing is assumed to be covered by solar cells, we consider here the exact surface required to balance the total electric energy consumed each day with the total electric energy obtained from the sun. Using equations (3.7) and (3.9), we obtain the required surface covered by solar panels :

$$A_{sc} = \underbrace{\frac{\pi}{2\eta_{sc}\eta_{cbr}\eta_{mppt}I_{max}\eta_{wthr}} \left(1 + \frac{T_{night}}{T_{day}}\frac{1}{\eta_{chrg}\eta_{dchrg}}\right)}_{a_9} P_{elec\ tot} \tag{3.26}$$

In order to obtain a module, the solar cells are interconnected electrically and then encapsulated between two non reflective transparent layers. Thus,

the final calculation of the solar panel mass has to take the cells and this encapsulation into account. This is done in equation (3.27) where k_{sc} and k_{enc} represent the surface density of the solar cells and the encapsulation respectively.

$$m_{sc} = A_{sc} \underbrace{(k_{sc} + k_{enc})}_{a_5} \tag{3.27}$$

3.4.4 Maximum Power Point Tracker

As mentioned previously, the MPPT is required to adapt the voltage of the solar panels so that they provide the highest power possible. With the growth of the photovoltaic market, there are a lot of commercially available MPPTs, but as they are used mainly for fixed applications (garden house, etc.), they are never optimized for low weight. For the development of our mass model, we will focus on trackers that were developed for solar airplanes and solar cars, two domains where the requirements for low weight and high efficiency are important. Figure 3.10 demonstrates clearly, based on six MPPTs, that the mass is proportional to the maximum power with a ratio of $k_{mppt} = 1/2368 \, kg/W$.

	Mass [g]	Power [W]	Eff [%]
Sky-Sailor	7.55	30	97
Sommerauer	45	100	98
AcPropulsion Solong	100	300	98
Biel MPPT	650	1200	99
Brusa Elektronik MPT-N15	1150	2600	99
Icaré 2	2058	5046	98
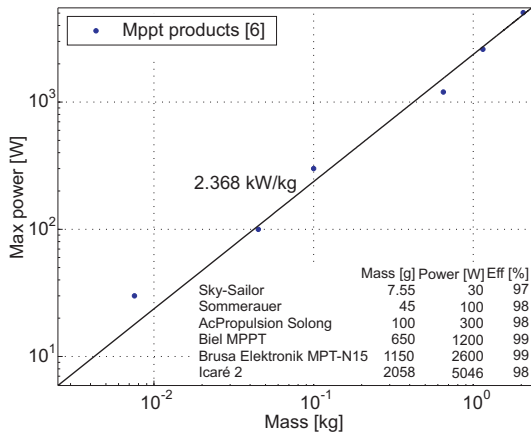
Figure 3.10: Power to mass ratio of high efficiency MPPTs

The maximum power required at the MPPT level is directly given by the maximum power output of the solar modules, which is proportional to their area (Equation 3.26).

$$m_{mppt} = k_{mppt} \, P_{solmax}$$
$$= \underbrace{k_{mppt} \, I_{\max} \, \eta_{sc} \, \eta_{cbr} \, \eta_{mppt}}_{a_6} \, A_{sc} = a_6 \, A_{sc} \qquad (3.28)$$

In order to be complete, it has to be mentioned that η_{mppt} is the product between the efficiency of the DC/DC converter alone and the efficiency of the tracking algorithm. In fact, the working point is never constantly on the maximum power point but oscillating around it.

$$\eta_{mppt} = \eta_{mppt\,dcdc} \, \eta_{mppt\,algo} \qquad (3.29)$$

For an MPPT that is well designed for a specific application, we can consider $\eta_{mppt\,dcdc} > 97\,\%$ and for the algorithm $\eta_{mppt\,algo} > 98\,\%$, leading to a total efficiency that should always be higher than $95\,\%$.

3.4.5 Batteries

Concerning the battery, its mass is directly proportional to the energy it needs to store, which is the product between power consumption and night duration, and inversely proportional to its gravimetric energy density.

$$m_{bat} = \frac{T_{night}}{\underbrace{\eta_{dchrg} \, k_{bat}}_{a_7}} \, P_{elec\,tot} \qquad (3.30)$$

3.4.6 Propulsion Group

Modeling the propulsion group is not an easy task, because it is composed of four subparts (control electronics, motor, gearbox and propeller) that all have their own power densities and efficiencies. In order to be consistent in this paragraph, we will use the unit kW/kg when referring to power density and kg/kW when referring to its inverse, the mass to power ratio. Additionally, we will always consider the maximum continuous power and not the short time peak power.

Looking at the past solar airplane designs, the main tendency is to assume a propulsion group mass that scales linearly with shaft power output. Also, many of them only take the motor into account, stating that it constitutes the major weight compared to the other parts. Table 3.3 presents a summary of the mass to power ratios and efficiency values that were considered in eleven solar airplane designs. Whereas all the sources agreed with a total efficiency

Table 3.3: Mass to power ratios and efficiencies used for propulsion group in various solar airplane designs in the literature

Designer	Plane type	Ctrl	Mot	Grbx	Prop	Total
Rizzo [110]	60 m HALE	-	4.5	-	-	4.5 kg/kW
		-	85 %	-	80 %	68.0 %
Youngblood [131]	84 m HALE	-	5.1	-	-	5.1 kg/kW
		-	-	-	-	-
Hall [68, fig.31]	100 m HALE	-	0.8	1	4.7	6.5 kg/kW
		-	90 %	97 %	92 %	80.3 %
Bailey [27, p.49]	29.3 m HALE	-	2.13	0.19	-	2.32 kg/kW
		90 %	95 %	99 %	90 %	76.2 %
Brandt [36, p.705]	61 m HALE	-	14.6			14.6 kg/kW
		-	80 %			80.0 %
Berry [31, p.3]	24.5 m HALE	-	-	-	-	-
		96 %	97 %	95 %	89 %	78.7 %
Colozza [50]	> 80 m HALE	-	5.5	-	-	5.5 kg/kW
		-	75 %			75.0 %
Boucher [34]	10 m model	-	-	-	-	-
		-	90 %	95 %	90 %	77.0 %
Rehmet [104, p.25]	Manned	-	0.5 - 2		-	-
		-	98 %	95 %	85 %	79.1 %
Schoeberl [115, p.46]	Manned	-	-	-	-	-
		-	89 %	97 %	86 %	74.2 %
Ross [114, p.4]	Manned	-	-	-	-	-
		98.5 %	93 %	-	77 %	70.5 %

between 70 % and 80 %, the power density varies more, i.e. between 2.32 to 14.6 kg/kW.

Coming now to real measured values of solar airplanes that were built and flown, the amount of data is far smaller. The 14 motors of Helios (1.5 kW each) had a mass to power ratio of 3.33 kg/kW, and in the case of Solair 2, this value was, for the motor and propeller together, only 0.76 kg/kW. The detailed data of Icaré 2 [119] show a value of 1.69 kg/kW for the entire propulsion group, from the control electronics to the propeller, with an overall efficiency of 79.7 %.

We can now wonder how these values evolve when downscaling the airplane. For their 38 cm solar powered MAV "SunBeam", Roberts et al. [111, 10] consider and verified an efficiency of 62.5 % for its 3.3 W 17 g motor. Wind tunnel tests showed an efficiency of 58 % for their 5 g propeller. Interestingly, at this scale the mass to power ratio is still in the range observed above with 6.66 kg/kW but the efficiency dropped to 36 %. Thus, the next sections will study the maximum continuous mass to power ratio for the different elements of the propulsion group separately.

Electric Motor

As we saw in section 2.6, there are several types of motors. However, from a market point of view and for the motors that interest us, we can distinguish basically three different motor categories :

- First, the cheap and low quality motors, mostly brushed DC motors that are used in low-cost products or toys. They are not suitable for a solar powered airplane for efficiency, durability and reliability reasons. Hence, they were not taken into account in this study.

- The second category includes high quality motors, both brushed and brushless, that are very reliable, robust, efficient and well documented. Maxon, Minimotor, Portescap and Faulhaber are the best companies present on this market. Encoders and polyvalent control units make them ideal for industrial applications.

- The third category contains motors specifically designed for model-makers building reduced scale airplanes, helicopters or cars. They are now exclusively brushless and the companies present on this market are often semi-amateur, even familial companies that emerged and expanded with the growing need of lightweight and very powerful motors in the model world. Here, the documentation is quite poor from a scientific point of view, and except the sensorless measurement from the controller that powers the motor, no special interface is available that would give a speed or position feedback. Despite all, companies like Hacker, Strecker, Plettenberg, etc. accumulated an impressive practical know-how that makes their motors far better that anyone else concerning power to mass ratio.

A large database of motor characteristics was created based on the data supplied by the various manufacturers. In figure 3.11, the maximum continuous power of more than two thousand motors is represented with respect to their mass in a logarithmic scale, allowing to show motors from $1\,mW$ to $10\,kW$ power on the same plot. For the brushed motors of the second category here above (red), an interpolation shows a power ratio of $0.09\,kW/kg$ $(11.1\,kg/kW)$. In the case of the third category, the model-makers brushless motors (green), this value increases to $3.4\,kW/kg$ $(0.29\,kg/kW)$. This impressive difference is mainly due to two reasons; first, the final application drives the designers' efforts in the direction of high power to mass ratio, using small but powerful magnets, and lightweight metallic alloy pierced as much as possible. This induces that efficiency is regarded as a second matter. Secondly, the majority of them are outrunners, which means that the outer part of the motor is the rotating part. Always containing many holes that let one see the inner stator, the rotation creates a very efficient cooling, allowing the use
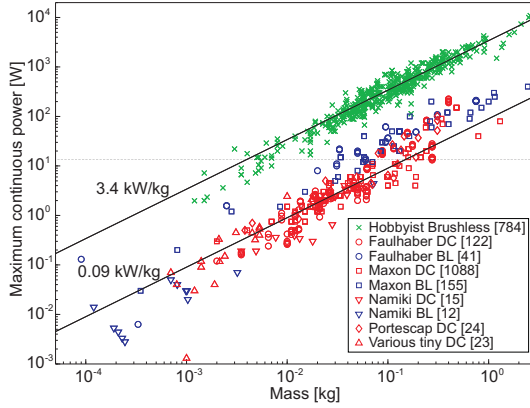
Figure 3.11: Power to mass ratio of 2264 commercial motors from a database created with the specifications of various manufacturers' products
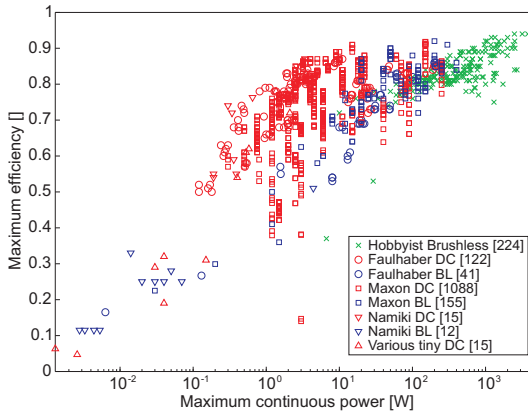
Figure 3.12: Maximum efficiency vs maximum continuous power of 1672 motors from a database created with the specifications of various manufacturers' products

of greater current than in the case of a hermetic brushed motor. The brushless motors built by the high quality motors companies (blue) are certainly better than the brushed ones, but not competitive with the ones from the model-making world.

As mentioned here above, we can wonder if this high power to mass ratio is not at the expense of efficiency. Figure 3.12 represents the maximum efficiency with regard to the maximum power, knowing of course that they

don't occur at the same time, the maximum efficiency occurring at roughly one seventh of the stall torque. From the 784 model-making brushless motors of figure 3.11, only 224 are plotted now, all the other having no maximum efficiency specified. Companies like Strecker or Hacker are thus not represented on this graph, but measurements achieved on their high quality motors used in the framework of this thesis show that their efficiency are competitive with the brushed DC motors. In a general point of view, the efficiency is very good for motors of more than 10 W but drops dramatically for motors below 1 W.

This is due to the imprecisions of small size motors that are much more difficult to produce with good tolerances and good quality. The ball bearings for example are hardly feasible at tiny dimensions. Of course, depending on the application, the motor optimization will take different directions. In an invasive medical tool for surgery for example, the volume is critical and thus a high power to volume ratio is preferred, even if the efficiency is poor, since the motor is being powered externally. Contrarily, for a watch, the motor efficiency will play a major role in order to ensure a long running time.

Gearbox

As mentioned in table 3.3, Hall and Bailey presented models to estimate the mass of a gearbox depending on its maximum continuous power. In order to verify these models, they were plotted in figure 3.13 with the characteristics of 997 Maxon and Faulhaber gearboxes.
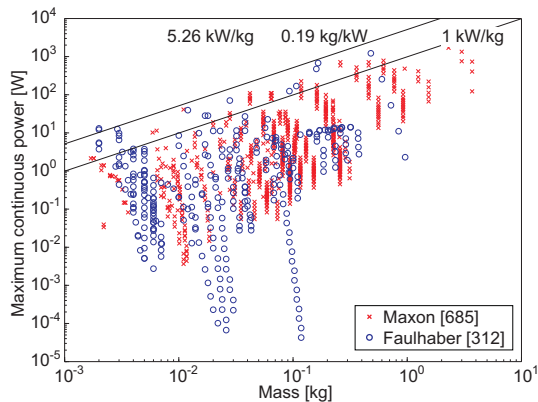
Figure 3.13: Power to mass ratio of 997 gearboxes

We can observe that the data set is quite diffuse but that the gearboxes with a good power to mass ratio located in the upper side are close to the

model of Bailey [27, p.49] with 0.19 kg/kW and to the one from Hall [68] who
considers a lower power density with 1 kg/kW. When studying deeper, we can
see that this upper region contains gearboxes with a small reduction ratio (1
to 20). In our case, the reduction ratio will also be in this range, as the goal
here is not to achieve a position control system but an airplane propulsion
group. For a well designed gearbox, 0.2 kg/kW should be reachable. That is
the value that will be considered later.

Concerning the efficiency, it drops inevitably at high reduction ratio, as
demonstrated in figure 3.14. In fact, keeping the dimensions of gears constant
requires more reduction stages and thus implies more friction. On the other
side, keeping the same number of stages implies smaller wheels with less
teeth, what also penalizes efficiency.
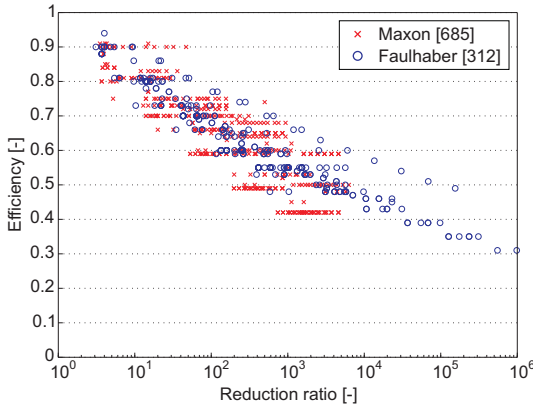
Figure 3.14: Efficiency vs reduction ratio of 997 gearboxes

Control Electronics

The motor control electronics are also a part of the propulsion group and have
to be studied. The control electronics needed for brushless motors are slightly
more complicated than for brushed motors. In fact, whereas the first can be
controlled with a constant voltage, the brushless motors are driven by three
sinusoidal signals that have to be synchronized with the position of the rotor.
Hence, this position has to be constantly measured by the electronics [108].

Here again, a database with standard products was created. The interpo-
lation on this data set is represented in figure 3.15 and shows a proportion-
ality of 0.026 kg/kW. Anyway, experience showed that a product optimized
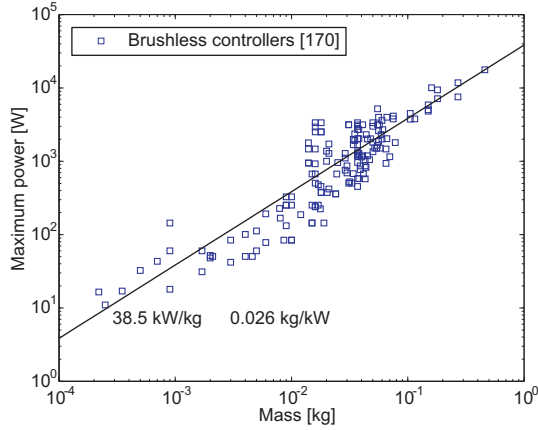
Figure 3.15: Power to mass ratio of 170 brushless controllers

for high efficiency requires often better components, bigger inductors and capacitors in order to reduce the losses, wider cables, etc. Thus it is reasonable to take a value of $0.06\,\text{kg/kW}$ into account.

Propeller

In literature, Colozza [50] considers for the mass prediction of the propeller a formula based on the airplane wing loading from Hall [69] $m_{plr} = 10.27\,(m_{tot}/S)^{0.5}$. Nicolai [89] proposes an equation for civil aircrafts that takes into account not only the engine power but also the propeller diameter. This relation was used for electric solar airplane design by Hall [68] and also by Keidel [71] who refined the constant factor, according to technological improvements in the field, and obtained :

$$m_{prop} = 0.12\, n_{bl}^{0.391} \left(d_{plr}\, \frac{P_{plr}}{1000} \right)^{0.782} \tag{3.31}$$

Where n_{bl} is the number of blades, d_{plr} the diameter and P_{plr} the power of the propeller. In our case, we will consider a linear relationship $m_{plr} = 0.25\,kg/kW\, P_{plr}$. It is based on the interpolation of a database containing propellers of civil aircrafts and a few solar airplanes such as Icaré 2, Velair [71] and SunBeam (Figure 3.16).

Concerning the propeller efficiency, it depends also on the power. The literature shows that for airplanes with a power of around $10\,\text{W}$, efficiencies
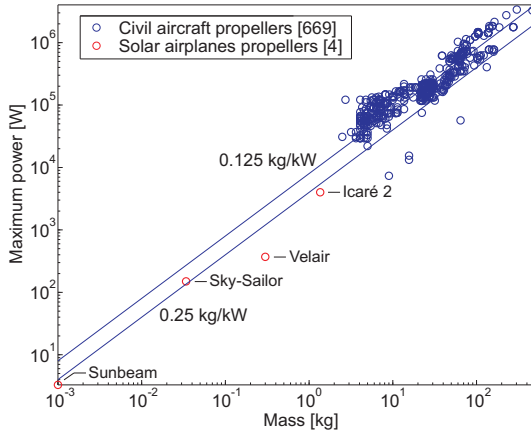
Figure 3.16: Power to mass ratio of 669 civil aircrafts propellers augmented with solar airplane propellers

between 85 % and 90 % can be expected, as written in table 3.3. However, it drops rapidly when downscaling. SunBeam, the 50 cm 3 W solar MAV [111], had a propeller efficiency measured at 58 %.

Model Summary and Adaptation to Launch conditions

The power to mass ratios of the propulsion group elements were given above for the maximum continuous power of each of them. Two adaptations have to be done before using these values in our solar airplane design :

First, the motor is quite inefficient at maximum power, because of the high Joule heat losses. A rule of thumb is that the maximum efficiency occurs at roughly one seventh of the stall torque and one third to one half of the maximum power. Therefore, the motor mass for level flight scales rather with 0.70 kg/kW considering the nominal power than with 0.29 kg/kW considering the maximum power.

The second point concerns the launch conditions. For an airplane taking off on a long runway, increasing gently its speed until lift-off, the difference between start power and level flight power is low. At the opposite, in the case of a hand-launched model airplane that needs to increase its speed and gain altitude rapidly, the motor has to provide a power at start that is far higher than the level flight power. This over-sizing is necessary for take-off but helps also flying with headwind and in turbulence. In the case of the Sky-Sailor prototype depicted in chapter 5, the over-sizing ratio is 10.

Table 3.4: Propulsion group mass to power ratio proposed depending on the power considered for the calculation

	Ctrl	Mot	Grbx	Prop	Total (k_{prop})
Maximum Power	0.06	0.29	0.20	0.25	0.80 kg/kW
Level flight Power (normal take-off)	0.06	0.70	0.20	0.25	1.21 kg/kW
Level flight Power (hand launched)	0.60	2.90	2.00	2.50	8.00 kg/kW

Table 3.4 summarizes the mass to power ratios considered in the various cases. Finally, the constant k_{prop} is used to predict the mass of the entire propulsion group using :

$$m_{prop} = k_{prop} \ P_{lev} = k_{prop} \ a_0 \ a_1 \frac{m^{\frac{3}{2}}}{b} \tag{3.32}$$

3.5 Summary and Resolution of the Design Problem

After having formulated the daily required energy, the solar energy available and developed all weight models, we can redraw the loop of figure 3.1 in a fully mathematical manner in figure 3.17. It summarizes in a compact way all equations that were given before and represents the problem of the solar airplane conceptual design in a compact graphical approach.

In order to be able to extract meaningful information, it is necessary, among the thirty parameters that our model contains, to distinguish between three different classes :

- The first group is composed of the parameters which are linked to a technology and are constant or can be regarded as constant for any good designs. This is for example the case of motor or propeller efficiencies that should be around 85 % when optimized for a specific application [119].
- The second group of parameters is linked to the mission; they are the air density, given by the flight altitude, the day and night duration, depending on the time and the location, and the mass and power consumption of the payload.
- Finally, the last group is composed of the parameters that we vary during the optimization process in order to determine the airplane layout, that is why we should use the term variable rather than parameter. They are the wingspan and the aspect ratio.
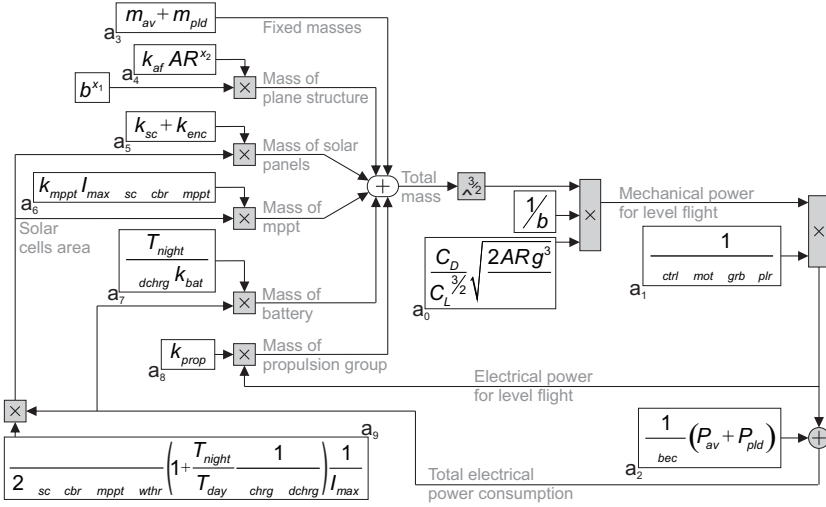
Figure 3.17: Schematic representation of the design methodology

A complete listing of these parameters is presented in tables 3.5 to 3.7. The values that are mentioned were used for the design of the Sky-Sailor prototype.

We will now solve mathematically the loop represented in figure 3.17 considering AR, b and m as variables for the airplane layout and all the others as parameters. This starts by summing up all the masses of the subparts to obtain the airplane take-off mass.

$$m = m_{fixed} + m_{af} + m_{sc} + m_{mppt} + m_{bat} + m_{prop}$$

$$= a_3 + a_4 b^{x_1} + a_0 a_1 a_9 (a_5 + a_6) \frac{m^{\frac{3}{2}}}{b} + a_2 a_9 (a_5 + a_6) \qquad (3.33)$$

$$+ a_0 a_1 a_7 \frac{m^{\frac{3}{2}}}{b} + a_2 a_7 + a_0 a_1 a_8 \frac{m^{\frac{3}{2}}}{b}$$

$$m - \underbrace{a_0 a_1 (a_7 + a_8 + a_9 (a_5 + a_6))}_{a_{10}} \frac{1}{b} m^{\frac{3}{2}} = \underbrace{a_2 (a_7 + a_9 (a_5 + a_6)) + a_3}_{a_{11}} + a_4 b^{x_1} \quad (3.34)$$

$$m - \underbrace{a_{10}}_{a_{12}} \frac{1}{b} \ m^{\frac{3}{2}} = \underbrace{a_{11} + a_4 \ b^{x_1}}_{a_{13}} \qquad (3.35)$$

Table 3.5: Parameters that are constant or assumed constant. The values correspond to the Sky-Sailor design.

Parameter	Value	Unit	Description
C_L	0.8	-	Airfoil lift coefficient
$C_{D\,afl}$	0.013	-	Airfoil drag coefficient
$C_{D\,par}$	0.006	-	Parasitic drag coefficient
e	0.9	-	Oswald's efficiency factor
I_{max}	950	$[W/m^2]$	Maximum irradiance
k_{bat}	190·3600	$[J/kg]$	Energy density of lithium-ion
k_{sc}	0.32	$[kg/m^2]$	Mass density of solar cells
k_{enc}	0.26	$[kg/m^2]$	Mass density of encapsulation
k_{mppt}	0.00042	$[kg/W]$	Mass to power ratio of MPPT
k_{prop}	0.008	$[kg/W]$	Mass to power ratio of prop. group
k_{af}	0.44/9.81	$[kg/m^3]$	Structural mass constant
m_{av}	0.15	$[kg]$	Mass of autopilot system
η_{bec}	0.65	-	Efficiency of step-down converter
η_{sc}	0.169	-	Efficiency of solar cells
η_{cbr}	0.90	-	Efficiency of the curved solar panels
η_{chrg}	0.95	-	Efficiency of battery charge
η_{ctrl}	0.95	-	Efficiency of motor controller
η_{dchrg}	0.95	-	Efficiency of battery discharge
η_{grb}	0.97	-	Efficiency of gearbox
η_{mot}	0.85	-	Efficiency of motor
η_{mppt}	0.97	-	Efficiency of MPPT
η_{plr}	0.85	-	Efficiency of propeller
P_{av}	1.5	$[W]$	Power of autopilot system
x_1	3.1	-	Airframe mass wingspan exponent
x_2	-0.25	-	Airframe mass aspect ratio exponent

This equation can be rewritten in the form of a cubic equation after a variable substitution :

$$a_{12}\,z^3 - z^2 + a_{13} = 0 \quad \text{with } z = m^{\frac{1}{2}} \tag{3.36}$$

$$z^3 - \frac{1}{a_{12}}z^2 + \frac{a_{13}}{a_{12}} = 0 \tag{3.37}$$

The equation (3.37) has only a positive non-complex solution, which makes physically sense, if :

Table 3.6: Parameters determined by the mission. The values correspond to the Sky-Sailor design.

Parameter	Value	Unit	Description
m_{pld}	0.05	$[kg]$	Payload mass
η_{wthr}	0.7	-	Irradiance margin factor
P_{pld}	0.5	$[W]$	Payload power consumption
ρ	1.1655	$[kg/m^3]$	Air density (500 m)
T_{day}	13.2·3600	$[s]$	Day duration

Table 3.7: Variables linked to the airplane shape. The values correspond to the Sky-Sailor design.

Parameter	Value	Unit	Description
AR	12.9	-	Aspect ratio
b	3.2	$[m]$	Wingspan
m	2.6	$[kg]$	Total mass

$$a_{12}^2 \, a_{13} \leq \frac{4}{27} \tag{3.38}$$

$$a_{10}^2 \, \frac{1}{b^2} \, (a_{11} + a_4 \, b^{x_1}) \leq \frac{4}{27} \tag{3.39}$$

$$a_{10}^2 \, a_{11} \, \frac{1}{b^2} + a_{10}^2 \, a_4 \, b^{x_1-2} \leq \frac{4}{27} \tag{3.40}$$

For a given airplane configuration, the feasibility of continuous flight is proved, if this inequality is respected and at the same time if the surface of solar cells is smaller than the wing area.

The conceptual design process can thus be summarized as follows : having set the mission requirements and chosen the technological parameters, we can try many possible airplane layouts by changing b and AR. The condition on equation (3.38) tells directly if the design is feasible or not with these wingspan and aspect ratio. In the case of a positive answer, the total mass m can be found by solving equation (3.35). It constitutes then the starting point for the calculation of the power and the characteristics of all the other elements. Hence, this method is not aimed at being used to optimize a precise and local element like the airfoil or the propeller, its objective is rather to help to choose the best combination and size of the different elements.

Chapter 4

Sky-Sailor Design

4.1   Introduction

The methodology that was presented in the last chapter will now be put into application, with the concrete example of the design of the Sky-Sailor proto-type. After the presentation of the airplane layout resulting from the design methodology in the next section, we will present a second tool to validate the concept before building a first prototype. It consists of a simulation environment that allows analyzing the energy flows on the airplane, between the solar panels, the battery and the power consuming elements second after second during a flight. This step is closer to the real experiments and constitutes an additional proof that the planned airplane will reach its objectives.

The goal of the Sky-Sailor project is to design and build an airplane that proves the feasibility of continuous flight, over 24 hours, as explained in section 1.1. This flight should be feasible within 3 months in summer, which sets the day duration to 13.2 hours according to figure 3.3. A 50 g payload consuming 0.5 W, representing a small camera and its transmitter, will be installed onboard. The airplane will fly at a low altitude of 500 m above sea level, 100 m above ground. These mission parameters are summarized in table 3.6 and the technological parameters in table 3.5.

4.2   Application of the Design Methodology

We will now investigate, with the mission and technical parameters that we considered, what would be the layout of an airplane capable of 24 h flight in these conditions. For this purpose, various airplane wingspans and aspect

ratios are tried methodically. For each combination, equation (3.38) determines if the solution is feasible. In the case of a positive answer, equation (3.35) is solved to find the airplane gross mass.
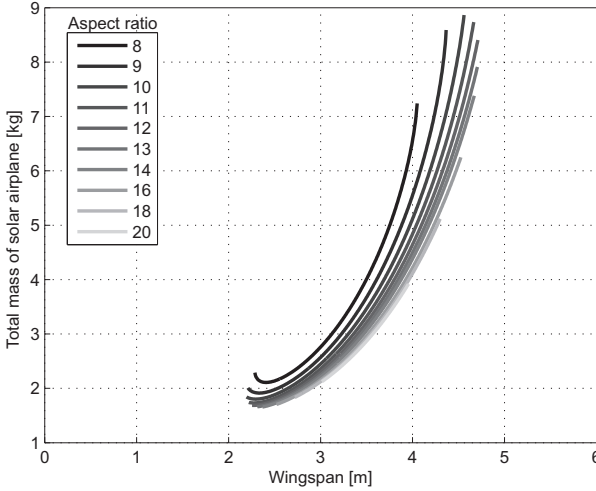
Figure 4.1: Possible configurations presenting the total mass as a function of the wingspan b and aspect ratio AR

Figure 4.1 presents the results. We can observe that the minimum wingspan the airplane should have for continuous flight is 2.5 m. There is also an upper limit, showing that with a wingspan greater than around 4.5 m continuous flight is no longer feasible. This might be surprising, but it has a very simple reason : with the weight prediction model that we considered, the airframe becomes too heavy above a certain wingspan so that it is no more possible to fly continuously with the available power. That means that going higher in dimension would require a lighter airframe weight model. This point will be further discussed below, with the help of figure 4.4.

Having found the total mass for each possibility, we can then introduce it into the loop represented in figure 3.17 to calculate precisely all the other airplane characteristics : powers at propeller, gearbox, motor and battery, surface of wing and solar panels, weights of the different subparts and also flying speed.
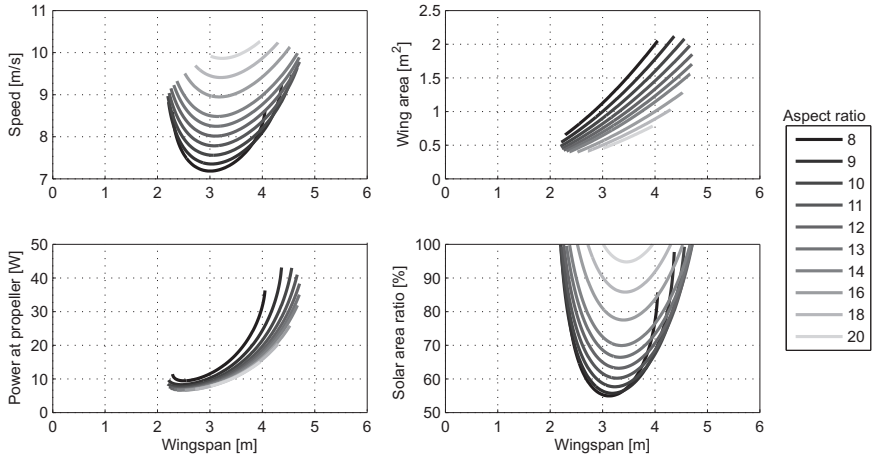
Figure 4.2: Aircraft and flight characteristics depending on the wingspan b and the aspect ratio AR

Figure 4.2 presents these data that are decisive for the final selection of the airplane layout. This selection will follow criteria that are determined by the application. They can concern speed, having a certain distance to cover in a limited time, or wingspan, the UAV being stowed in a limited volume and launched by hand. Thus, with the help of these plots, a final configuration can be selected. In the case of Sky-Sailor, one key objective was to study the stowage of the airplane in a very limited cylinder, what would be the case of a system sent to Mars. With a cylinder of a diameter of 1 m, the airplane folded into three parts could have a wingspan of around 3 m (Figure 4.3).
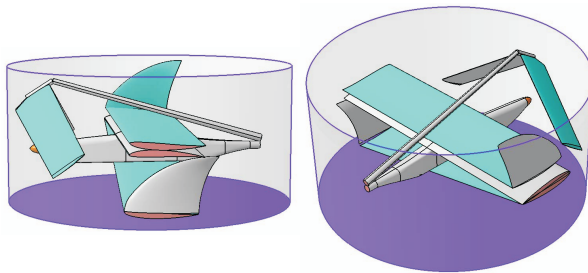
Figure 4.3: Stowage in an aeroshell for the entry phase into Mars atmosphere

Finally, a wingspan of 3.2 m including the winglets is considered with an aspect ratio of 13, giving a chord of 25 cm. The targeted airplane weighs 2.55 kg, the 196 Wh battery and the fuselage representing 40 %, respectively 34 % of this amount, as the mass distribution in figure 4.4 tells us. This plot is very useful to see what percentage of the total weight each element represents, in order to orient the research efforts accordingly. One notable point is the airframe weight that sees its percentage increase from 17 % to 39 % when increasing the wingspan from 2.3 to 4.7 m. As the model is roughly cubic, this percentage grows and above a certain wingspan, continuous flight is no more ensured without using a lighter construction technique. Coming back to the selected layout, the mechanical power required for level flight is only 9.42 W, but considering the efficiencies of the propulsion group elements an electrical power of 14.2 W will be needed. When adding the autopilot and payload power consumption, the total electrical power is 17.22 W. Level flight should take place at a nominal speed of 8.3 m/s. The wing surface is $0.787\,\mathrm{m}^2$, from which $0.525\,\mathrm{m}^2$ are covered by solar cells giving a maximum power of 74 W at the output of the MPPT.

Instead of varying only b, m and AR, it is also possible to fix one of these three variables and use a parameter that was considered as constant as a new variable. For example, we can fix the aspect ratio and then see the impact of air density on the flight feasibility in order to calculate the maximal altitude for a 24 h flight, keeping the same mission objectives. In fact, a potential future step in the project is to fly higher than a few hundreds of meters above the ground. The battery technology being the one that will see improvements the most rapidly in the next years, it is interesting to see the evolution of this altitude with respect to the gravimetric energy density values. This is represented in figure 4.5 that confirms the 3.2 m wingspan as a good optimum.

Thus, with this approach it is possible to do far more than just designing an airplane, as a multi-disciplinary optimization (MDO) program would do it. We can easily analyze the impact of some of the design parameters on other parameters or variables. This kind of sensitivity analysis is very useful to observe into which technological domain it is interesting to put efforts in order to increase a certain capability, for example the flight duration.

The design methodology that led to the plots here above was implemented under Matlab$^{\circledR}$. The code is simple and composed of 210 lines divided in four m-files available in the appendix so that the reader can test the methodology himself. In fact, in our design methodology, the added value is not only the program itself but mainly the good models that the methodology is based on. The equations relating them are themselves very simple.
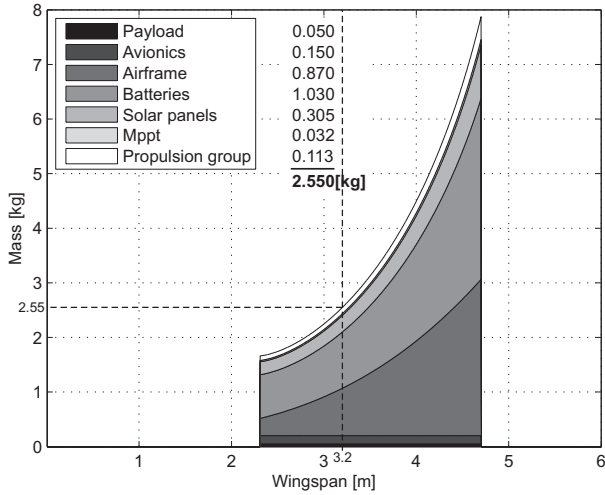
Figure 4.4: Mass distribution considering an aspect ratio AR of 13. The values for a wingspan of 3.2 m corresponds to the Sky-Sailor Design.
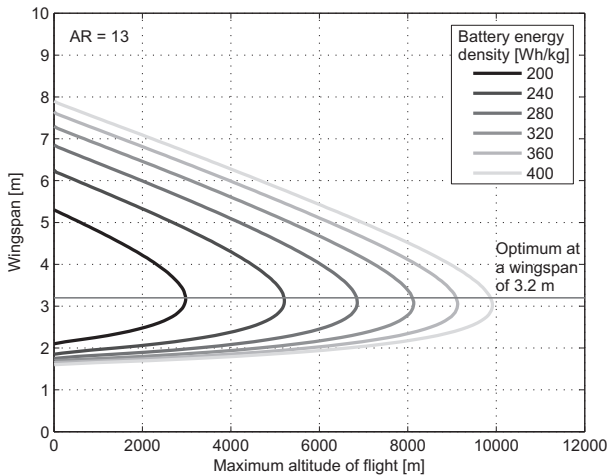
Figure 4.5: Evolution of the maximum reachable altitude depending on the battery gravimetric energy density k_{bat} and the wingspan b. In 2008, the best lithium-ion batteries offer 240 Wh/kg.

4.3   Real-Time Simulation Environment

In the methodology and its application example presented above, the irradiance is averaged over the whole day, so what comes out at the end is a solution that makes solar flight feasible during this day. However, we might also want to see the flight evolution second per second with an irradiance that varies during the entire day instead of being averaged. It is then possible to monitor all state variables and analyze the energy flows on the airplane from dusk till dawn and from dawn till dusk. This allows validating the design a second time before building the real prototype, but it has other purposes.

Such solar flight simulation can predict the charge status of the battery in order to see what the energy margin in the morning will be. This information is very useful then during the real experiments to control for example in the middle of the night if the voltage profile is close to the prediction or not, in which case special measures have to be taken. A second purpose is to see the influence which the alteration of some parameters has on the continuous solar flight. For example, by reducing the efficiency or the area of solar panels, we can simulate dust deposition or damages and evaluate the impact on the feasibility of 24 hours flight. Also, instead of considering only level flight, we are able to test various types of flight at different moments in the day. One example is to start climbing at the end of the afternoon, once the battery is fully charged. Thus the surplus of energy is stored into potential energy. After dusk, when the sun power is not sufficient to power the level flight anymore, a descent to the nominal altitude with the motor off is engaged.

Hence, this new tool is definitely not redundant to the design methodology, it is rather complementary.

4.3.1   Description of the Simulation Environment

This simulation tool was developed under Matlab® Simulink®. It is represented in figure 4.6 where we distinguish three main parts :

- The left side contains the irradiance model, derived from "Solar Engineering of Thermal Processes" from Duffie and Beckman [54]. Based on the time in year, the orientation of the panels with respect to the sun, the geographic location on Earth and the albedo, it outputs the irradiance in W/m^2. Considering then the surface of solar panels and the efficiencies of the cells, their configuration (see section 3.4.3) and the MPPT, we obtain the available solar electrical power.
- The lower right corner contains the power consuming elements, including the autopilot system, the communication electronics and the
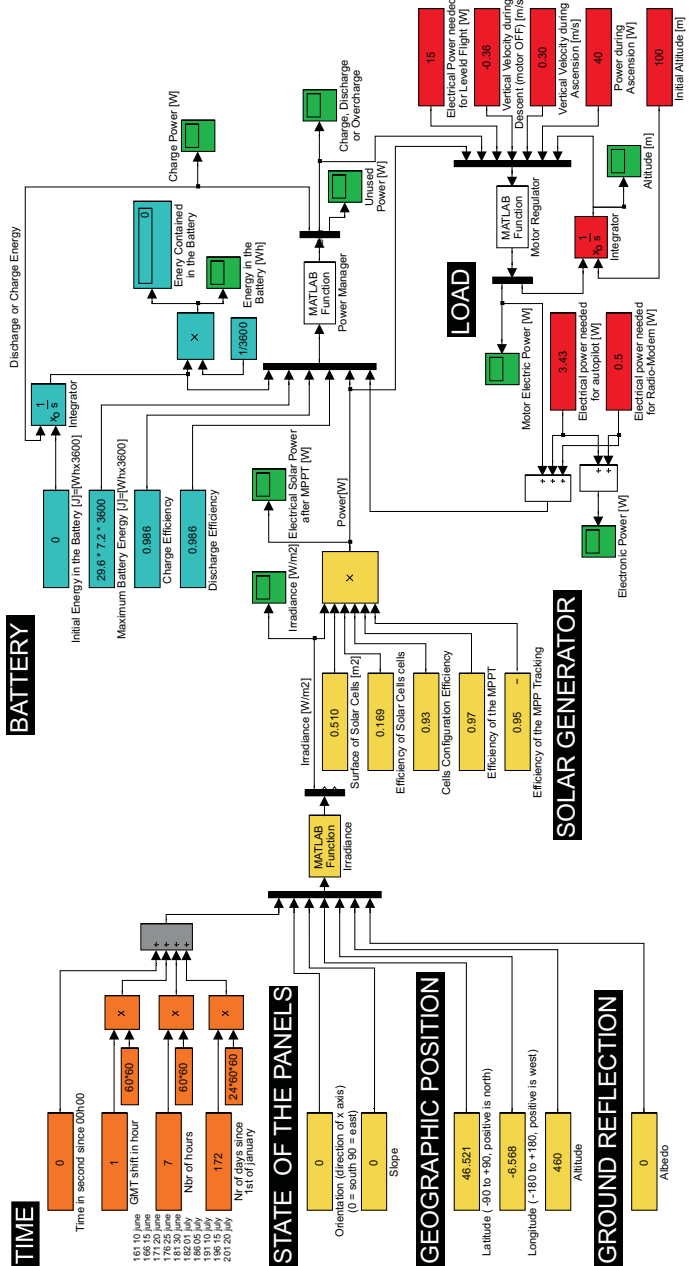
Figure 4.6: Simulation environment of the solar flight implemented with Matlab®
Simulink®

propulsion group. For the latter, we can simulate level flight, using the electrical power required in this case, but it is also possible to consider storing energy into potential energy by gaining altitude, as said before. Thus, vertical gliding and descending velocities, as well as the power needed in this case and the initial altitude are required. The "Motor Regulator" block is responsible to adapt the flight mode between gliding, ascending or level flight based on the current solar power available and the airplane power consumption.

• The upper right corner represents the energy storage, in the present case the battery. We consider here the initial energy in the battery and its maximum capacity, but also the charge and discharge efficiencies. A more complex model that simulates the battery chemistry could be developed, but it was not the case here.

At the intersection of these three parts lies the "Power Manager" block, responsible to orient the energy flows into the appropriate direction. Considering the electrical power retrieved from the solar generator, it simply subtracts the total power consumption and charges the battery with the surplus or discharges it with the difference if the solar cells don't provide enough power.

This simulation environment is already one step into the direction of real experiments. In fact, the power consumption can be based on the theoretical aerodynamics coefficients, but we can also directly enter the power consumption that was measured during a test. This is also the case of the battery capacity, its charge and discharge efficiency, the autopilot power consumption, etc. Hence, it allows simulating the flight but with real data acquired experimentally.

4.3.2   Simulation of a 48 Hours Flight

The simulation of a 48 hours flight on the 21st of June and starting at 7h00 in the morning is presented in figure 4.7. This day has theoretically the shortest night duration and is thus the optimal period to fly continuously. The left part concerns the power transfers. Considering only level flight, the total power consumption in green is constant, but of course the electrical power coming from the solar panels augments until a maximum of 72 W at around noon. During this period, the battery is charged with the power surplus. At 12h10, the battery is charged and during the afternoon, only a power equal to the power consumption is acquired from the solar panels. This is similar to what happens in the reality, meaning that having a full battery, it is not necessary to dissipate the power surplus through a heating resistor because
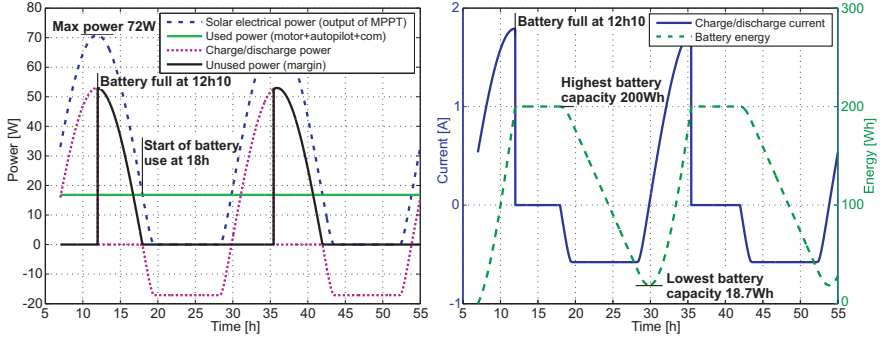
Figure 4.7: Continuous flight simulation on the 21st of June

the MPPT itself places the working point below the maximum power point so that only the consumed power is retrieved. At 18h, the solar power is not sufficient anymore and the battery starts to be used, with a phase where both the solar panels and the battery are supplying power. During night, the supply comes from the battery only.

Thus, the bold curve shows that almost half of the energy is not used. The reason is that this graph shows ideal sun conditions, whereas in reality some clouds can obstruct the sky during some periods and thus lowers the available solar power. In this case, the battery would be fully charged later than the prediction, or if the solar power is really lower than the power consumption, the battery would even be discharged during the day. If this last situation occurs during a short time in the middle of the afternoon, it is not so critical as the battery can be fully charged again before dusk arrives. This is precisely why in our design a margin factor η_{wthr} was considered (Equation 3.8). If it happens precisely at dusk or at down, this becomes more problematic because the battery will start, or respectively end its nocturnal discharge before the planned hour, what could prevent achieving a new 24 h cycle. In the present case, the right part of figure 4.7 shows that we have a battery capacity margin of 18.7 Wh, what represents more than one hour of flight.

In order to be consistent, we should also mention that an ideal battery model was considered. In reality, the power charging the battery has to be limited during the second charge phase with constant voltage and decreasing current (Figure 2.12). Hence, the charging time is slightly lengthened compared to the case where the battery is constantly charged at 1 C (see section 2.4.1).

Now we can do the same simulation but one and a half month later,
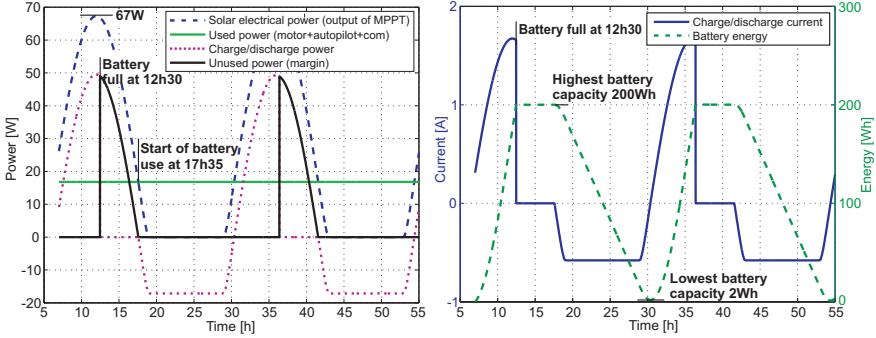
Figure 4.8: Continuous flight simulation on the 4th of August

as we considered a feasibility margin of three months in summer. Figure 4.8 presents the case with the same airplane and also starting at 7h00 in the morning, but on the 4th of August. The maximum solar power already decreased by 7 % but this is not critical as a certain margin was considered. It results only in a battery that needs slightly more time to be charged. The problem comes from the night which lasts longer now. As a consequence, the battery starts its discharge 25 minutes earlier than on the 21st of June, leading to a minimum capacity of only 2 Wh at the end of the night.

After this date, the feasibility is no more ensured. That shows clearly that for achieving continuous solar flight far away from the 21st of June, what becomes problematic is not the day duration that decreases but mostly the night duration that increases. And the reason lies simply in the fact that even with the best energy storage technology available now, the battery is still very heavy, constituting around 40 % of the airplane's weight.

Chapter 5

Sky-Sailor Realization and Testing

5.1 Introduction

After the presentation of the conceptual design in the last chapter, this section addresses the preliminary and detailed design of the Sky-Sailor solar airplane. In fact, whereas so far only the sizes and masses of the airplane elements were determined using the weight prediction models, the target is now to choose the exact parts that will be assembled to build the prototype.

This chapter will thus be very practical, presenting not only the selection of each component but also discussing the possibilities that were offered and then the criteria and the approach that led to each final choice. In order to validate the theory, we will then also compare the real characteristics obtained with the theoretical predictions. The last part of the chapter will present the flight experiments that were conducted with the fully functional prototype and compare them with the capabilities that were predicted.

5.2 General Configuration and Structure

According to the results of the design study using the methodology presented before, a fully functional prototype was built with the name Sky-Sailor.

The general configuration of the airplane is a 3 axis motorized glider, meaning that the control surfaces are the ailerons, the elevator and the rudder. Figure 5.1 presents the drawings and dimensions of the airplane that has a dihedral wing and a V-tail. The aerodynamic design and construction of the

structure was achieved by Walter Engel, a world expert in ultra-lightweight
high performance model sailplanes. The basis layout was adapted from his
Avance glider that set two world records in distance (424.5 km) and dura-
tion (15 h 12 m 30 s) in the F5P category of FAI in 1998 [21]. The empty
airframe, including the control surfaces and their actuators, weighs 0.725 kg,
for a wingspan of 3.2 m and a wing area of 0.776 m^2. It is thus slightly better
than the 5 % model developed for the design phase (Figure 3.7) that predicted
0.870 kg.
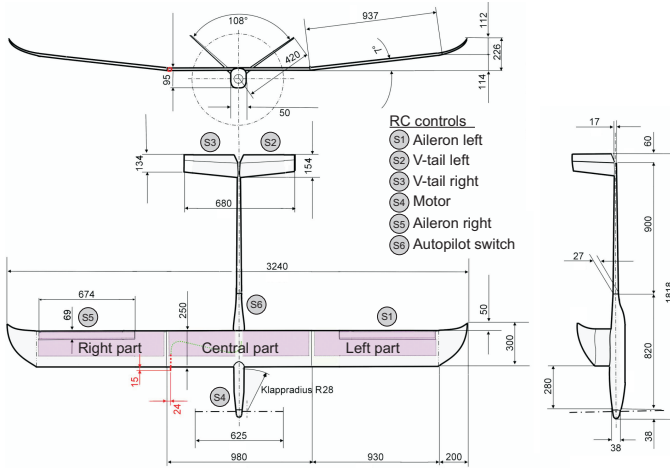
Figure 5.1: Drawings and dimensions of the Sky-Sailor prototype

The wing structure is essentially made of composite materials, i.e. carbon,
aramide, Kevlar and balsa wood. A main spar carries the bending and torsion
loads along the wing, and wing ribs, disposed in the direction of flight but
also in diagonal to improve resistance to torsion, give the aerodynamic shape
to the wing. The lower side is covered by a polyester film (Oracover®116712)
while the upper side is directly closed by the solar panels that are glued on
the spar and the ribs, and follow exactly the airfoil shape thanks to their
flexibility. The wing is in fact composed of three parts (left, central and
right) that are connected mechanically using dihedral braces. On the two
sides of each of these parts, where they are connected to each others, a zone
of 2 cm width was not covered with solar panels for two reasons. First, high
torques and forces are transmitted between the parts, which could break a
solar cells placed too close to this junction. Second, for the flight experiments
a very resistive Kapton tape is applied on this zone to add security at the

junction between the two parts. Figure 5.2 presents the right and the middle part of the wing, with and without solar panels so that the reader can observe the ribs architecture.
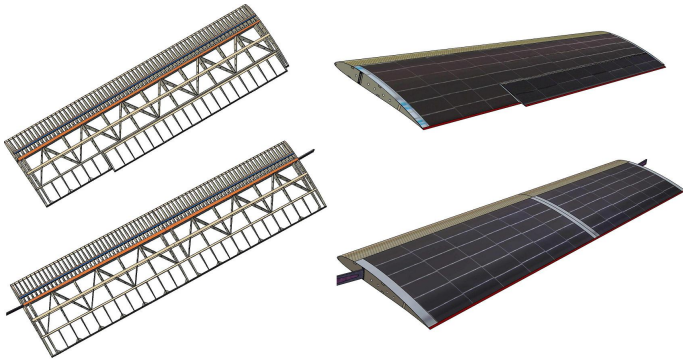
Figure 5.2: Right and middle part of the wing, with and without solar panels

The front side of the wing delimited by the border of attack and the spar represented in figure 5.3 is commonly named the "D box". This closed D shape is responsible for withstanding the torsion moments along the wing whereas the flexion forces are supported by the spar only. The shape of the border of attack must be perfect in order to meet the aerodynamics characteristics calculated theoretically. In order to avoid sagging between ribs, the leading edge is made of a composite structure of aramide and carbon fiber that is molded separately. It is then glued onto the ribs that are more numerous than for the rear part, as it can be seen in figure 5.2.

The main spar and the ribs are made of a sandwich structure of balsa wood between two thin layers of carbon, which ensures low weight and high resistance. A second spar on the rear part supports the ailerons and, combined with the diagonal ribs, adds rigidity which is especially important at high speed in order to avoid resonance problems. Compared to a wing molded in one piece, the spar-ribs technique is quite laborious as it takes a lot of time and needs several pieces to be assembled together. However, the experience shows that it proves to be far lighter.

The wing has a constant chord because it eases the integration of solar cells. Thus, in order to reduce the induced drag, two winglets made of molded Depron are placed at the wing tips. They also contain two LEDs that allow the pilot to light up the airplane during the night in case of emergency. As this option requires 1 W, they are not constantly turned on but only on demand.
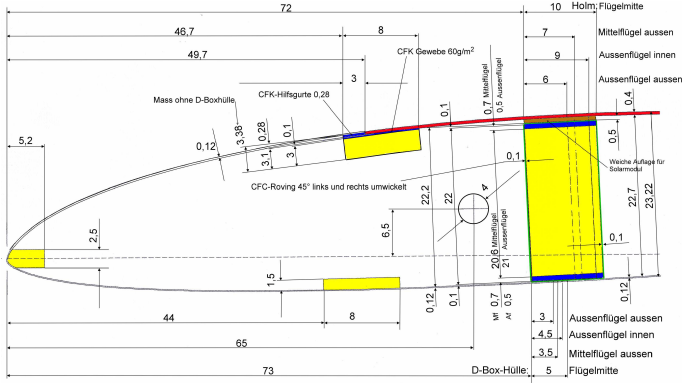
Figure 5.3: Partial view of the wing section with the leading edge and the main spar
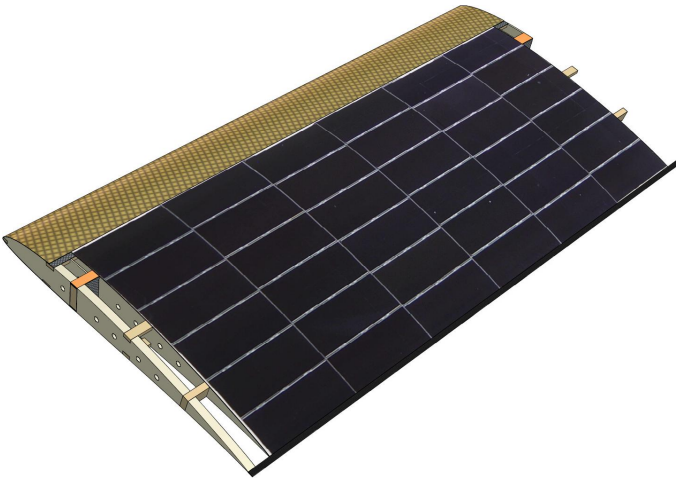
Figure 5.4: View of the integration of the solar modules on the wing

The two V-tail parts, built with the same technique, are connected to the fuselage through a carbon fiber tail boom. Compared to a T configuration, the V-tail has the advantage to be made of two symmetrical but almost identical parts, it is lighter and well suited for belly landing because the risk of contact with the ground is low. The drawback is that the rudder and elevator commands are not separated as it is the case for a T-tail where each

one is linked to its own actuator. With a V-tail, for both an elevator and a rudder correction, a combination of the two surfaces deflection is necessary. The fuselage itself is made of aramide and glass fiber that are molded to form a honeycomb structure. It doesn't contain carbon fiber in order not to disturb the radio communications. There is no landing gear as the airplane is thrown by hand and lands on its belly.

As previously mentioned, a 3 axis configuration was chosen, which differs from two axis by the fact that, additionally to the rudder and elevator on the tail, two ailerons are added on the wing. In comparison, a 2 axis sailplane doesn't need servo actuators in the wing which reduces the weight, but the drawback is that the turn sequence is more complicated : it needs first a yaw rotation using the rudder, inducing then a roll rotation due to the wing dihedral, and then, pulling on the elevator, it acts on the pitch and the airplane turns correctly. This has two disadvantages :

- The turns are more complex to realize and take more time
- The aircraft wing needs to have a consequent dihedral, unless the induced roll is small. That means that on Sky-Sailor, if we wanted to switch to 2-axis actuation, the dihedral angle should be at least doubled, which would lead to some problems for collecting the solar energy and add more aerodynamic drag.

5.3 Airfoil

In the design process of an airplane, the airfoil selection is very important and always different because of the various applications, flight speeds, etc. In the present case, the selection criteria are first the ratio $C_D/C_L^{3/2}$ that is part of equation (3.5) for the calculation of the level flight power. The airfoil should also be especially good at low speed because of the low Reynolds number. At level flight, Sky-Sailor will have a speed of $8.3\,\mathrm{m/s}$ what leads to a Reynolds number of around $150\,000$ using equation (2.3).

There are many programs to calculate the lift, drag and moment coefficients of a wing section. In addition to the complex Computed Fluid Dynamics (CFD) programs that use finite elements methods, there are several other programs that are limited to 2D calculations. We can mention X-foil, Javafoil, Winprof among many others. The mathematical models that they use to calculate the pressure distribution vary and as consequence, they are all efficient for a specific flight domain. Some will give good results for the selection of an heavy high speed aircraft profile, some others are more suitable for lightweight slow gliders. For this reason, we shouldn't be astonished to see different results coming out of two programs while the profiles and flight

conditions entered are similar. It is just important to take their domain of validity into account.

Whereas the airfoil used for the V-tail is a standard symmetrical profile NACA0008, the one used for the wing was specifically designed by W. Engel for that precise application and named WE3.55-9.3 (Coordinates in appendix C). The lift and drag coefficients are plotted in figure 5.5 for different Reynolds number using the program X-foil. For angles of attack between -2° and 8°, the airflow around the profile is laminar what gives valid data. Outside this domain, one can observe that the drag increases rapidly due to the fact that an airflow separation occurs leading to turbulent zones, as explained in section 2.2. The behavior then becomes very difficult to predict and even if the software outputs data, it should be considered very carefully. In fact, only real experiments in a wind tunnel can correctly predict what happens then.
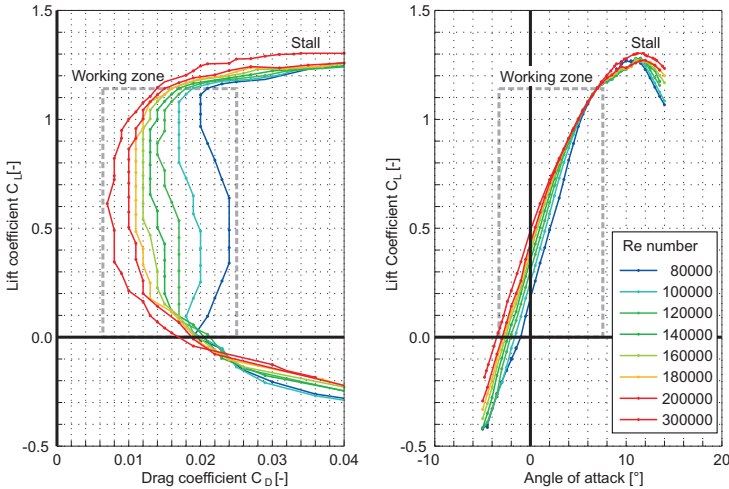
Figure 5.5: Polars of the WE3.55-9.3 airfoil using X-foil

The angle of attack used in the case of Sky-Sailor for nominal flight will be such that it gives a lift coefficient $C_L = 0.8$ and a drag coefficient $C_{D\,afl} = 0.0122$. Then considering the induced drag $C_{Dind} = 0.0152$ and a parasitic drag $C_{Dpar} = 0.0065$ calculated with the Winprof program, we end with a total drag of $C_D = 0.034$ what leads to a glide ratio of 23.5 at a speed of 8.3 m/s . It would be possible to choose a higher angle of attack that would slightly reduce the power required for level flight, but the speed would then be very close to the stall speed. It is therefore very important to choose an

angle of attack that gives a certain margin before stall for the flight in normal conditions. Of course, in the case of very calm atmospheric conditions, it is possible to increase the angle of attack of the main wing by some tens of degrees using the elevator in order to be at the minimum power point.

Equation (3.4) allows plotting the power required for level flight as a function of the airplane's gross mass. This is done in figure 5.6 considering always the same wing surface of $0.776\,\mathrm{m}^2$ and battery capacity of $196\,\mathrm{Wh}$. This plot is more useful than it may look like at a first glance. In fact, it will facilitate the selection of the various components by showing the relation between a gain in weight, efficiency and autonomy. As an example, we can wonder if it is worth trading a motor controller that offers $94\,\%$ efficiency for a new one with $97\,\%$ efficiency but $20\,\mathrm{g}$ heavier. This plot and the equations behind help determining if the weight penalty is compensated by the power reduction thanks to the better efficiency.
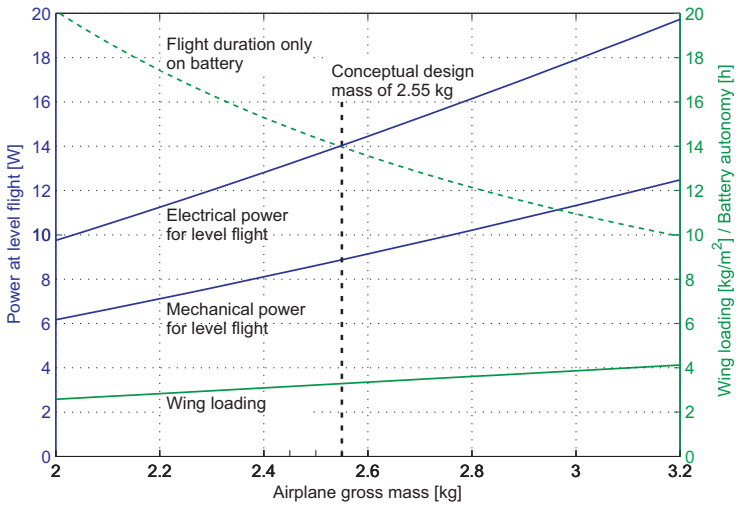
Figure 5.6: Variation of motor power, autonomy and wing loading with the airplane's mass during level flight. The wing surface is considered constant to $0.776\,\mathrm{m}^2$ and the battery capacity as well with $196\,\mathrm{Wh}$.

Concerning the control surfaces on the wing, the ailerons are controlled differentially to act on the roll. In order to have a similar drag and not to induce a yaw rotation, the up angle has to be two times bigger when the aileron is up than the angle value when the aileron is low. The two ailerons are also used as flaps, which means that additionally to the asymmetric commands

that control the roll, a symmetric up angle can be given to both of them
in order to significantly increase the drag. This allows low speed landings
on a very short runway, which limits the risks of damages. It is also highly
necessary when encountering too strong upwind that could push the aircraft
out of sight quite rapidly. In this case, without flaps, the only way to loose
altitude in a short period of time would be to point the nose down but the
high speed would then risk destructing the airplane.

The airplane is of course optimized for the solar flight conditions, meaning
a speed of 8.3 m/s with calm atmospheric conditions. However, it is also
necessary that it can withstand higher speeds for the case where it has to fly
against strong winds or in case of turbulence. The wing was thus designed
accordingly and flight tests at more than 30 m/s (110 km/h) proved to be
secure. However, even falling after stall, the airplane automatically finds a
good flight orientation thanks to its auto-stability and thus never reaches the
high speed mentioned above.

5.4 Propulsion Group

The choice of the components that compose the propulsion group, i.e. the mo-
tor and its controller, the gearbox and the propeller has to be done carefully
with the objective to increase the efficiency while keeping the total weight
low. The selection first began with the propeller, because their availability is
very restrictive.

5.4.1 Propeller

A fixed pitch two carbon blades propeller with a diameter of 60 cm and a
weight of 34 g is used. Named Solariane, it has a Goe795 profile and was
designed and built by the high efficiency propeller expert, Prof. Dr. Ernst
Schöberl, also a pioneer in solar and man-powered airplanes. Variable pitch
propellers are more suitable if the flight conditions often change, because
adapting the pitch can ensure the highest efficiency at each speed, which can
even be done automatically with an in-flight thrust measurement. However,
this solution requires additional mechanics and control, which means more
weight. In the case of Sky-Sailor, flying at constant speed except for the
launch and the landing, the fixed pitch solution is the best. A spring system
retracts the two blades when they are not turning, which is necessary for
landing. Once powered again, they open thanks to centrifugal forces.

The propeller data, especially power, efficiency and thrust, with respect to
the rotating and forward speed were simulated using the program WinProp

v. 3.01 from W. Westphal, Helmut Schenk and Norbert Graubner. This program bases its calculation on experimental data.
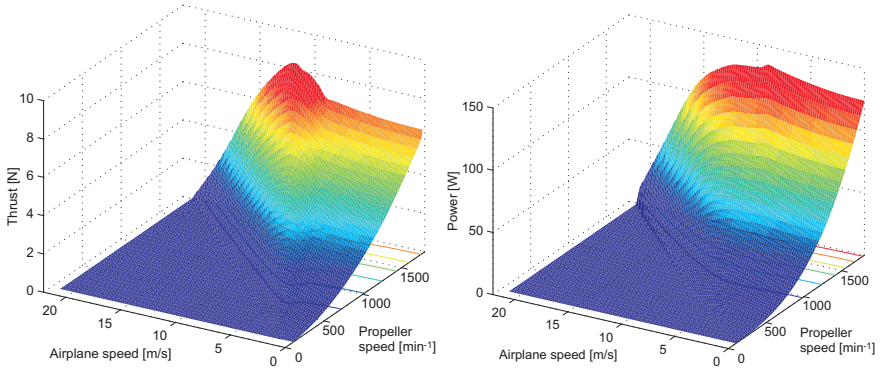
Figure 5.7: Thrust and power characteristics of the Solariane propeller depending on its rotational speed and the flight speed
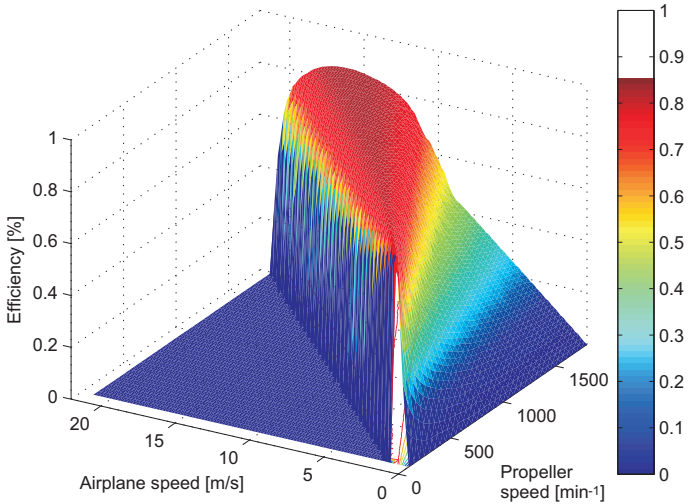
Figure 5.8: Efficiency of the Solariane propeller depending on its rotational speed and the flight speed

The maximum theoretical efficiency of the propeller is 86 %. The nominal speed of Sky-Sailor is 8.3 m/s and according to the calculation, the needed

thrust at level flight is 1.1 N, so the efficiency of the propeller in this case will be 85.6 % with a rotational speed of 880 rpm. At start, the needed thrust is 4 N assuming that the hand launch speed is 5 m/s, the efficiency of the propeller that turns at 1410 rpm is in this case only 32 % which is quite poor.

5.4.2   Motor and Gearbox

Having the propeller, a suitable motor has to be found that, combined to a gearbox with the appropriate reduction ratio, maximizes the efficiencies product of the three elements. It was not the goal here to design and build a special motor, but rather to find the most suitable commercially available one. In order to do this, a routine was written in Matlab® that simulates the operation of a motor, a gearbox and a propeller.

A database of more than 2600 motors for which the no load current, speed constant, resistance and weight information were available was created. It contains mainly all the Maxon motors and includes the Motocalc database, very well known among the model-makers and containing all the main model-making brushless motors on the market.

Contrary to the motor, the gearbox will not come from the market but will be built specifically. Hence, it is possible to reduce the weight compared to commercial products and choose a very precise and optimal reduction ratio. Gearboxes with reduction ratios from 1 to 20 with a step of 0.1 were considered. The limit is set to 20 because above this value, the efficiency starts to drop below 90 % which is not desirable (Figure 3.14).

Then, all the combinations between these motors, gearboxes and the propeller were simulated to find the best trade-off in terms of efficiency and weight. The theory behind this program and the results are shown here after.

Selection Program

The propulsion group is represented schematically in figure 5.9, the objective now is to model it in order to simulate it. The equations of a motor were already presented in details in section 2.6.1.

The second element in the propulsion group is the gearbox that is only characterized by its efficiency η_{grb}, considered here as constant, and its reduction ratio r. The problem here is to define the torque M_{plr} and speed ω_{plr} at the output of the gearbox with an input torque M_{mot} and an input speed ω_{mot}. That is done in equations (5.1) and (5.2).

$$P_{plr} = \eta_{grb}\, P_{mot} \qquad\qquad (5.1)$$
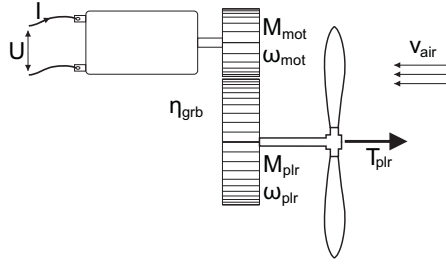
Figure 5.9: Schematic view of the propulsion group

$$M_{plr}\,\omega_{plr} = \eta_{grb}\,M_{mot}\,\omega_{mot} \Rightarrow \begin{cases} \omega_{plr} = \frac{\omega_{mot}}{r} \\ M_{plr} = r\,\eta_{grb}\,M_{mot} \end{cases} \qquad (5.2)$$

We can substitute these results in equation (2.9) that expresses the motor voltage with respect to its speed and torque, and thus obtain :

$$U = r_a\left(i_0 + \frac{M_{plr}}{r\,\eta_{grb}\,k_m}\right) + r\,k_u\,\omega_{plr} \qquad (5.3)$$

As in the case of the motor, the equations show that, assuming a fixed voltage, torque and speed are linearly dependant.

$$\omega_{plr} = -\frac{r_a}{\eta_{grb}\,r^2\,k_m^2}\,M_{plr} + \frac{U - r_a\,i_0}{r\,k_m} \qquad (5.4)$$

$$M_{plr} = -\frac{\eta_{grb}\,r^2\,k_m^2}{r_a}\,\omega_{plr} + r\,\eta_{grb}\,k_m\left(\frac{U}{r_a} - i_0\right) \qquad (5.5)$$

In each of these two equations, there are not three but two variables, as the propeller speed ω_{plr} and torque M_{plr} are linked as seen in figure 5.7. Thus, for a certain motor voltage U and a certain flight speed v, there will be a unique propeller speed ω_{plr}, what leads the to unique torque M_{plr}, power P_{plr} and thrust T_{plr}.

How this was concretely applied for the selection of the motor is explained hereafter. Each combination of the 2600 motors and the gearboxes were simulated in two flight conditions, at start and at level flight. The criteria for the selection were the followings :

- At hand launch, thus at a speed of $5\,\text{m/s}$, the propulsion group should be able to give a thrust higher than $4\,\text{N}$ to ensure a good start. This means the full battery voltage of $33\,\text{V}$ is applied to the motor.

- During level flight at a speed of 8.3 m/s, the propulsion group should be able to provide a thrust of 1.1 N at an overall efficiency higher than 70 %.
- In the two cases, the motor should be able to thermally withstand the power asked.

Each time a combination met these three conditions, it was retained, else it was discarded. The disadvantage of the method is the fact that it is very exhaustive. All possibilities being tested, it is highly improbable to miss a successful combination, but of course, a lot of combinations that would immediately look senseless to an engineer are anyway tested. However, the rapidity of execution makes this point acceptable.

Results of the program

Out of the few possibilities that were retained, the DC motor M118752 from Maxon was found to be the best with an efficiency $\eta_{mot} = 86.8\%$ used with a gearbox of 8:1. This motor was used for the preliminary test of Sky-Sailor but had the drawbacks that it was quite heavy with 130 g and that it heated dramatically at start. Rated at 20 W, it was only capable to withstand the more than 100 W at start during less than 8 s.

In the selection program, many combinations with brushless motors were tested, but despite very good results at start, they suffer from a relatively bad efficiency at level flight. The reason is that in their use in model airplane making, they are often optimized to have a high efficiency at high speed where they are mainly used. For this reason, two brushless manufacturers were asked to build a special motor meeting our needs with an improved efficiency at low speed. Finally, an outrunner from the company RS-Strecker was found to be the best with a reduction ratio of 9:1, leading roughly to the same efficiency as the M118752 but with a weight of 55.3 g only. Also, it is able to withstand the 120 W at start indefinitely, thanks to the cooling that the outrunner configuration gives. Considering this value, its mass to power ratio is 55.3 g/120 W = 0.046 kg/kW, slightly higher than the 0.03 kg/kW predicted.

For the gearbox, a spur gearhead was preferred to a planetary gearhead because of its lower friction and higher efficiency. For both the Maxon and the RS-Strecker motor, individual gearboxes were built with the objective to obtain efficiencies around 97 % at level flight while keeping the weight as low as possible by using thin gears with the inner parts made of aluminum. The use of high quality grease that reduces the friction and that remains on the teeth even after 24 hours operation is also recommended. In the present case, the Molykote YM 103 was used. Finally, the mass to power ratio of the

gearbox is $29.7\,\text{g}/120\,\text{W} = 0.25\,\text{kg/kW}$ which fits very well with the prediction in table 3.4.

5.4.3   Motor Controller

For the first motor which was a DC type, a dedicated motor controller was developed with priority on weight and efficiency. As DC motors are simpler to control, the final controller contained a few components and weighed only 10.5 g. Considering the 120 W it was able to supply, it had a weight to power ratio of 0.087 kg/kW what is in the range of our prediction (table 3.4).

With the RS-Strecker motor, a Jeti Advance 45 Opto Plus brushless controller is used, that can give up to 45 A for a maximum continuous power of 1550 W and a weight of 20 g without the cables. It is of course oversized but in the present case, the efficiency and the reliability of the controller were important selection criteria. In fact, some poor quality brushless controllers may not be able to restart a motor after a power cut-off, which is unacceptable for long endurance flight. Moreover, the high efficiency at around 15 W is more important than saving 10 more grams at a poor efficiency. This efficiency is also depending on the phase shift between the rotor's position and the command signal, a parameter that can be fine tuned with this model. As it was already mentioned in figure 5.6, we see again that there is always a trade-off between efficiency and mass. When we compare the weight prediction of 0.06 kg/kW and the current $0.02\,\text{kg} / 120\,\text{W} = 0.16\,\text{kg/kW}$, it is almost 3 times heavier, because a commercial product was chosen and not modified. However, designing a dedicated controller would make it certainly gain some grams and fit to the model.

Finally, the propulsion group including the motor controller weighs 139 g and considering the 120 W of start, it has a weight to power ratio of 1.15 kg/kW which is 43 % higher than the 0.8 kg/kW predicted for the reasons explained separately here above. Concerning the efficiencies, it was not possible to experimentally measure the value for each element separately. In fact, special instruments are needed concerning the three phases of the controller electronics. For the gearbox and the propeller, input and output torque, speed as well as propeller thrust should be measured in a wind tunnel. However, the power measurements in flight were very close to the calculations which shows that the propulsion group efficiency is close to the 66.6 % predicted.

5.5   Control Surfaces Actuators

The four control surfaces, i.e. the two ailerons and the two parts of the V-tail, are actuated by what is called in the model-making world "servomotors" and often abbreviated "servos". A servomotor has an axis, the angular position of which can be precisely set in a limited range of less than one turn, generally around 90 °. It is composed of a DC motor, a very high reduction ratio gearbox and electronics that steer the motor based on the angle measured with a potentiometer connected to the main axis.

Many products are available on the market, but generally of very poor quality and without any specifications on their reliability during long periods of use. For these reasons, a test bench was built where many servos were tested with the same torque and angle deviation as on the airplane. The current consumption and the temperature were monitored continuously. The worst servomotors broke or saw their temperature dramatically increase after less than 24 hours. The most common reason was the rapid usury of the potentiometer contact that blocked the axis. However, the best products held 20 days without any problems or significant power consumption increase. This was the case of the S100 from Becker, a 13 g coreless servomotor with metallic gearbox, which was used for the ailerons. For the V-tail, two Dymond D47 weighing 4.7 g with plastic gearbox were used. They showed fatigue after seven days but were still the best in this low weight category. Thus, for a 24 or 48 hours flight commercial products can be used after a careful selection, but a one week solar flight would for sure require a special development.

5.6   Battery

As it was demonstrated in figure 4.4, the battery constitutes more than 40 % of the total airplane's mass, even considering the best lithium-ion technology. In our case, the capacity needed is around 200 Wh. During the four years of developments on Sky-Sailor, three batteries were built. The first two packs were made of 48 lithium-ion-polymer cells from the model airplane market. From the first pack to the second, the housing was reduced in order to increase the gravimetric energy density to more than 200 Wh/kg. Since 2005, the battery manufacturers for model airplanes mainly improved the admissible discharge rate and no more the energy density. However, this quest stayed the main objective of computer battery manufacturers, where the cells for the new battery pack used in 2008 were found, leading to a gravimetric energy density of almost 240 Wh/kg.

Table 5.1: Characteristics of the three battery packs built for Sky-Sailor

Pack		2004	2005	2008
Cell name		Kokam 1200	Kokam 1200	NCR 18650
Cell capacity	[Ah]	1.2	1.2	2.9
Cell voltage	[V]	3.7	3.7	3.6
Pack configuration[1]		8S6P	8S6P	8S3P
Nominal voltage	[V]	29.6	29.6	28.8
Nominal capacity	[Ah]	7.2	7.2	8.7
Theoretical energy	[Wh]	213	213	251
Measured energy (charge)[2]	[Wh]	249	249	267
Measured energy (discharge)[2]	[Wh]	233	233	253
Cycle efficiency	[%]	93.5	93.5	94.8
Weight (incl. housing & cables)	[kg]	1.205	1.150	1.056
Energy density[3]	[Wh/kg]	193.4	202.6	239.6

[1] S stands for the number of cells in series, P in parallel
[2] Measurements were achieved with a Schulze ISL 6-430d
[3] Energy density is calculated with the measured energy during discharge

5.7   Solar Generator

5.7.1   Solar Modules

The solar cells used are RWE-S-32 silicon cells from the company RWE Space that have an efficiency of 16.9 % and a weight of 320 g/m^2 at a thickness of 130 μm. Despite their high fragility, they are slightly flexible and constitute an excellent trade-off between highly flexible cells that have a poor efficiency of some percents and very efficient multi-junction cells that are far heavier and cannot be bent. The wing is covered by 216 of them separated equally on the 3 parts of the wing, always in a configuration of 36 in series, 2 times in parallel. This gives a voltage of around 19 V for a current that reaches a maximum of 1.6 A. From the 72 cells that are on each left and right part, 54 are on the fixed wing and 18 cells are located on the moving aileron (Figure 5.1). In total, there are five solar panels, one panel for the middle wing and two for each side wing.

For their integration on the wing, they are encapsulated using a mechanically favorable symmetrical laminate combined with a fiber glass reinforced plastic coating what gives finally five non-reflective highly flexible modules. Figure 5.10 shows a 40 cm sample of these modules that was used for preliminary tests. This encapsulation was realized by Gochermann Solar Technology. The cells cover a surface of 0.51 m^2, which increases to 0.58 m^2 when considering the panels' surface that includes spaces between the cells and on the border. This last value represents 75 % of the wing area. Concerning
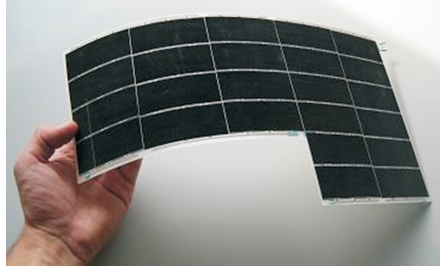
Figure 5.10: Flexible solar module made of encapsulated silicon cells

the weight, this encapsulation adds 91 % of additional weight, which includes not only the plastic films but also all the electrical connections, leading to a total solar modules weight of 313.25 g. At maximum irradiance conditions AM1.5 (at noon in summer with $1000\,\mathrm{W/m^2}$ irradiance, see section 2.3), the available power is around 30 W per third of wing, which offers a total of 90 W.

5.7.2   Integration in the Wing

The solar panels are directly glued on the ribs and the spar, where a special notch with the same thickness was made to ensure a good continuity of the profile. Thus, they constitute, thanks to their flexibility, the extrados of the airfoil. The wing was designed to be very stiff so that the solar panels don't encounter flexion or torsion moments that could potentially break the solar cells. The glue, containing silicon, is especially important as it has to hold very well but at the same time allow small elastic displacements due to torsion. More generally, for all assemblies on the airplane, a correct selection of the glue to use is very important and according to the various locations and materials, different types of glue have to be used, some are even charged with carbon fibers to make it stiffer or others contain special tiny plastic bubbles to save weight.

The electrical connection between the wing and the ailerons is especially important and has to withstand the thousands of deflections during the flights. In the case of Sky-Sailor, it is done using very flexible wires, but for an airplane staying in the air for many weeks or months, the use of metallic hinges should certainly be preferred. For the connections between the three wing parts, special connectors were realized in order to save weight.
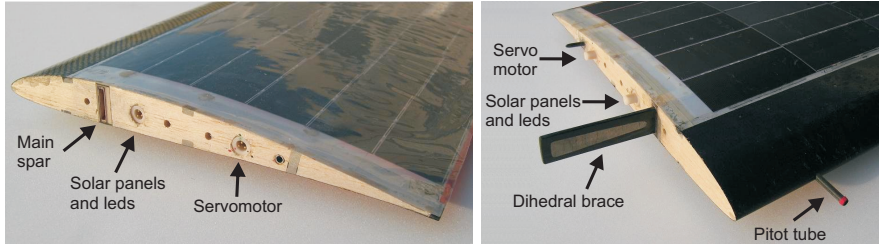
Figure 5.11: Mechanical and electrical connections between the middle and the right part of the wing. On the left image, the panel is covered by a protection film removed just before the flight
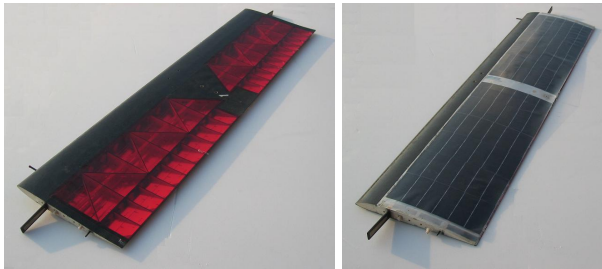
Figure 5.12: Upper and lower side of the middle part of the solar wing

5.7.3 Alternative Solar Cells Integration Possibilities

The other parts of the airplane were not covered by solar cells, first because the surface on the wing was already big enough even taking a margin into account. Additionally, the cells disposed on the fuselage would have a higher risk of breaking at belly landing but also during the hand launched take-off. Also, the small surface, curvature radius and the various orientations (cf. figure 3.4) would give some problems for the design and the efficiency of the panel. On the tail, this would add an additional weight on the rear, considering also the cables along the tail boom, which wouldn't be good in the case of Sky-Sailor in terms of center of gravity adjustment and stability. Also the small surface would make the disposition of the cells, which are large with respect to them, quite difficult. Anyway, for a bigger airplane with runway landing and take-off, this additional solar surface could be an appreciated advantage, especially on a vertical tail that would allow capturing the sun energy more efficiently than the horizontal wing at sunrise and sunset, two

very critical moments for a solar airplane.

Going on with the idea to put solar cells on non lifting surfaces, there have been already a few original concepts where the solar cells are disposed on a flat panel that is oriented actively in order to track the sun and ensure an angle of incidence near $90°$ during the entire day [71,122]. The advantages of this solution are that the power at dawn and dusk is retrieved more efficiently than when having the cells on the wing and that even rigid cells can be used. However, the additional drag, weight and power to track the sun, added to the fact that the airplane is far more sensitive to side winds makes the concepts not so beneficial. Moreover, we saw enough times that the critical part is not the day but the night, where the surplus of weight and drag of such system is especially undesirable.
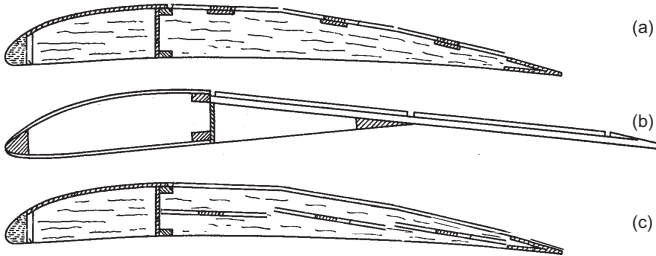
Figure 5.13: Different techniques for the integration of solar cells [38]

When using stiffer cells that cannot be bent enough to follow the wing profile, we can integrate them two different ways. The first solution consists in adapting the airfoil that will contain some straight parts on the extrados, as depicted in figures 5.13a and 5.13b. The problem is then the reduction of the aerodynamic efficiency of the airplane, which is even more reduced if the cells are not covered by a sheet that closes the surface. The second solution is to place the cells on a flat support directly inside the wing, as shown in figure 5.13c. The airfoil properties are then not affected as in the previous case, but the heat caused by the black solar cells, which cannot be evacuated as well as if they were in direct contact with the airflow, can increase the temperature. This reduces their efficiency and it can also lead to deformations of the parts or the cover sheet.

When the airplane wing is molded, we can also directly integrate the solar cells during the process, with or without cover sheet, like in the case of AcPropulsion's Solong shown in figure 5.14. They then follow the airfoil shape very precisely which gives very good aerodynamic properties, but as

Figure 5.14: Integration of the solar cells during the molding process (AcPropulsion's Solong)

explained before, this technique leads to a heavier wing compared to the spar-ribs method.

In all cases, a crucial attention has to be paid to the selection of the cover sheet. In fact, tests showed that using standard sheets used in the model-making world decreases the electrical power given by the cells by 30 % to 40 % because of their reflectivity. The so called solar transmittance is thus between 60 % and 70 %. It is better to use special non-reflective films, like Dupont$^{\text{TM}}$ Teflon$^{\circledR}$ fluoropolymer films that offer a very good transmittance of up to 96 % at a thickness of 50 μm. They are specifically made for flexible photovoltaic panels and offer good mechanical properties and moisture protection over more than 20 years.

In order to increase the power output from the solar panels, we can also use bifacial solar cells, where the lower side of the cells receives the albedo, i.e. the light reflected from the ground. This was the case of the 62 120 cells of Helios. It requires then also to take care of the lower cover sheet, but allows the bifacial modules to produce from 10 % up to 50 % more energy.

5.7.4   Maximum Power Point Tracker

After a survey of the market, no off-the-shelf MPPT seemed to be available, that fitted our application and met our tight requirements. That is the reason why an own MPPT was designed. Five successive versions were built with, at each step, improvements in the direction of dimensions, weight and efficiency.

Hardware

The MPPT is composed of three DC-DC converters with adjustable gain controlled by a microcontroller, put together on a single printed circuit board.

Their inputs are connected separately to each of the three solar panels and
their output is connected in parallel to the battery (figure 5.16). A good
design is necessary to minimize the losses that reduce the efficiency, especially
occurring in the inductor (L1) and the conducting diodes (D1-D4) that were
put in parallel to minimize the individual currents and thus the dropout
voltage [90].
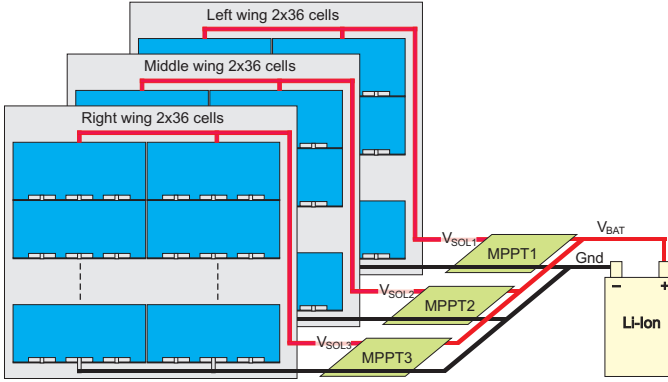
Figure 5.15: Schematic of the solar generator
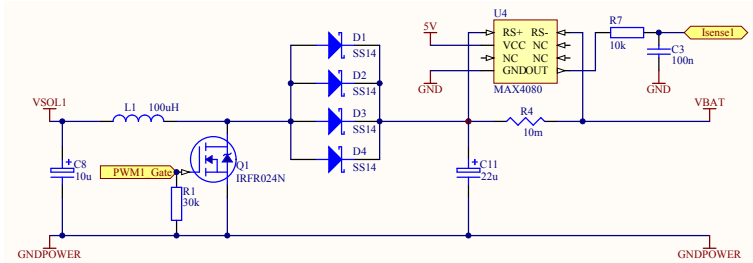
Figure 5.16: DC/DC converter block of the maximum power point tracker for a
single solar panel. The two other blocks and parts like the microcontroller, tem-
perature sensors, MosFet drivers and voltage sensor were omitted here (see [90]).

The high switching frequency of 100 kHz with currents that can go up to
5 A in total can cause electromagnetic interferences that disturb the antennas
present on the airplane. For this reason, a shielding in a special material
named mu-metal covers the board on which the last layer is a ground plane.
The shielding itself is also connected to the ground. The last version of the

MPPT has a measured efficiency between 95 % and 97 %, depending on the power that can go up to 100 W. It weighs 25.86 g yielding a power to weight ratio of 3.87 kW/kg . This is higher than the 2.37 kW/kg predicted with the interpolation in figure 3.10.
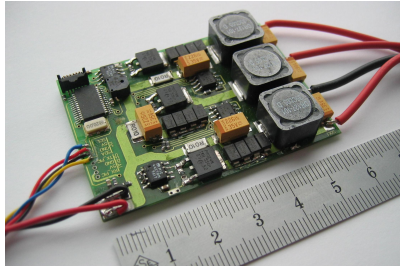
Figure 5.17: Sky-Sailor high efficiency and lightweight MPPT

Software

A "Hill Climbing" method was used for the algorithm. At a frequency of 100 Hz, the current and voltage are measured on the output of each DC/DC converter. The calculated power once compared with the previous value allows changing the gain into the correct direction. This technique was tested and found to be efficient enough to track the maximum power point even when the irradiance conditions change rapidly.

An additional function of the MPPT is to monitor the current and the voltage of each solar module and make that information available for the control and navigation system through an I^{2}C protocol (Figure 5.22). This information is communicated to the interface on the ground control station so that the operator is aware of the energy received from the sun in real-time. According to the efficiency mentioned here above, 3 % to 5 % percent of the solar energy are lost and converted into heat, especially in the diodes, transistors and inductances. Considering the very small surface of the MPPT, this can make its temperature increase up to 110 °C at noon. In order to monitor this effect, two temperature sensors are placed on the printed circuit board and connected to the microcontroller. It is thus possible to react from the ground if necessary by stopping the MPPT or limit the current to a certain threshold.

Experiments

A complete solar charge experiment is presented in figure 5.18. It was realized on the 16th of July 2007 from dawn until the beginning of the afternoon with the second Kokam battery that was almost empty at the beginning of the test. The airplane was not in flight but placed on the ground. We can notice the increasing power until the point where the battery reaches the maximum voltage. The algorithm then holds the voltage constant whereas the power needed to recharge the battery decreases. These two phases are similar to the non solar charge presented in figure 2.12. One can notice that the power curve has some variations due to the non constant sun conditions. Also, due to the dihedral angle of the wing, the 3 MPPTs give different power especially at the beginning of the day. The power dropout at 11h30 represents the shut down function of the MPPT being tested.
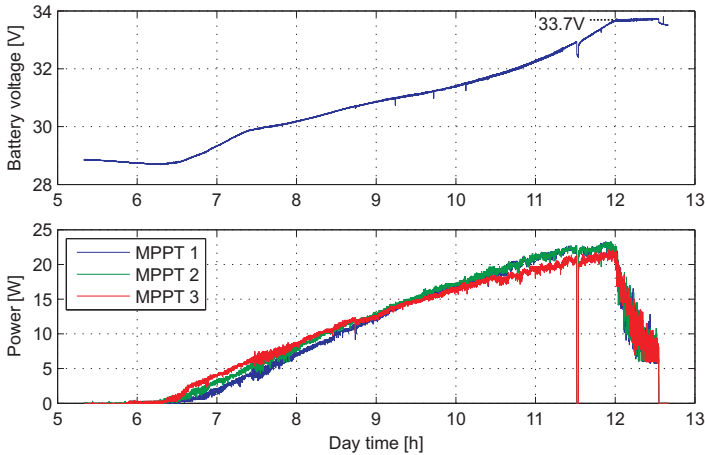
Figure 5.18: Solar charge of the battery with the MPPT

The solar panels didn't give their maximum power of around 30 W each because the highest irradiance occurred at 13 h and at this time, the battery was already full, with a total energy of 232.8 Wh given by the panels. The MTTP temperature reached 110 °C but this value is reduced once the airplane is in flight thanks to the airflow.

5.8   Control and Navigation System

The objective with Sky-Sailor prototype was not only to have an airplane autonomous in terms of energy, but also in terms of navigation and control, requiring an autopilot system. Several products are available on the market, but none met the weight and power requirements offering all the special features that a solar airplanes needs, for example monitoring the power retrieved from the three solar panels.

Thus, a lightweight and low-power consumption autopilot dedicated to our application was designed and built. The system is mainly based on a DsPic33 microcontroller that is interfaced to the various sensors and other electronics boards on the airplane, as depicted in figure 5.19. An external EEPROM memory is used to store various configuration and mission parameters. The choice of the main processor is a trade-off between computational power and electrical consumption. A first approach was to use a single board computer running Linux, but this solution turned out to be far too much power consuming, requiring already 4 W, meaning a third to a fourth of the motor power consumption.

Processor and Sensor Board

The sensor board contains an Xsens MTX inertial measurement unit for the attitude measurement, two absolute and differential pressure sensors for altitude and airspeed and a ultra low power GPS from Nemerix. The GPS offering also speed and altitude information, it could seem useless to add two additional pressure sensors. However, in the case of the airspeed, it is very important to have the relative airspeed and not only the absolute ground speed that is not equal to the first one in case of wind. Also, the GPS offers a low accuracy altitude information at short term but very stable at long term. For the pressure sensor, it is exactly the opposite as the atmospheric pressure changes with the weather conditions. Thus a fusion of those information is an advantage. All these sensors are disposed in the fuselage except the Pitot tube that was installed in the wing on the border of attack and connected electrically to the autopilot. It is also possible to place this sensor on the autopilot board and connect it with at tube to the border of attack, but this solution is heavier. The control, explained in more detail in section 5.11, is entirely done on the DsPic33 that outputs the desired commands to the actuators, i.e. the motor and the servomotors of the control surfaces.
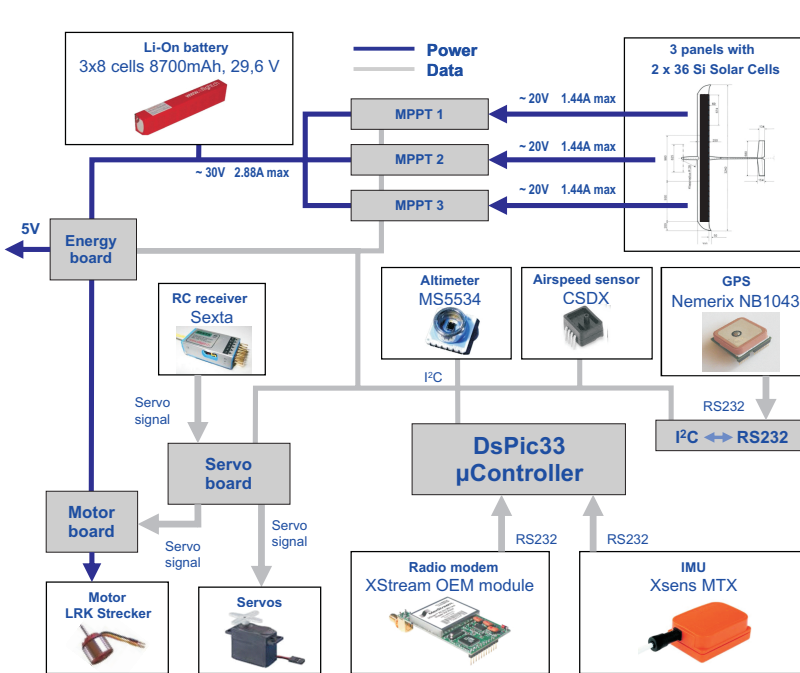
Figure 5.19: Schematic of the autopilot system

Servo Board

This is done through a servo board that receives the digital orders on the I^2C bus and converts them into PWM signals for the servomotors and the motor controller. This board also receives orders from a second source, a standard Sexta 35 MHz RC receiver connected to a remote control in the hands of the operator on the ground. Based on the value of an additional channel coming from the remote control, the board switches from one source to the other. This ability to switch between manual and autopilot mode is necessary for the take-off, landing and during preliminary experiments in order to tune the controller. When the RC remote control is switched of, the mode is on autopilot by default. Normal RC pulses are between 1 ms and 2 ms. Here, we are able to code them from 0.5 ms and 2.5 ms on 10 bits (1024 angular positions) which is useful as in some cases higher angles are desirable and possible to obtain, for the flaps for example.

This board controls also two LEDs located in the winglets that can be switched on or off using the remote control or the user interface. The light

emitted allows locating the airplane during the night and land safely in case of an emergency problem.

Energy Board

Especially for a solar airplane, it is necessary to monitor in real time the energy flows between the solar panels, the battery, the motor and the rest of the electronics. For this purpose, the processor first gets the average power retrieved from the solar panels each second from the three MPPTs. Moreover, the energy board monitors precisely the battery voltage, the current given to the motor, the servos and the onboard electronics.

Communication

The communication between the airplane and the ground is achieved using a MaxStream radio modem operating at frequency of 900 MHz and that acts as a normal RS232 serial link at a baud rate of 9600 bps. The outdoor line-of-sight range with a dipole antenna is maximum 11 km at a power consumption of 400 mW.

Autopilot Subsystems Placement

An important issue in the integration of all these avionics elements is their placement in the fuselage. In fact, the power and digital parts have to be separated, in order to avoid electrical disturbances, especially on the antennas. For this reason, the MPPTs and the energy board are placed in the front, near the motor and its controller. The rear part of the fuselage is occupied by the autopilot.

Also, the choice of cables and wire types is very important and in each case a trade-off needs to be found between thick cables that weigh too much and thin wires that have more risks of breaking if connectors are plugged and unplugged several times. They also have a higher electrical resistance, leading to Joule heat losses when passed by high current as it is between the solar panels, the battery, the MPPT and the motor.

Each second, 750 bytes are exchanged on the I^2C bus between the autopilot board and the various modules. The communication lines from the rear to the front side measuring 50 cm, the bus capacitance is quite high and very rare errors or even communication conflicts can occur. Considering the duration of the tests that exceeds 24 h, the system has to be reliable and robust to such problems. That is the reason why watchdogs were implemented in the different modules that induce a reset in the case of an inactivity of one

Autopilot V2
Electric Schematic &
Registers v 7.0

Power
- Ground
- Battery V+ [24-33.7V]
- Bec V+ [5.6 V]

Digital Electronics
- Ground
- 5V regulated
- 3.3V regulated
- I²C clock line (SCL)
- I²C data line (SDA)
- Other data line (PPM, RS232)

Sky-Sailor Project, A. Noth, Jan 2007

0xA0 — Module address (0x50 in PicWatch)

Addr	r/w	Name	Unit
0xA0		MPPT Temperature1	[°C]
0x22	r	MPPT Tempertaure2	[°C]
0x23	r	Current MPPT 1	[1/100 A]
0x24	r	Current MPPT 2	[1/100 A]
0x25	r	Current MPPT 3	[1/100 A]
0x26	r	Voltage lsb	[1/1000 V]
0x27	r	Voltage msb	[1/1000 V]
0x28	r		
0x29	r/w	Working Mode	
		10 – sleep mode (0x0A)	
		11 – track mode (0x0B)	
		12 – reset mode (0x0C)	
0x2A	r/w	Duty Cycle MPPT 1	[]
0x2B	r/w	Duty Cycle MPPT 2	[]
0x2C	r/w	Duty Cycle MPPT 3	[]
0x2D	r/w	Current limitation	[1/100A]

0x60 — Module address (0x30 in PicWatch) [Internal Unit]

Addr	r/w	Name	Unit
0x60		Pressure lsb	[IntU]
0x22	r	Pressure msb	[IntU]
0x23	r	Raw pressure lsb	[IntU]
0x24	r	Raw pressure msb	[IntU]
0x25	r	Pressure offset lsb	[IntU]
0x26	r	Pressure offset msb	[IntU]
0x27	r	Speed lsb	[1/100 m/s]
0x28	r	Speed msb	[1/100 m/s]
0x29	r		
0x2A	r/w	Melody	
		1 – waiting gps	
		2 – gps fixed	
		3 – Do-Ré...Do	
		4 – Music	
		11-19 Warning nr 1-9	
0x2B	r/w	Reset Pressure 1 – reset 0 – else	
0x2C	r/w	Sensor Type	
		10 – DSDX (0x0A)	
		11 – CSDX (0x0B)	

0x80 — Module address (25Hz) (0x40 in PicW)

Addr	r/w	Name	Unit
0x80		Voltage batt lsb	[1/1000 V]
0x22	r	Voltage batt msb	[1/1000 V]
0x23	r	Voltage bec lsb	[1/1000 V]
0x24	r	Voltage bec msb	[1/1000 V]
0x25	r	Current motor lsb	[1/1000 A]
0x26	r	Current motor msb	[1/1000 A]
0x27	r	Current servo lsb	[1/1000 A]
0x28	r	Current servo msb	[1/1000 A]
0x29	r		

0x40 — Module address (0x20 in PicWatch)

Addr	r/w	Name	Unit
0x40		Pressure lsb	[1/10 mbar]
0x22	r	Pressure msb	[1/10 mbar]
0x23	r	Temperature lsb	[1/10 °C]
0x24	r	Temperature msb	[1/10 °C]
0x25	r	Altitude lsb	[1/10 m]
0x26	r	Altitude msb	[1/10 m]
0x27	r	Error	
0x28	r	Time hour	[hr]
0x29	r	Time minute	[min]
0x2A	r	Time second	[sec]
0x2B	r	Latitude degree	[deg]
0x2C	r	Latitude minute	[min]
0x2D	r	Latitude 10000th lsb	[1/10000 min]
0x2E	r	Latitude 10000th msb	[1/10000 min]
0x2F	r	Latitude direction	[N/S]
0x30	r	Longitude degree	[deg]
0x31	r	Longitude minute	[min]
0x32	r	Longitude 10000th lsb	[1/10000 min]
0x33	r	Longitude 10000th msb	[1/10000 min]
0x34	r	Longitude direction	[E/W]
0x35	r	Satellite fix 1=ok, no fix=0	
0x36	r	Number of satellite	
0x37	r	Altitude GPS lsb	[1/10 m]
0x38	r	Altitude GPS msb	[1/10 m]
0x39	r	Speed GPS lsb	[1/100 m/s]
0x3A	r	Speed GPS msb	[1/100 m/s]
0x3B	r	Heading lsb	[1/10000 rad → North]
0x3C	r	Heading msb	[1/10000 rad → North]
0x3D	r	New data ready 1=new data, old=0	
0x3E	r/w		

0x20 — Module address (0x10 in PicWatch)

Addr	r/w	Name
0x20		RC Signal no signal = 0, signal = 1
0x22	r	Signal source RC=0 AP=1
0x23	r	LED switch OFF=0 ON=1
0x24	r	RC receiver channels 1to8 + 2
0x30	→	Value is between 0-1024
0x39		channel 5 is RC/AP switch
0x40	r/w	Autopilot channels 1to8 + 2
0x49		Value is between 0-1024

Block labels: Radio-Modem 900 Mhz · FILTER · Autopilot Board · Multi Purpose Pic module · GPS Altitude module · FILTER · StepDown 3.3v · LDO 5V · ServoBoard · FILTER · RC Receiver 35 Mhz · Energy Board · LDO 5V · BEC · FILTER · Li-Ion Battery · MPPT 100 kHz · Motor Controller 100 kHz · No Mass to avoid current loop

Figure 5.20: Autopilot electric schematic and registers

Figure 5.21: Placement of the elements

second. This traffic was also found to be a source of interferences for the 35 MHz RC receiver, degrading significantly the range between this latter and the remote. Ferrite beads and capacitors were used to clean the different lines and stop interferences with success.

Power Consumption

An important criterion for the choice of the various components of the autopilot system was low power consumption. As they all require either 5 V or 3.3 V, we need a step-down converter to obtain this voltage from the battery that varies between 26 V to 33.7 V. The conversion efficiency is thus an important parameter that has to be taken into account. The solution retained was to use first a commercial step-down converter that lowers the voltage to a fixed 5.6 V. It is called battery eliminator circuit (BEC) and is used to power servomotors that can have very sudden high current demands. Its efficiency depends on the current and reaches 65 % for the present case, according to measurements. From these 5.6 V a low dropout regulator (LDO) is used to obtain the 5 V. For the 3.3 V, a DC/DC converter was designed in order to have a good efficiency despite the high dropout.

Table 5.2 presents an overview of the power consumption of all the different parts of the autopilot system at the level of the BEC. Finally, the power consumption of the avionics is 1.313 / 65 % = 2.02 W at the battery level. This value was verified by measurements. At that point, we also have to add the power consumption of the servomotors. It varies significantly depending on

Table 5.2: Power consumption of the avionics subsystems

Device	Voltage	Current	Power	η_{conv} from 5.6V	Power @ BEC
	[V]	[mA]	[mW]	[-]	[mW]
Radio Modem (XStream)	5	80	400	89 %	449
IMU (Xsens MTX)	5	70	360	89 %	404
CSDX (Sensortechnics)	5	7	35	89 %	39
Pic16F876-Autopilot	5	7	35	89 %	39
Pic16F876-Energy Board	5	7	35	89 %	39
MS5534 (Intersema)	3.3	1	33	92 %	36
GPS (Nemerix NB1043)	3.3	20	66	92 %	72
DsPic33-Autopilot	3.3	27	99	92 %	108
DsPic33-Servoboard	3.3	27	99	92 %	108
Pic16LF877-Autopilot	3.3	5	17	92 %	18
Total			**1.179**		**1.313**

the atmospheric disturbances that require corrections to be done in order to
follow the trajectory. What also influences this value is whether the airplane
is remotely piloted or flies autonomously. Whereas a pilot has the tendency
to give discrete corrections, the autopilot sends new orders to the servomotors
at a high rate which can need more power in windy conditions. However, an
average power consumption of 0.6 W at the level of the BEC was measured.
Hence, it has to be added to the total power consumption in table 5.2.

5.9   Ground Control Station

The user can interact with the airplane using the ground control station
(GCS) composed by a graphical user interface (GUI) and the bidirectional
radio modem for communication. The state of the airplane during flight
is monitored and a visual feedback is given with virtual instruments and a
3D representation on a terrain map. The user can tune the controller by
editing its parameters while the airplane is airborne, and also send high level
commands to modify the trajectory. Additionally, the current, voltage and
power retrieved from each panel, the power consumption of the motor and
the charge status of the battery are represented graphically (Figure 5.22).

For security, all commands coming from the ground are validated by the
autopilot to the GCS again. Also, in case of communication losses, abnormal
attitude or GPS problems, the interface warns the user so that he can quickly
act according to the problem by controlling it with the remote control.
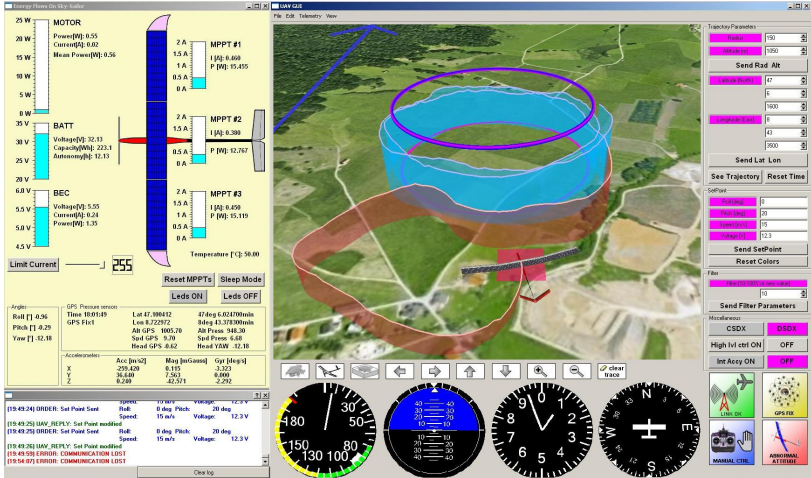
Figure 5.22: Graphical user interface of the ground control station. The experiment represented on the 3D view shows an autonomous flight (blue) followed by a landing in manual mode (red)

5.10   Final Prototype

Along the different phases of the project, two fully functional prototypes were built and tested. They only differed by the fact that the first one didn't embed any solar cells but was covered instead by a sheet with exactly the same weight. This model was used during the first experiments where the goal was to validate the aerodynamics, the flight behavior, the autopilot systems, the different sensors and to tune the controller for the autonomous flight. In parallel, the second prototype, this time with solar panels, was built. The experience gained with the first one was used to improve the efficiencies and decrease as much of the total weight as possible. This was done for example by removing housings, like in the case of the IMU and the RC receiver, changing heavy coaxial connectors and cables with thinner versions and taking off the plastic cover of the radio-modem antenna. This zero tolerance approach against parasitic weight is really crucial and leads to important savings once all the efforts summed up. The resulting total mass during the last experiments in the end of June 2008 was 2.444 kg, with a weight distribution that is presented in table 5.3. As discussed separately along this chapter when presenting the various elements, the weight prediction models fit quite well with the real data. The final version of Sky-Sailor is shown in figure 5.23.

Table 5.3: Weight distribution of the airplane elements and comparison with the predicted values (figure 4.4)

Part	Dimensions [mm]	Mass [g]	Predicted [g]	Δ m [%]
Autopilot sensor board	127 x 33 x 8	8.37		
IMU	48 x 33 x 13.5	15.00		
GPS & patch antenna	25 x 22 x 8	10.96		
On/Off Switch	23 x 14 x 13	4.85		
Energy board (incl. BEC & shield)	65 x 24 x 6	17.70		
Servoboard	42 x 24 x 8	6.51		
RC Receiver	47 x 19 x 10	9.80		
RC Receiver Antenna	1000	1.30		
Radio Modem & Antenna	75 x 40 x 11	26.48		
Cables		60.32		
Avionics system		**161.30**	**150**	**+7.5 %**
Wing part middle	980 x 250 x 25	196.10		
Wing part left (incl. servos)	1130 x 300 x 25	161.60		
Wing part right (incl. servos)	1130 x 300 x 25	167.10		
3 Wing Screw M4		0.95		
Fuselage with tail boom	1720 x 94 x 54	168.85		
2 V-tails	41.5 x 15.5 x 1.2	54.00		
Airframe		**748.60**	**870**	**-14.0 %**
Li-Ion battery	283 x 60 x 33	**1056.00**	**1030**	**+2.5 %**
Solar panel middle	980 x 202 x 0.4	105.90		
Solar panel left	937 x 208 x 0.4	104.40		
Solar panel right	937 x 208 x 0.4	102.90		
Solar panels		**313.20**	**305**	**+2.7 %**
MPPT + shield	42 x 42.5 x 9	**25.86**	**32**	**-19.2 %**
Motor Controller	52 x 25 x 10	20.00		
Brushless motor (Strecker)	Ø30 x 25	55.30		
Gearbox	Ø33 x 29	29.70		
Solariane Propeller & support	600	34.05		
Propulsion group		**139.05**	**113**	**+23.5 %**
Total take-off mass (21.06.2008)	3240 x 1818 x 295	**2444.00**	**2500**	**-2.2 %**
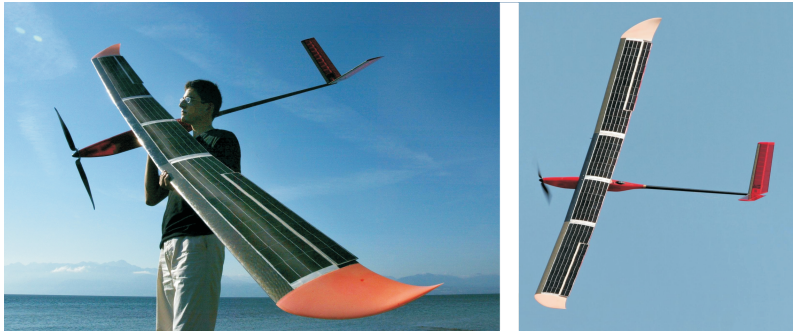
Figure 5.23: The Sky-Sailor prototype held by the author and during a flight

5.11   Modeling and Control

In the case of autonomous aerial robots, where a failure or a crash is fatal for the platform, the ability to simulate and tune a controller before implementing it on the real machine is very important. That is the reason why a mathematical model of the Sky-Sailor was developed in Matlab® using Lagrange-Euler formalism [92].
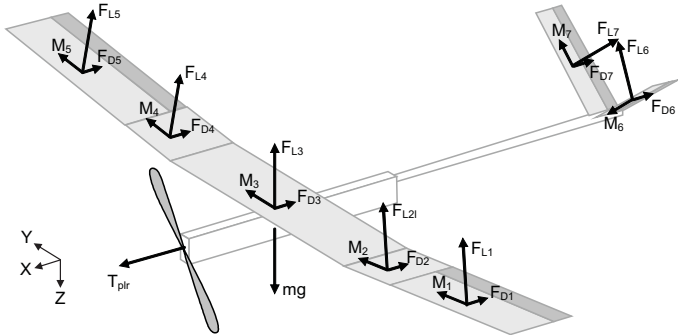
Figure 5.24: Modeling the Sky-Sailor

The aircraft is first cut into subparts, as shown in figure 5.24 where the forces acting on the airplane are represented, i.e. the weight located at the center of gravity, the thrust of the propeller in the forward direction and the aerodynamic forces, i.e. lift and drag, of the seven subparts of the wing and the V-tail. The sum of non-conservative forces and moments are :

$$F_{tot} = F_{plr} + \sum_{i=1}^{7} F_{Li} + F_{Di} \tag{5.6}$$

$$M_{tot} = \sum_{i=1}^{7} M_i + F_{Li} \times r_i + F_{Di} \times r_i \tag{5.7}$$

These are depending on the relative airspeed, the angle of attack and the angle of the control surfaces, i.e. the ailerons, elevator and rudder. The moments are the aerodynamic moments and those induced by forces acting at a certain distance of the center of gravity. The final model was developed and implemented on Matlab® where it was validated with real experimental data. Typical effects like induced roll due to a yaw rotation can be observed.

$$\begin{cases} F_{plr} = f(\dot{x}, U_1) \\ F_{Mi} = C_{Li} \frac{\rho}{2} S_i v^2 \\ F_{Di} = C_{Li} \frac{\rho}{2} S_i v^2 \\ M_i = C_{Mi} \frac{\rho}{2} S_i v^2 \, chord_i \end{cases} \tag{5.8}$$

$$\begin{cases} [C_{L1} \; C_{D1} \; C_{M1}] = f(Aoa_1, U_2) \\ [C_{Li} \; C_{Di} \; C_{Mi}] = f(Aoa_i) \;\; | \;\; \text{for i} = 2, 3, 4 \\ [C_{L5} \; C_{D5} \; C_{M5}] = f(Aoa_5, U_3) \\ [C_{L6} \; C_{D6} \; C_{M6}] = f(Aoa_6, U_4) \\ [C_{L7} \; C_{D7} \; C_{M7}] = f(Aoa_7, U_5) \end{cases} \tag{5.9}$$

The controller is constituted by two different parts, an inner loop the role of which is to keep the stability of the system and an outer loop used to plan and follow the trajectory [79]. For the low level, an optimal linear state feedback control method, namely a Linear Quadratic Regulator is used. It is based on the dynamic model explained above. For the high level part, the choice was to adapt an algorithm proposed and tested for the path tracking of a non-holonomous robot [39]. After simulation with the airplane dynamic model, the final controller shows to be very robust in various conditions. Other simulation environments were used to test the controller, like the Matlab® Aerospace Blockset and the excellent flight simulator X-Plane where the airplane was modeled. The objective of this thesis being not to focus on the control part, the reader can read on about this subject in [79].
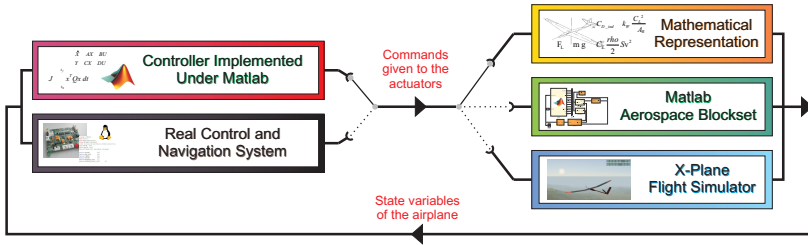
Figure 5.25: Control simulation environment with hardware in the loop

5.12   Flight Experiments

More than 50 flight experiments were realized with the two Sky-Sailor prototypes with a total of more than 100 hours in the air. They all took place at different locations in Switzerland and always at an altitude of around 200 m

AGL, for security and legal reasons. At first, it was with the non-solar version but once the many elements on the airplane validated and fully tested, the final solar powered prototype was flown. The individual tests will not be described in detail, but the most important results and lessons learned will be summarized.

The first experiments had the objective to validate the power needed for level flight. The theoretical values in figure 5.6 were verified only during one or two tests after sunset, when the air was extremely calm. With a wing loading of $3.22\,\mathrm{kg/m^2}$, the airplane is very sensitive to the smallest turbulence and even during a calm day, the air is never completely still. That is why the power required to stay at the same level during the day was always 10 to 20 % higher than the theoretical value of $14.2\,\mathrm{W}$ electrical power.

Many settings were also crucial before the flight. The center of gravity, which one can adjust by moving heavy parts such as the battery, has to be precisely located at the millimeter, $100\,\mathrm{mm}$ from the border of attack. Also coincidence of the propeller axis with the flight axis and the zero positions of all control surfaces were to be verified in order not to create parasitic drag.

Concerning the autopilot system, some sensors clearly showed their limitations during the autonomous flights. The inertial measurement unit, for example, showed difficulties to give a correct roll information when the airplane was in a curve. Also the GPS sensor not featuring an active but a passive antenna in order to save energy occasionally encountered some loss of signal when under alto stratus clouds.

5.12.1 Continuous 27 h Solar Flight

From the 20th to the 21st of June 2008, a continuous solar flight of more than 24 hours was attempted. It took place in Niederwil, Switzerland at a take off altitude of $430\,\mathrm{m}$ above sea level. The irradiance was very good, but the conditions were quite turbulent with wind. The airplane was launched at 12h33 with a 60 % full battery in order to ensure a safe launch. During the afternoon, the half square meter of solar cells gave enough energy to power the motor and at the same time completely charge the battery, while the airplane was following a circular trajectory at $200\,\mathrm{m}$ above ground. Figure 5.26 shows the battery status and as well the solar power available.

During the afternoon, the wind conditions were quite difficult, with sporadically strong upwind and downwind. As the airplane's objective was to stay between $200\,\mathrm{m}$ and $400\,\mathrm{m}$ AGL, the power given to the motor was here set manually to stay in this range, which can be seen depicted in figure 5.27. At around 18h, the decreasing solar power was not high enough to supply the
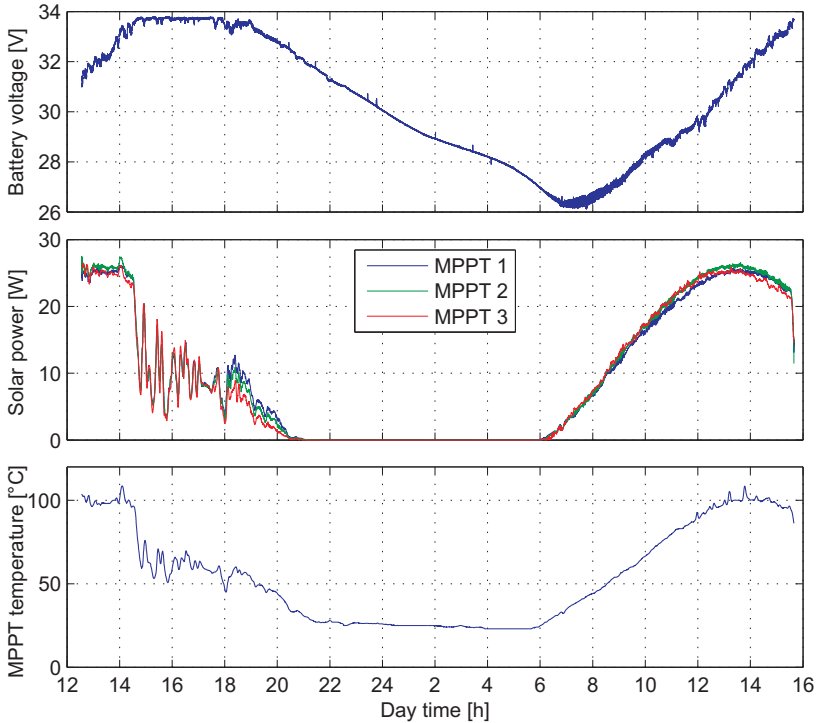
Figure 5.26: Evolution of the battery voltage, the power supplied by the solar panels and the MPPT temperature during the 27 h flight

motor and the onboard electronics, the battery then slowly started its discharge. In the evening, the wind conditions got slowly better what is proven on 5.28 by the fact that the relative air speed and the ground speed began to be very close, whereas there were a lot of variations during the day. From 23 h until the morning, the airplane was able to fly with the minimum power. It is also interesting that also the power needed for the servomotors decreased significantly.

In the early morning at 6h10, the solar panels started progressively to supply power again. Only one hour later, they gave enough energy to supply the motor and the avionics entirely, but also to charge the battery that still had 5.8 % of capacity. The morning saw again turbulent atmospheric conditions which required more power to the motor and led to a longer battery charge. However, at 15h35 on Saturday 21st, the battery was completely full,
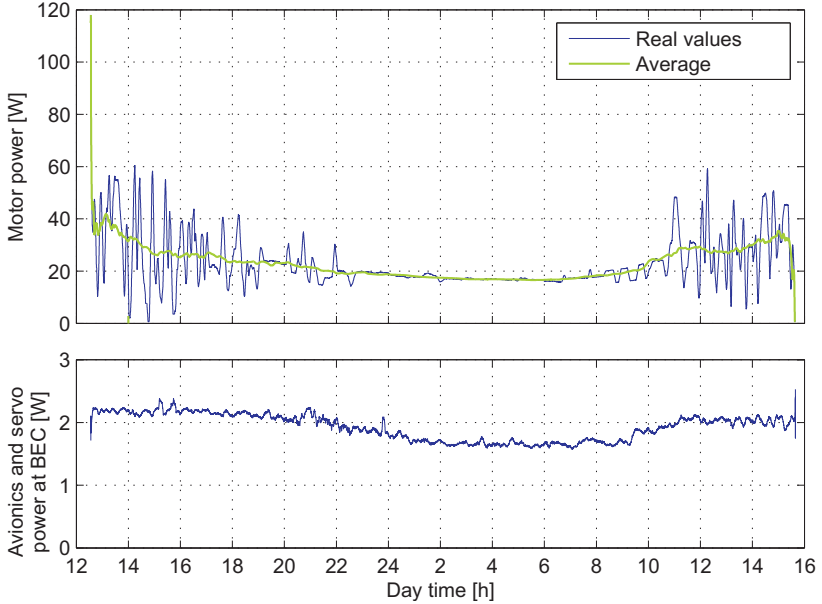
Figure 5.27: Evolution of the power required by the motor and the avionics during the 27 h flight. We can observe a reduction of the power required for the motor and the servomotors during the calm night.

ready for a new night cycle. That proved the feasibility of continuous flight using solar energy only. The airplane landed some minutes later after a flight of more than 27 hours.

With an average speed of 32.3 km/h (8.97 m/s), it covered more than 874 kilometers. The flight was achieved at 98.9 % in autonomous mode. In fact, the launching and landing phase were remotely piloted and the motor's throttle was given manually in some cases like strong upwind. At start, 120 W were needed in order to ensure a safe launch but the mean power required during the entire experiment was 23 W for the motor and 1.93 W for the avionics and the servos at the level of the BEC. During this cycle, the total energy used was 675 Wh whereas 768 Wh were obtained from the solar panels.
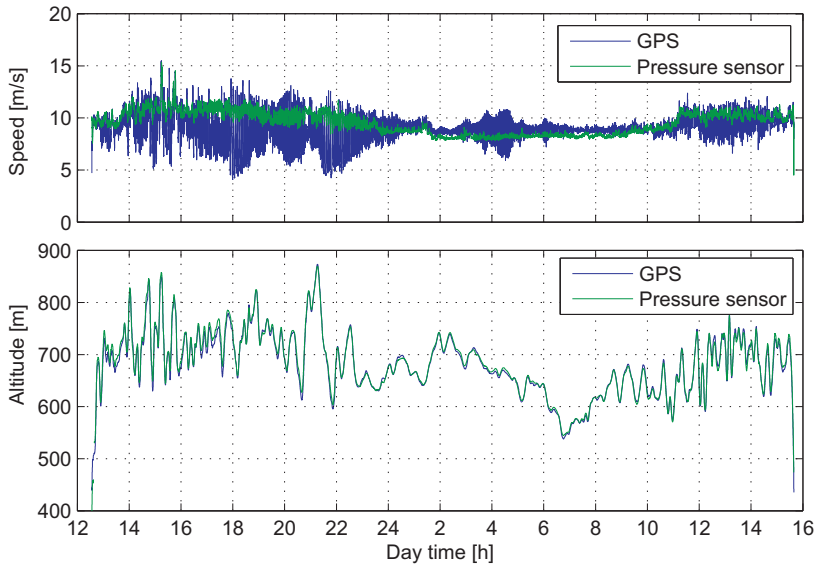
Figure 5.28: Evolution of speed and altitude during the 27 h flight. The high variations between the ground speed given by the GPS and the airspeed given by the pressure sensor show clearly the wind speed during the experiment.

Chapter 6

Scaling Considerations and Other Designs

6.1 Introduction

After having shown one application of the methodology that was validated through the realization of a prototype, this chapter aims at presenting additional designs at different scales, in order to emphasize the portability of our methodology, but also the limitations of solar power when scaling up or down.

Thus, we will see how to adapt the methodology to take care of such special cases and still be able to use it to help finding the layout of a future airplane. The cases of solar micro aerial vehicles, manned solar airplanes and high altitude long endurance platforms will be presented. Moreover, we will also treat special airplanes or flight configurations that could enhance the flight duration, such as using altitude to store potential energy or use swiveling solar panels to track the sun.

6.2 Scaling Down : Solar Micro Aerial Vehicle

With the miniaturization of processors, sensors and communication chips, the development of efficient robotic platforms is not only possible at the UAV size, but also at the MAV size, i.e. for aircrafts with a span of less than 6 in (15.24 cm) and a mass of less than 100 g [65]. Several projects have been started in the two last decades in this domain with various study goals, such as aerodynamics, system design, obstacle avoidance, bio-inspired algorithms,

etc. But unfortunately what all these prototypes have in common is a poor endurance that rarely exceeds 15 to 20 minutes.

A solution to expand this endurance for MAVs is the use of solar energy. With solar cells integrated in their structure, they would be able to acquire energy from the sun and use it for flight propulsion, the eventual surplus being stored for higher power demands.

6.2.1   Scaling Down Advantages and Drawbacks

In the last chapter, we saw the application of the methodology with a validation at the UAV size, but now one might wonder how the feasibility of solar flight evolves when scaling down. The analytical character of the design method and its mathematical models allow investigating these scaling issues on the different airplane parts, which will be the subject of the following subsections.

Airframe

The airplane structure is the only part that scales down in a favorable manner. In fact, as presented in figure 3.7, its weight is proportional to the cube of a reference length, the wingspan for example, and this law is a great advantage at small size. In fact, dividing the wingspan by a factor of 2 reduces the surface, and thus the solar power, by 4 but the weight of the structure by 8.

Additionally, the structure stiffness and the stress related to the mass scale linearly with the reference length. This is a great advantage for smaller systems which are intrinsically more robust against destruction forces related to their own mass. Also, an MAV has a much better chance to survive a free fall than a big airplane because of the increasing ratio between air drag and mass. Nature gives us a nice example that illustrates this principle; an ant easily survives a fall from a multi floor building whereas the elephant is seriously hurt when falling from around one meter [41].

Low Reynolds Number Airfoil and Propeller

Unfortunately, there are many problems occurring when scaling down. On the aerodynamic side, it is well known that the lift to drag ratio decreases significantly for Reynolds number smaller than 10^5 (Figure 6.1).

That is basically why natural selection made the smallest birds and insects flap their wings, in order to increase Reynolds number, instead of gliding. Whereas the lift to drag ratio of the 3.2 m wingspan Sky-Sailor is around 24,
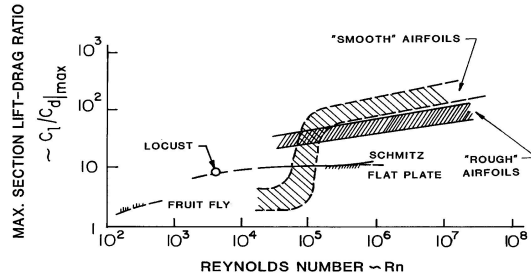
Figure 6.1: Low Re number performance of smooth and rough airfoils [81]

this value decreases dramatically to 6 for both the Black Widow of AeroVironment [65] and the 2 g Glider of UC Berkeley [129], both in the MAV category.

This low Reynolds number effect is negative for the main wing airfoil, but also for the propeller that sees its efficiency decrease dramatically. The measured propeller efficiency of the SunBeam, a 50 cm solar MAV [111], was 58 %, which is far away from the 85.6 % of the Sky-Sailor. For the 56.5 g Black Widow, it was clear for the builders at the beginning that an off-the-shelf propeller would lead to a poor efficiency. That is the reason why they designed and molded an optimized propeller with a reported measured efficiency of 80 % [65].

Actuators

Going on with the propulsion group, the scaling down of electromagnetic motors is not favorable either. The study of more than two thousand motors, presented in section 3.4.6 showed clearly that even if we can consider the mass to power ratio as constant for good quality motors, the efficiency tends to drop dramatically below 1 W. Moreover, the control electronics of the brushless models is slightly more complicated than for the normal DC motors.

Here again, this is confirmed by the Black Widow that has a motor-gearbox efficiency of 50 %. This leads to a propulsion group efficiency of 40 %. It emphasizes the fact that a very important point is the correct matching between motor, gearbox and propeller. Unfortunately, the market proposes far more products for the UAV than for the MAV range. It is thus even more difficult to find a good matching. The only solution remains to design and build a dedicated motors, gearboxes and propellers that fit perfectly to MAV applications.

For very low power, it seems that piezoelectric actuators could play an important role as their efficiency, poor compared to traditional electromagnetic motors at big dimensions turns out to be higher at low dimensions [125]. However, their command requires high voltages which induces more complex and heavier control electronics. But this technology was already demonstrated with success on the EPSON micro-helicopter [2].

Concerning the actuation of the control surfaces, servomotors are generally used for UAVs, but at the MAV size, it is more difficult to find lightweight and still reliable products. Other elegant solutions are the use of magnet-in-a-coil actuators [132] or shape memory alloys [73].

Solar Cells

Solar cells don't scale with the cube of the reference length but with the square. In fact, when reducing the wing surface of an MAV, less cells are used but the thickness remains the same. Their weight percentage then increases compared to the total MAV mass. Another problem is that scaling down an airfoil decreases its curvature radius, making it far more difficult to install the fragile cells on a cambered wing.

A solution to this problem is to place them flat inside the wing, closing the profile with a transparent sheet, as it was presented in figure 5.13. This latter has to be non-reflective, unless it induces additional losses. Highly-flexible solar cells (FlexCell, PowerFilm) can be applied on low curvature radius airfoils, but do not currently have high enough efficiency to be considered for continuous solar flight. They can however be used on an MAV that can recharge its batteries on the ground between two flights [59].

Maximum Power Point Tracker

The MPPT is responsible for interfacing the battery with the solar panels ensuring that they work at the maximum power point. Its efficiency also decreases at low dimensions where the operating voltage is reduced. This loss is due to the diode dropout voltage, which is 0.4 V for good schottky diodes. In the case of the Sky-Sailor that has a battery voltage of 30 V, this is not critical, but on an MAV powered by a single lithium-ion cell at 3.7 V, this means a loss of 11 %. This is the reason why in some low voltage designs, the solar cells are directly connected to the battery, choosing the number of solar cells in series so that their maximum power point voltage corresponds to the battery's nominal voltage.

Energy Storage

On the side of energy storage, high gravimetric energy density lithium-ion or lithium-ion-polymer cells are not easily scalable. Current battery technology is driven by the market of mobile devices, thus the cells with the best energy to mass ratio are always of the "18650" type, a standard size in portable computer battery pack. One cell weighs around 45 g, which is not a problem for a large airplane using a multiple of them, but for tiny MAVs, one unit is already too heavy. The only choice is then to select tiny batteries where the mass percentage of the housing is higher, which inevitably reduces the gravimetric energy density.

Control

If the MAV is aimed at being autonomous, the development of a navigation and control system becomes very critical at small scales, especially on the sensor side. It is no longer possible to embed GPS or IMU, the smallest of these two devices currently weighing around 10 g including the antenna for the GPS. Also the power consumption of the sensors and the communication cannot stay constant but has to be reduced, which means lower communication range. Hence, the expectations concerning the control capabilities have to be reduced. This limitation forces engineers to develop lightweight and power efficient devices to sense the environment, taking inspiration from nature like Zufferey et al. who used optical flow to avoid walls [132].

Also, the control of such MAVs itself is more difficult as they are more dynamic than larger UAVs. In fact, if we consider the angular acceleration formula $M = I\alpha$ and an airplane with a reference length l, the following reasoning can be made; moments on the airplane are the product of length and aerodynamic forces :

$$M \sim l\,F \sim l\,S\,v^2 \sim l^3\,v^2 \tag{6.1}$$

In order to find how the speed scales with the reference length, we can use the lift force and put it into equality with the weight, obtaining the flight speed at level flight

$$v = \sqrt{\frac{2\,m\,g}{C_L\,\rho\,S}} \sim \sqrt{\frac{l^3}{l^2}} \sim \sqrt{l} \tag{6.2}$$

Substituting equation (6.2) in (6.1) shows clearly that $M \sim l^4$. Concerning the inertia, we know that

$$I \sim m\,l^2 \sim l^5 \tag{6.3}$$

Considering again the angular acceleration formula, we can write

$$\alpha = \frac{M}{I} \sim \frac{l^4}{l^5} \sim \frac{1}{l} \tag{6.4}$$

This result proves that the smaller an aerial vehicle is, the more dynamic it will be. Consequently in the case of MAVs, it tends to be more difficult to maintain a constant angle of attack and thus stay at an optimal angle where an aerodynamic characteristics like the lift to drag ratio is the highest.

6.2.2   Application Example on a Solar MAV

After having seen the many problems occurring when scaling down a solar airplane, we will try to adapt the parameters that were used for the Sky-Sailor to the MAV size. Basically, the aerodynamics coefficients quality is reduced, as well as the propulsion group efficiencies. The new values were taken from the SunBeam and the Black Widow case studies. The induced drag is taken into account this time with an Oswald factor of 0.6. Concerning the airframe weight prediction, the mean interpolated model of figure 3.8 is considered instead of the 5 % model. The reason is that the control being more dynamic and difficult as explained in section 6.2.1, the structure has to be able to withstand potential bad landings. Of course, the mission objectives are also reduced in terms of payload mass and power, as well as the avionics system.

Using these new parameters, the first result is that it is impossible to find a configuration that can fly continuously over 24 hours in the MAV size, even without payload in summer. This accomplishment is already a real challenge at the UAV size, thus with the lower efficiencies and aerodynamic problems at MAV size, this infeasibility becomes understandable.

6.2.3   Methodology Adaptation : Day Flight Only

The methodology can be slightly modified to design an airplane that flies only during the day. For this purpose, we can set $T_{night} = 0$ and give T_{day} any value higher than zero. A quick look at figure 3.17 to see the influence of this modification shows that no battery will be considered and that the area of solar cells will be lower, which is logical as no battery needs to be charged during the flight. In this case when we consider a mean irradiance, the value of I_{max} has to be multiplied by $\pi/2$ because it was divided by the same value to obtain the mean irradiance on an entire day, as written in equation 3.8.

Table 6.1: Parameter changes at the MAV size

Parameter	Value	Unit	Description
C_L	0.5	-	Airfoil lift coefficient
$C_{D\,afl}$	0.05	-	Airfoil drag coefficient
e	0.6	-	Oswald's efficiency factor
k_{af}	5.58/9.81	$[kg/m^3]$	Structural mass constant
m_{av}	0.005	$[kg]$	Mass of autopilot system
η_{grb}	0.81	-	Efficiency of gearbox
η_{mot}	0.62	-	Efficiency of motor
η_{plr}	0.80	-	Efficiency of propeller
P_{av}	0.1	$[W]$	Power of autopilot system
x_1	3.18	-	Airframe mass wingspan exponent
x_2	-0.88	-	Airframe mass aspect ratio exponent
m_{pld}	0.01	$[kg]$	Payload mass
P_{pld}	0.00	$[W]$	Payload power consumption

The results presented in figures 6.2 and 6.3 show that the minimum airplane wingspan is around 30 cm for a speed between 6 to 8 m/s. An MAV has generally been defined as having a span of less than 6 in (15.24 cm), and a mass of less than 100 g, so even choosing the solution with 30 cm, it cannot be considered an MAV [65]. It is also not wise to make a selection at the limit of the solution domain because a small change in one of the models, for example a slightly heavier airframe, would cause the solar MAV not to reach the objectives anymore (Figure 6.2). Also, an airplane with a very low aspect ratio like the black widow will have more agile dynamics around the roll axis than with a high aspect ratio. Taking this into account and considering a low speed as selection criterion, a nice solution would be an airplane with an aspect ratio of 10 and a wingspan of 80 cm (Figure 6.4).
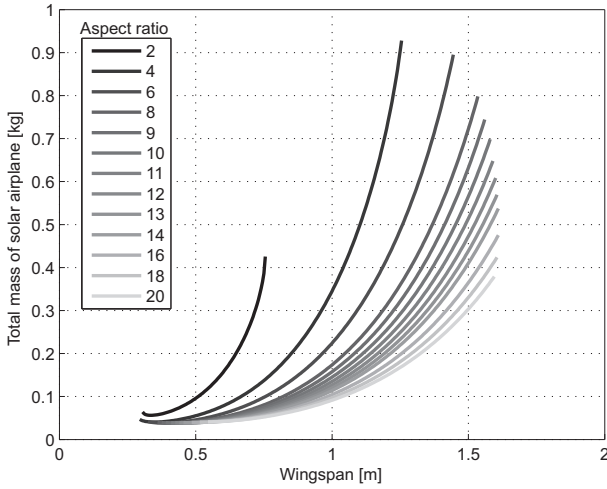
Figure 6.2: Possible configurations for a solar mini UAV depending on b and AR
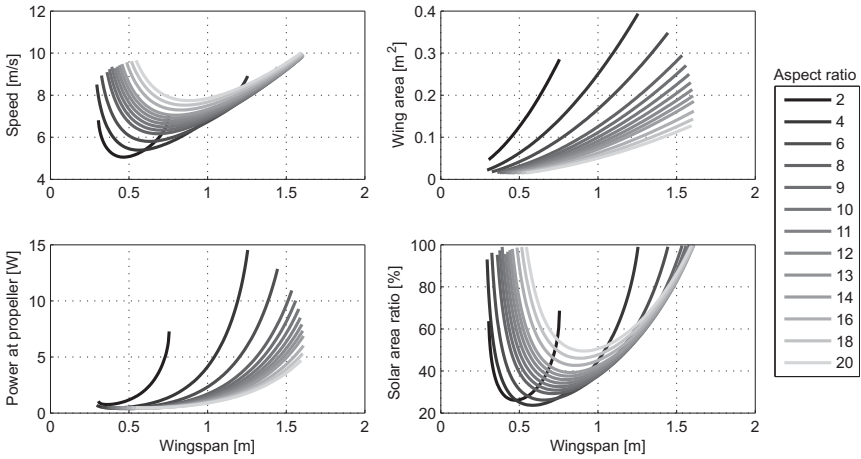
Figure 6.3: Aircraft and flight characteristics depending on b and AR
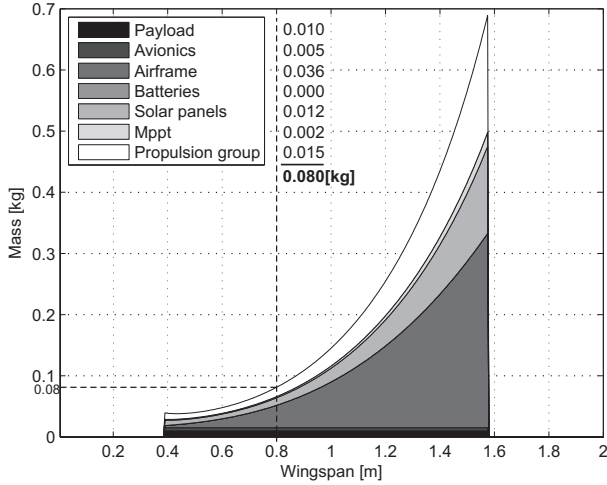
Figure 6.4: Mass distribution for $AR = 10$

Two successive prototypes with a wingspan of 77 cm, named SunSurfer 1 and 2, were realized during students projects [52, 58]. It emphasized all the problems that were mentioned above, especially the lack of choice in commercially available motors, gearboxes and propellers, and the low performances of the existing ones. The study focused also on the various airframe construction techniques and ended with the conclusion that the spar and balsa wood ribs is lighter than hot wire cut foam or molding methods, even if with the latter, the solar cells can be molded in the wing without any need of other encapsulation. A low voltage MPPT for two lithium-ion cells was also designed, allowing to emphasize precisely the increasing losses coming especially from the diode dropout voltage and leading to a poor total efficiency. Finally, both airplanes were tested with a small battery for the launch phase. The propulsion group being less efficient than expected because of a non optimal matching of commercially available parts, the solar power was not high enough to fly on solar energy only, but rather only increased the autonomy of the battery.

The fact that the choice of components, i.e. motor, propellers, batteries, etc., on the market is very poor at this size implies that the realization of a solar MAV first requires a careful design and the manufacturing of dedicated parts specifically for the application. In these conditions, and by decreasing the payload to 2 g and avionics to 2 g enables a solar MAV in the range of 15 g to achieve level flight at noon in summer. Improvements on the side of

flexible and efficient solar cells, tiny batteries as well as lightweight sensors
and actuators are required to extend this capability.

Considering other flight concepts, we could also envisage the building
of a solar version of a flapping wings UAV. The thin and flexible Mylar$^{\circledR}$
films that are used to cover their wings could be replaced by solar sheets.
The problem would then be the poor efficiency of flexible solar cells and the
very fast changing irradiance angle on the moving wing. It would require an
MPPT able to track the maximum power point a the same speed.

6.3   Scaling Up : Manned Solar Airplane

Having discussed the feasibility at a very reduced size, we will now go in
the other direction and consider the case of a manned solar airplane at low
altitude. A body mass of 80 kg is assumed to which we add 40 kg of addi-
tional equipments, i.e. a seat, a parachute, food, beverages, etc., yielding a
total payload of 120 kg. We will also consider 20 kg for the avionics system,
including navigation instruments and communication means that require an
electrical power of 100 W.

6.3.1   Scaling Up Advantages and Drawbacks

Aerodynamics and Efficiencies

Contrary to the case at MAV size, scaling up is very beneficial on many
aspects. Concerning aerodynamics, the Reynolds number is higher and we
expect better lift to drag ratio and propeller efficiency. This efficiency in-
crease is also true for the other elements of the propulsion group such as the
motor, its controller and the gearbox [106]. If the airplane takes off on a
runway, the difference between the take-off power and level flight power is
not as high as in the case of a hand launched UAV, as it was explained in
section 3.4.6. It is thus no more required to oversize the motor which im-
plies a more favorable constant k_{prop} (Table 3.4). An advantage to have a
higher propulsion power is that it can be distributed into several propulsion
groups instead of one, without major efficiency drop. This distribution along
the wing is an advantage because the mass being no more concentrated at
one point, the concentration of constraints decreases what results in lighter
structures.

Solar Cells and MPPT

Considering the same single cell surface for a larger wing area, there is much more possibilities to adopt a configuration of solar cells where each series sees the same irradiance. We remind here that in a series, the cell with the lowest irradiance penalizes all the others, which is the reason why we considered an efficiency η_{cbr} (Figure 3.4). Also, high power MPPTs, such as DriveTek AG products, approach an efficiency of $99\,\%$. In fact, with a more elaborated DC/DC architecture and using powerful digital signal processors running efficient tracking techniques, the losses can be considerably reduced.

Airframe Structure

Unfortunately, the single part that doesn't scale up in a positive manner is the airframe. In fact, keeping the same parameter k_{af} in the new airframe weight prediction model, thus assuming the same construction technique, it is clearly not possible to have an airplane embedding $120\,\mathrm{kg}$ for a $24\,\mathrm{h}$ solar powered flight. The reason is that the airframe becomes far too heavy due to the cubic scaling law (Section 3.4.2). Already in the case of Sky-Sailor it was clear that when increasing the wingspan, the airframe was taking a bigger and bigger part in the total mass distribution, until a value where the feasibility was no more ensured (Figure 4.1). In order to build large solar airplanes, engineers have to develop construction techniques that are far lighter than for normal aircrafts, even the one used for high performance sailplanes. Keeping the cubic tendency of our airframe weight prediction model, this amounts to decrease the k_{af} constant, which corresponds to place the future airplane in figure 3.8 on a parallel above the $5\,\%$ model. This is confirmed by the position of Helios that had a k_{af} value 20 times lower than the one used for Sky-Sailor.

   Inevitably, the airframe becomes more fragile and ideally requires more than a single support to the ground. This is confirmed by the NASA prototypes that have several wheels to distribute the loads and avoid constraints concentration on a single point. Moreover, the airframe cannot be completely stiff but possesses certain flexibility. Thus, the fixation of the solar modules has to be realized so that the wing torsion doesn't break the cells.

6.3.2   Application Example on a Manned Solar Airplane

All the mission and technological parameters modifications that are needed at the manned size are summarized in table 6.2. Having done these changes, we can reuse our program to design a manned solar airplane.

Table 6.2: Parameter changes at the manned airplane size

Parameter	Value	Unit	Description
C_L	1	-	Airfoil lift coefficient
k_{prop}	0.00121	$[kg/W]$	Mass to power ratio of prop. group
k_{af}	0.44/9.81/15	$[kg/m^3]$	Structural mass constant
m_{av}	20	$[kg]$	Mass of autopilot system
η_{sc}	0.19	-	Efficiency of solar cells
η_{ctrl}	0.98	-	Efficiency of motor controller
η_{mot}	0.88	-	Efficiency of motor
η_{plr}	0.87	-	Efficiency of propeller
P_{av}	100	$[W]$	Power of autopilot system
m_{pld}	120	$[kg]$	Payload mass
P_{pld}	0	$[W]$	Payload power consumption

It has to be recalled that the scenario here is still a flight at low altitude. According to figure 6.5, the feasibility starts at a wingspan of around 30 m. Interestingly, we can observe in figure 6.6 that the flying speed is pretty low and not so different than for the Sky-Sailor UAV. This is of course the nominal level flight speed, but during the day, a surplus of energy coming from the fact that a margin was considered in the design with η_{wthr} would allow the aircraft to fly faster.
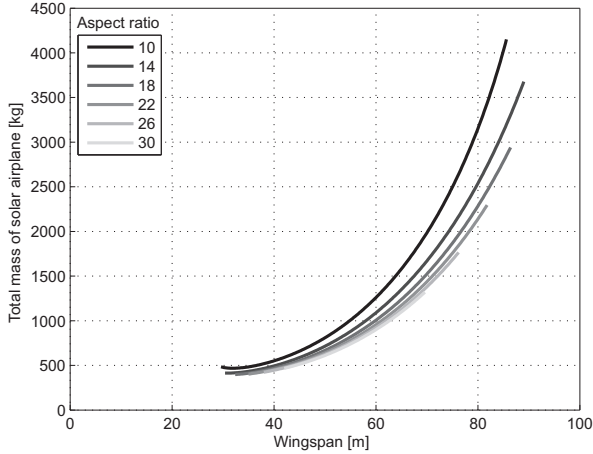
Figure 6.5: Possible configurations for a manned solar airplane designed for 24 h flight depending on b and AR
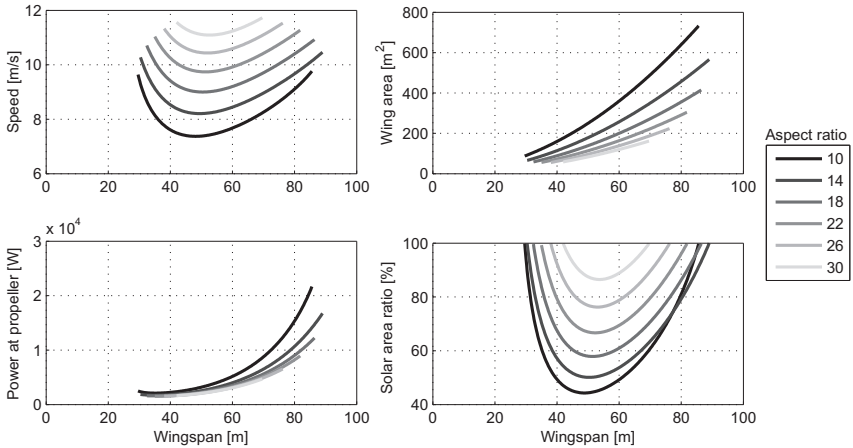
Figure 6.6: Aircraft and flight characteristics depending on b and AR

The speed lays here between 8 and 10 m/s (28.8 to 36 km/h), this value would only increase to 12 to 14 m/s (43.2 to 50.4 km/h) for a new design with a flight altitude of 8000 m, what is the limit for a un-pressurized cockpit. That means that in the better case here above, it would take more than 5 days to travel from Zürich to New York, whereas an actual A330-200 requires 8h45 to

cover the 6340 km. Thus, it appears that this low speed would be a limitation of solar powered airplane as a mean of human transportation.

Considering the choice of an airplane with 60 m wingspan and an aspect ratio of 26 as in figure 6.7, the flight speed would be around 10.7 m/s (38.52 km/h). Following the same rule as in section 6.2.1 where we proved that the angular accelerations vary with the inverse of a reference length, we can expect the airplane to have a slow flight behavior. It will require certainly long delays to achieve heading modifications and other manoeuvres.
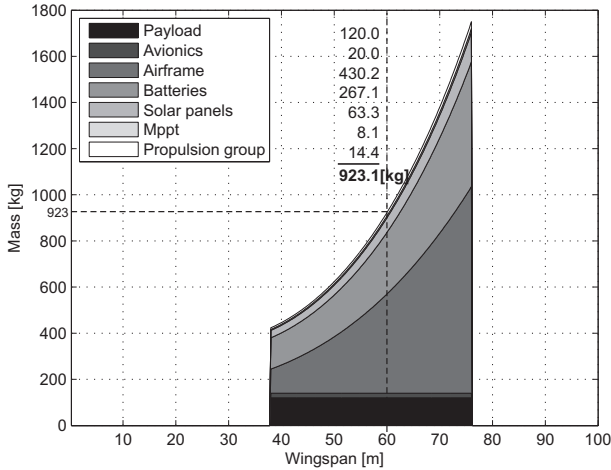
Figure 6.7: Mass distribution for $AR = 26$

6.3.3   Ideal Airframe Weight Model

We noticed that the cubic law of the airframe weight model is a very limiting factor when increasing dimension. Hence, we can wonder what shape should this structural weight scaling law have to make continuous flight possible with all wingspan, considering no more payload than just the airplane weight.

This can be done, using our methodology, by setting k_{af} to zero which means that we consider an ideal wing structure that has no mass. Then, we can search what the maximum payload weight that can be embedded is, for a specified b and AR. Hence, this value will also be the maximum weight that the wing can have if we assume no payload. Starting with equation (3.39), we have :

$$a_{10}^2 \ (a_2 \ (a_7 + a_9 \ (a_5 + a_6)) + a_3) \ \frac{1}{b^2} \ \leq \frac{4}{27} \qquad (6.5)$$

Isolating a_3 which corresponds to the payload mass, we obtain :

$$a_3 \ \leq \frac{4}{27a_{10}^2}b^2 - a_2 \ (a_7 + a_9 \ (a_5 + a_6)) \qquad (6.6)$$

We can express the maximum admissible wing structure mass depending on its surface.

$$m_{af} \ \leq \frac{4 \ AR}{27a_{10}^2}S - a_2 \ (a_7 + a_9 \ (a_5 + a_6)) \qquad (6.7)$$

The objective is then to transform this last equation in order to plot it on the great flight diagram. Hence, the wing loading follows :

$$W_{af}/S \leq \frac{W_{af}\frac{4 \ AR}{27a_{10}^2}}{W_{af}/g + a_2 \ (a_7 + a_9 \ (a_5 + a_6))} \qquad (6.8)$$

The result is represented graphically in figure 6.8 where the zone in which this equation is true is drawn for three different AR. Hence, only airplanes present in this area have an airframe light enough to achieve continuous solar flight. Interestingly, the 5 % model that was interpolated from sailplanes and that we took as weight prediction model for the airframe crosses these zones only in the UAV domain. This demonstrates mathematically why it is easier to build a solar airplane that achieves continuous flight at the UAV size than at the MAV or at the manned size. Of course these zones depend on the technological and mission parameters, but the shape that considers here the values used in the case of Sky-Sailor (Table 3.5 and 3.6) changes only slightly with other values. If we didn't consider a minimum electronic power for the autopilot system, the zone limits would be vertical, meaning that ideally, the mass of the wing structure should vary with the square of the wingspan. In fact, having a_2 equal to zero in equation (6.7) shows that the airframe mass over its surface should be below a constant value. When taking this minimum power into account, the zones are narrowed at small dimensions.

Lets consider an airplane in this feasibility zone and increase its size. If we follow the 5 % model, we will at one point go out of this zone. In order to stay in it when increasing the dimension, the only way is to have a lighter airframe weight prediction model that will be a parallel above the 5 % model. Concretely, this leads to find lighter construction techniques, and when having a look at the large solar airplanes built so far, they are precisely trying not to follow the cubic law, but trying to be lighter and enter the feasibility
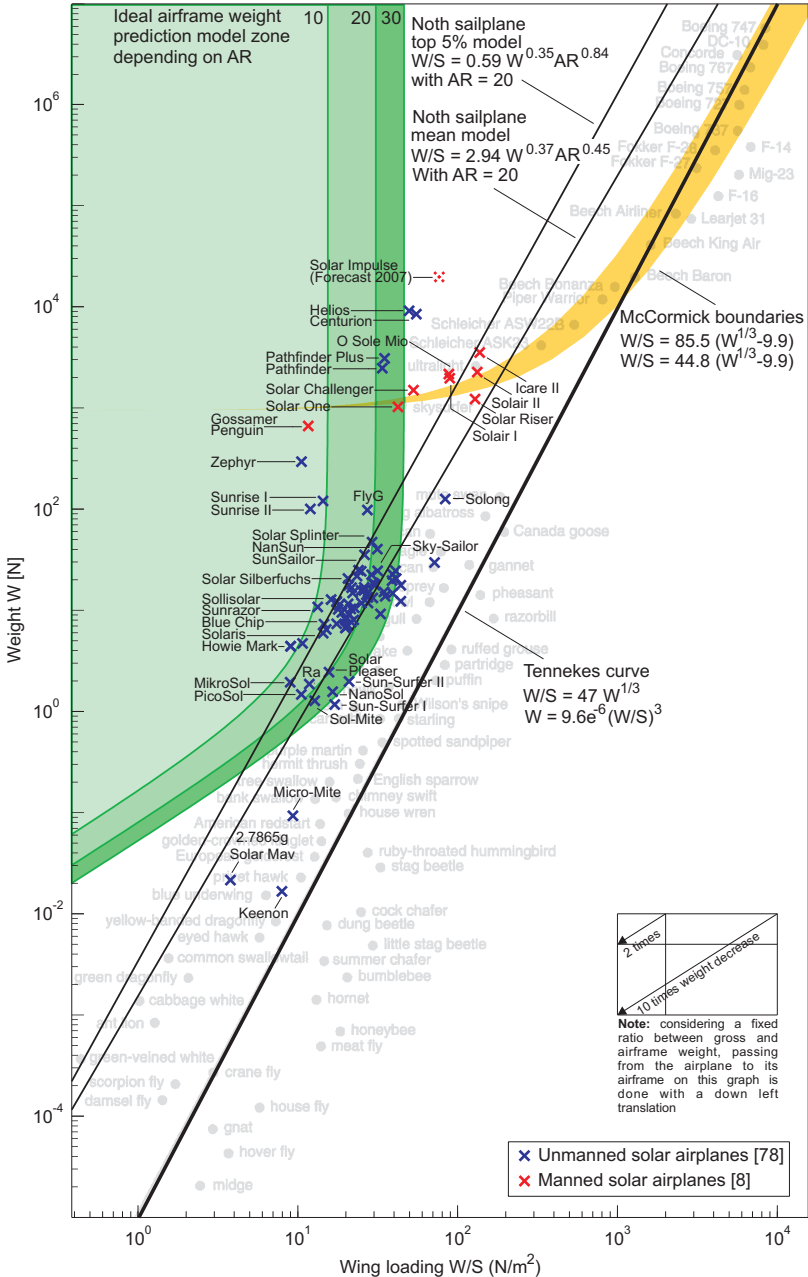
Figure 6.8: Maximum admissible wing surface density

zone. This is especially true for the Helios and the future Solar Impulse. The disadvantage is that the airplane becomes then more fragile, what explains why the large solar HALE cannot withstand dynamic manoeuvres, whereas the Sky-Sailor can achieve rapid turns and would survive a looping.

If we consider the weight prediction models of Stender and Rizzo that were plotted in figure 3.9, they lead to a completely opposite conclusion. In fact, when increasing the airframe weight, we enter in the zone where the feasibility of continuous flight is ensured. That is precisely why the author consider them as far too optimistic. This is confirmed by the fact that, when looking at Tennekes graph in gray color, no airplane or animal has ever existed that would be located at one extremity of their curve, i.e. on the top left or the bottom right corner of the great flight diagram.

We have to be careful about the fact that the three regions correspond to the airframe only, thus its weight with respect to the empty weight to surface ratio. At the opposite, the 86 solar airplanes are plotted with their gross weight with respect to the gross wing loading. The reason is that the information about the airframe weight only for all these prototypes were not available. Anyway, if we assume that the airframe constitutes generally a constant percentage of the airplanes gross weight, the difference is only a 45 degrees translation in the down left direction when passing from the gross weight to the airframe weight.

6.4   Scaling Up : High Altitude Long Endurance Platforms

Satellites in orbit around the Earth, whether they are aimed at imaging or telecommunication, could be replaced advantageously by high altitude long endurance platforms. Compared to the satellites, they would be far less expensive and more ecological to deploy. They wouldn't follow always the same predefined orbit but could be directed to specific location, or even land in case of a maintenance necessity or payload modification.

An ideal altitude for such platform is around $21\,000\,\mathrm{m}$ where the average wind speed is minimum, as depicted in figure 6.9. However, the temperatures at high altitude are low, approximately -57 °C (216 °K) between 11 and $20\,\mathrm{km}$. This has a very small beneficial impact on the solar cells and the motor efficiency because of the lower resistance. However, it induces structure deformation due to the dilatation and penalizes significantly the batteries that would reveal to be very inefficient. In such case, they have to be isolated and eventually kept at an ideal temperature with a dedicated heater,
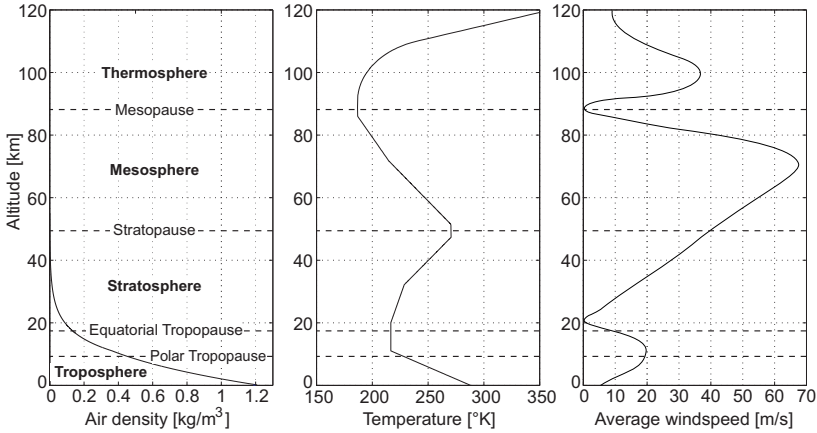
Figure 6.9: Evolution of density, temperature and wind speed with the altitude. Values vary with season and location. Source : COSPAR International Reference Atmosphere

if the heating due to the internal losses is not enough. Also, the atmospheric moisture and the formation of ice can be problematic.

Above all, the biggest issue is the low density of the air. Considering the same lift and drag coefficient and the same mass in a first approximation, equation (3.5) shows that an airplane flying at $10\,000\,$m would need already $71\,\%$ more energy than at sea level. In fact, despite the reduction of gravity of $0.3\,\%$, the reduction of air density from $1.225\,\text{kg/m}^3$ to $0.413\,\text{kg/m}^3$ is very disadvantageous. At $21\,000\,$m, at a density of $0.0757\,\text{kg/m}^3$ and $0.7\,\%$ less gravity, the power required is 4 times higher than at sea level.

We will consider the case of an airplane aiming at transporting a payload of $300\,$kg at $21\,000\,$m during 3 months in summer continuously. Using the parameters of the manned airplane (Table 6.2), the design methodology doesn't output any feasible solution for such a solar HALE platform. The efficiencies taken into account for the propulsion group being already quite high, the improvements to make it feasible concern the solar cells, the battery and the airframe. It is only when using a battery energy density of $1000\,$Wh/kg and a k_{af} four times lighter than we used in the low altitude manned airplane case, thus sixty times lighter than our $5\,\%$ model, that this becomes feasible with a minimum wingspan of $80\,$m. A better efficiency of the solar cells also has a beneficial impact on the feasibility, but this effect is not predominant, the battery technology and the airframe construction technique being clearly the most crucial issues. In conclusion, such concept is not feasible today and

needs future improvements in structure and energy storage methods, which could be batteries or regenerative fuel cells.
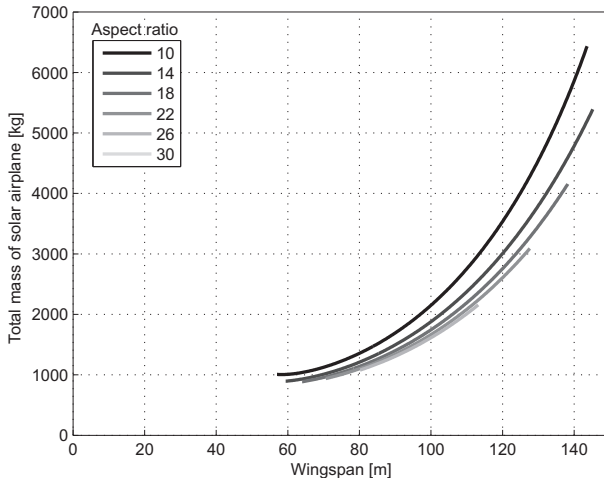
Figure 6.10: Possible configurations for a HALE platform designed for 24 h flight depending on b and AR
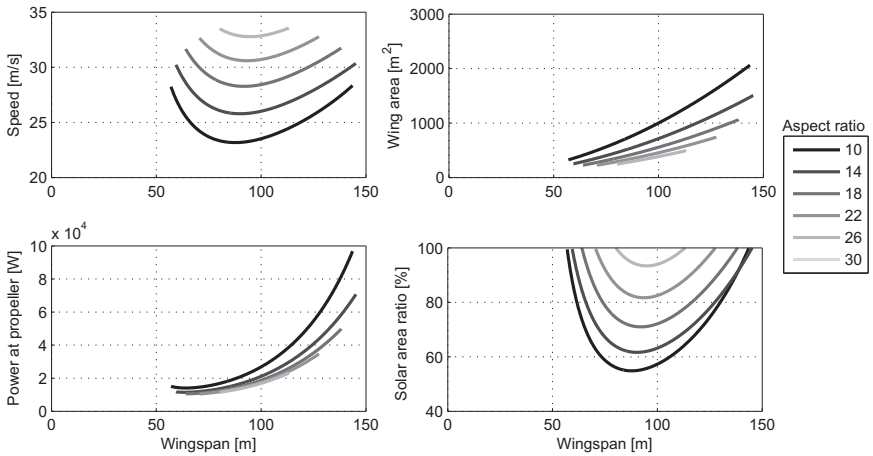
Figure 6.11: Aircraft and flight characteristics depending on b and AR
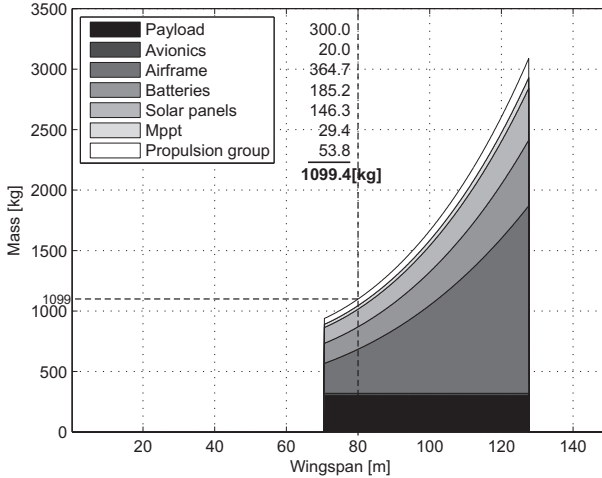
Figure 6.12: Mass distribution for $AR = 22$

Other concepts to embed large payloads at high altitudes propose to use lighter than the air objects, such as blimps filled with Helium, instead of heavier than the air airplanes [71]. Thanks to their buoyancy, they don't need a forward speed to generate the lift, however, they suffer from many disadvantages. Compared to a solution with an airplane embedding the same weight, the volume needed is very large, what requires an important power to resist to winds in order to maintain a constant position. There are also many issues concerning the envelope covered by flexible solar cells that has to be perfectly hermetic and resist to the low temperatures. The fixation of the payload has also to be done trying to limit the stress concentration on the envelope.

6.5 Storing Potential Energy in Altitude and Using Thermals

We mentioned already that many applications would require the solar unmanned airplane to stay at a constant altitude, whether it monitors forest fire a 500 m AGL or acts as a communication platform at 21 000 m. However, in the opposite case, one way to reduce considerably the airplane weight is to store energy not only in the battery but also in potential energy by gaining altitude. As a matter of fact, this way to store energy can be compared to

a battery without any weight, which is interesting, recalling that this part constitutes always around $40\,\%$ of the airplane's gross mass.

There are anyway drawbacks with such strategy. The air density gets lower with the altitude (Figure 6.9) and thus the nominal flight speed increases. Concerning aerodynamics, this makes then more difficult to design an airfoil and a propeller that will show good characteristics over a wide range of altitudes. Trade-offs have thus to be found. For the propulsion for example, a variable pitch propeller becomes necessary. There is also the problem of low temperature that was discussed in the last section.

6.5.1   Methodology Adaptation : Gaining Altitude

The methodology developed in chapter 3 can be adapted to take this strategy into account. In fact, the total energy required during the night stays the same, but it is composed now of a reduced amount of energy coming from the battery to power the motor at a reduced speed and of potential energy, the airplane loosing altitude.

$$E_{night} = T_{night}\,P_{elec\;tot} = E_{bat} + E_{pot} = m_{bat}\,k_{bat}\,\eta_{dchrg} + mgh \qquad (6.9)$$

Here the maximum altitude gain h is an additional mission parameter. Concerning the mass of the battery, that means a reduction of :

$$m_{bat} = \frac{T_{night}}{\eta_{dchrg}\,k_{bat}}\,P_{elec\;tot} - m\,\underbrace{\frac{gh}{\eta_{dchrg}\,k_{bat}}}_{a_{14}} \qquad (6.10)$$

Introducing this change in equation (3.33), we obtain in the compact form of equation (3.33).

$$m - \frac{a_{12}}{1+a_{14}}\,m^{\frac{3}{2}} = \frac{a_{13}}{1+a_{14}} \qquad (6.11)$$

leading to a modification of the condition for the feasibility :

$$\frac{a_{12}^{2}\,a_{13}}{(1+a_{14})^{3}} \leq \frac{4}{27} \qquad (6.12)$$

It is intuitively understandable that a solution that is unfeasible when not considering gaining altitude can then become feasible, the left part of this equation being smaller while the right part stays the same. This adaptation can be used for small altitude increase where the air density and other

parameters can be considered as constant, but for high altitude gain, their variation have to be taken into account.

The plots in figure 6.13 show the exact same case that was presented in section 4.3.2 where the Sky-Sailor was simulated on a 48 h flight on the 21st of June. However, this time, the surplus of energy when the battery is fully charged is used to gain 2000 m in altitude. At sunset, when the solar energy slowly decreases, the airplane starts its descent with the motor cut off. If we compare to figure 4.7, we observe that it allows postponing the start of battery discharge of 1h30 what leads to a higher capacity margin in the next morning.
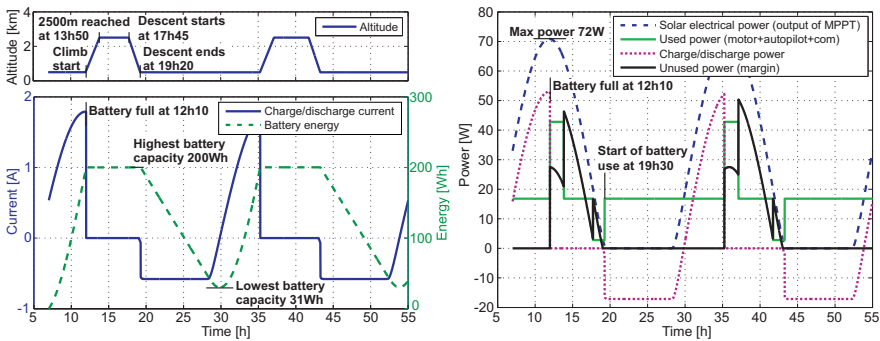
Figure 6.13: Continuous flight simulation with gain in altitude on the 21st of June

6.5.2   Using Thermals

An other way to save energy is the use of ascending thermal winds. The topology of a terrain and the disparity of the elements constituting this terrain is the source of such winds. For example, a zone of rocks exposed to the sun will get warmer than the forest near by. Thus, the air heated at this place will go up and create thermal updrafts, which can be used by an airplane to gain altitude as it is already done by many birds to stay longer in the air spending the minimum amount of energy.

Research in this area were also conducted within the framework of the Sky-Sailor project [56, 57]. The first issue concerns the detection of the thermals, that was not done here using additional sensor but only by monitoring how the airplane was behaving. A different force on the two sides of the wing resulting in a roll moment, or comparing the kinetic and potential energy with the energy supplied to the motor can give information about the

instantaneous updraft strength. With a set of data acquired during flight at different location, we can then try to fit a mathematical model of the thermal. Having predicted its center and size, the airplane can then describe a circular trajectory that maximizes the vertical velocity. This process has to be executed continuously. The set of data is refreshed each second, getting new values that replace the oldest one, before fitting the model again.

Such method was so far only simulated, using the airplane dynamic model depicted in section 5.11. It gave very good results, the airplane being able to follow a fast moving thermal updraft. With the many experiments that they conducted at NASA Dryden research center, Allen and Lin showed excellent results working on autonomous soaring algorithms with their 4.27 m UAV [24].

We could also think about using the propeller and the motor as a generator. During a descent, the propulsion group would produce energy and charge the battery. However, this energy conversion is definitely not efficient and it is much more interesting to achieve a slow glide, giving no throttle to the motor during a long period than gaining in short time energy at poor efficiency after what the motor has anyway to be turned on for level flight. This solution is only interesting if there is a limit altitude at which the airplane flies already, with the battery not fully charged yet, and if there are still solar energy and updrafts.

6.6   Mars Solar Airplane

The Sky-Sailor project started with the objective to study the feasibility of solar flight on the planet Mars. We will show here the basic layout of an airplane that would fly continuously at low altitude on the red planet, embedding a 0.5 kg payload. There are fundamental differences in the flight conditions compared to the Earth. The air density is 81 times lower, and despite the 3 times lower gravity, the level flight power required, considering in a first approach a similar airplane, is two times higher. On the other hand, due to its distance to the sun, the irradiance is approximately two times smaller. Concerning the day duration, they are very close. Due to these constraints, continuous solar flight is currently not possible on Mars. It will need improvements in energy storage and photovoltaic technologies in the following years before such a mission can be envisaged.

We will however try to design such an airplane. Compared to the design of Sky-Sailor on Earth in section 4, we will only change the flight conditions discussed above and consider a two times lighter airframe model and a 1000 Wh/kg battery or fuel cell, what can be hoped to arrive in a decade or

Table 6.3: Parameter changes for a solar powered airplane flying continuously on Mars

Parameter	Value	Unit	Description
I_{max}	589	$[W/m^2]$	Maximum irradiance
g	3.72	$[m/s^2]$	Gravity
k_{bat}	1000·3600	$[J/kg]$	Energy density of energy storage
k_{af}	0.44/9.81/2	$[kg/m^3]$	Structural mass constant
m_{av}	0.15	$[kg]$	Mass of autopilot system
m_{pld}	0.5	$[kg]$	Payload mass
η_{wthr}	1	-	Irradiance margin factor
P_{pld}	0.5	$[W]$	Payload power consumption
ρ	0.015	$[kg/m^3]$	Air density (500 m)

two. All these modifications are listed in figure 6.3. The possible layouts are shown in figure 6.14.
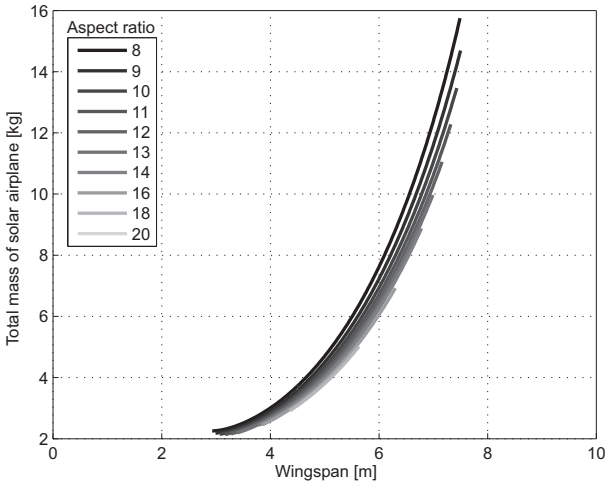
Figure 6.14: Possible configurations for a Mars airplane designed for continuous flight depending on b and AR

The results show that the wingspan would be in the range of 3.5 to 7 m. The airplane would fly at around 35 m/s (126 km/h) which is much faster than on Earth but understandable as the air density is lower.
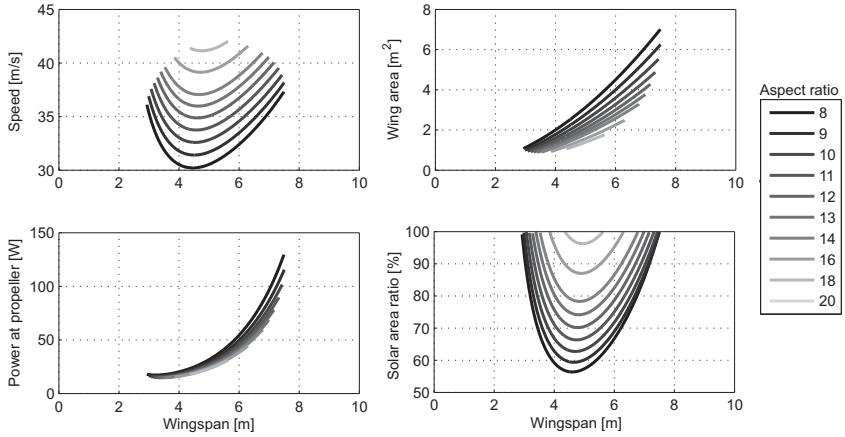
Figure 6.15: Aircraft and flight characteristics depending on b and AR
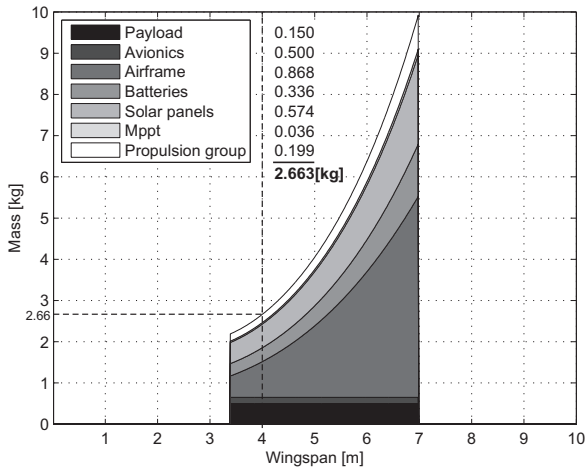
Figure 6.16: Mass distribution for $AR = 13$

Of course, this is only a conceptual design and many things would have to be studied specifically such as the aerodynamics at these low air densities, the control and navigation with adapted sensors, since the global positioning system is not available. Also, a lot of problems should be solved such as the behavior of the temperature sensitive elements, for example the battery, in the -130 °C to 30 °C temperature range of Mars.

Chapter 7

Conclusion

7.1 Main Achievements

This thesis presented a new methodology for the conceptual design of solar airplanes. It has the advantage to be very versatile and usable for a large range of dimension, from UAVs with less than one meter wingspan to manned airplanes. It is purely analytical and based on the concepts of energy and mass balances during one day using mathematical models that put the sizing of all elements on the airplane in relation. These models are used for efficiency or weight prediction and constitute a key part of such design method. They were not only studied in a limited domain, but over a very large range, for some models with up to 7 orders of magnitude, showing for example on the same graphics a tendency that encompasses motors from $1\,\mathrm{mW}$ to $10\,\mathrm{kW}$. Finally, the design methodology consists of a simple routine that takes 5 parameters linked to the mission and 25 to the technologies used as inputs. It allows the designer to output the layout of a solar airplane rapidly, with size, weight and power informations.

The methodology was used for the conceptual design of a prototype that would embed a small payload and with the objective to prove the feasibility of continuous flight on Earth. It also allowed emphasizing some general principles. For example, it was clearly demonstrated that the most limiting technology at this time is the energy storage. Even with the best lithium-ion batteries, the energy storage constitutes more than $40\,\%$ of the airplane's gross weight. For that reason, what is critical for a continuous solar flight is not the day that has to be the longest, but the night that has to be the shortest.

Following the obtained design, a prototype was built and fully tested.

Named Sky-Sailor, it validated the theoretical part of this thesis through experiments and proved the efficiency of the design methodology by achieving a flight of more than 27 hours using only solar power. This achievement is a record for a UAV that doesn't use altitude gain or thermal updrafts. With the development of this prototype, a considerable amount of practical knowledge and experience was acquired in various fields such as aerodynamics, lightweight structure construction, solar energy management, sensor fusion, efficient electronics, control, etc. For all of the airplane components, trade-offs were to be made between efficiency, power consumption and weight. Figure 7.1 presents the losses on the energy train from the solar cells to the propeller and emphasizes the fact that a careful design of each part is necessary. This results in a precious know-how that wouldn't have been acquired if the project had stayed at a simulation level.
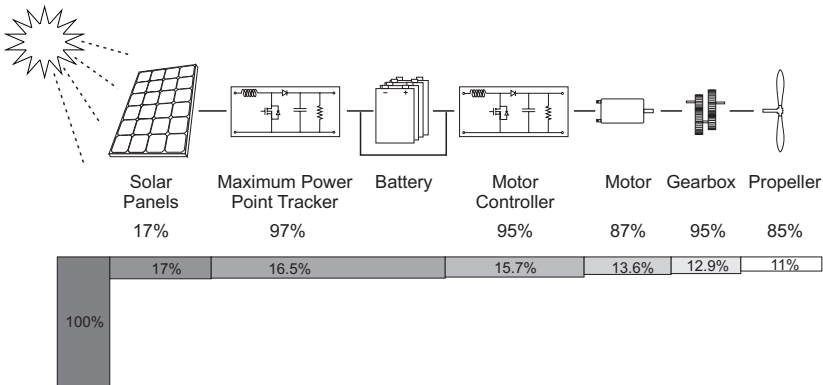
Figure 7.1: Energy train on the Sky-Sailor solar airplane with the cumulated efficiencies

The design methodology being valid over a wide range of dimensions, a part of this thesis was also dedicated to study the scaling of solar airplanes and thus to clearly identify what becomes problematic at large or small dimensions.

- When scaling down, the lower Reynolds number are deteriorating the aerodynamics, which see reduced lift to drag ratios, and also the propeller that sees its efficiency dropping. For the other elements of the propulsion group that are the motor and the gearbox, this drop of efficiency was also demonstrated, especially below 10 W. Other problems were also identified, such as the bending of the solar cells on a smaller

curvature radius and the difficulty to find lightweight avionics systems and sensors.

- When scaling up, the efficiency of the various elements is no more a problem, even if their design is not straightforward and needs a careful attention. But what becomes the nightmare of engineers is the airframe. It was proved in this thesis that, considering the same construction method, the airframe weight increases with the cube of a reference length and that ideally it should go with the square to make the feasibility of continuous flight independent of the dimension.

7.2 Outlook

The design methodology in this thesis was kept at a simple level with a low number of parameters, but we could increase this complexity. It would for example be interesting to express the efficiencies, which were considered as constant, as a mathematical function of the power.

Intelligent control algorithms that automatically adapt to the atmospheric condition and thus minimize the power consumption is another interesting topic. It would adapt the angle of attack, choosing a high value in calm conditions to fly very slowly but lowering this angle in order to increase speed when encountering some turbulence. Thermal soaring would also allow saving energy by using another form of solar energy. Within the framework of this thesis, it was shown to be very efficient in simulation and a next step could be to conduct experiments with a real glider.

Concerning the structural design, the ultimate goal would be to include the solar cells and the actuators in the wing as structural elements. A. J. Colozza presented such a futuristic concept called the "solid state aircraft" where the wing would consist of a sandwich structure composed by the solar array, the battery and the actuators all made of different layers. The entire wing would be flexible and there would be no more discrete control surfaces separated from the rest of the wing [48]. In this case, the battery that would be used as a structural element should be more robust to shocks than our current lithium-ion batteries.

7.3 Potential Applications and the Future of Solar Aviation

Without intending to predict the future, the experience gained during this thesis allows us to foresee the direction that solar aviation will take and the

applications that it might cover. It is obvious that the technologies involved in the construction of solar powered airplanes will see many improvements these following years, with the growing need of green solutions for transportation, consumer electronics, etc.

The first solar powered airplanes used for concrete applications will probably have a size between 3 to 6 m. In fact, it was proved in section 6.3.3 that this range is somehow optimal and allows already now continuous flight with the current technologies. Moreover, applications such as law enforcement, border surveillance, forest fire fighting or power line inspection would require a payload of not much more than 1 kg what is precisely the capacity in such wingspan range. So for these applications, the next 10 years will certainly see a rapid and important development of solar powered UAVs at the size of some meters.

At the MAV range, improvements will be necessary before seeing a flying robots of the size of a hummingbird, powered by the sun only. The low Reynolds number will always be a limiting factor, but with more efficient solar cells and propulsion group elements, added to a better energy storage, the dream should once come true. Miniaturization of the electronics and the avionics will also play a major role.

At large scale, we saw already in chapter 6 that with the current state of technology, embedding a human person or for instance a payload of 150 kg for a perpetual flight imposes a huge wingspan and requires a very lightweight wing that turns out to be fragile, leading to an airplane that is not easily steerable. One could of course say that with improvements of technology, it will become feasible in some years, as it was not predictable after the Wright brothers' flight that there would once be airliners crossing the Atlantic with 500 passengers onboard. The author thinks that this will never happen, for many combined reasons. The first limitation comes from the sun irradiance that even with 100 % efficiency solar cells would never provide enough power to not only carry the passengers, but also a minimum of comfort which implies a lot of additional weight. Linked to this, the cubic tendency of the airframe's weight is not compensated by the square tendency of the solar cells surface, as it was demonstrated in section 6.3.3. The large surface of solar cells needed leads then to impressive wingspans. Also, we observed that the speed of a solar airplane doesn't exceed 50 km/h making trips last several days instead of hours as with an actual airliner. That lets us believe that solar propulsion has a future for transportation only for trips that don't exceed 24 hours and for one or two persons onboard.

Even in this case, a far better solution would still consist in using solar energy, but in a concentrated form. In fact, one could cover the roof of

airports and hangars with solar panels and use this energy to hydrolyze water into hydrogen and oxygen. The hydrogen would then be stored and used on the airplane in a fuel cell. To summarize, what makes solar airplane not so ideal is that they have to embed the whole factory that converts the few energy coming from the sun in real-time, which is, as we saw, a heavy and not so efficient undertaking. Thus, the better idea is to let this heavy factory on the ground, concentrate the energy, and then only use it on a fast airplane with reasonable dimensions and thus a correct manoeuvrability. One part of the wing could still be covered by solar panels, but to cover only a small percentage of the electrical power consumption.

For solar HALE platforms anyway, it is different. The reason is that here the objective is not to transport something from A to B in a minimum of time but rather to ensure the presence of a given payload at a certain location and altitude during months or years. In this case, no energy storage method available now is good enough to embed the whole energy needed for the flight as a concentrated form. Thus the collection of solar energy directly onboard the airplane is so far the only solution. Such platforms will certainly be used in some years for telecommunication or Earth monitoring. Nevertheless, the payload they will be able to carry will always be very limited, due to the problems that were mentioned here above.

Appendix A

List of Solar Airplanes Flown to Date

The table below lists all the solar powered airplanes that were built and flown, until 2008, and from which it was possible to obtain dimension and weight characteristics. From the 1 gram SolFly to the 600 kg Helios, they are all sorted here according to the year of their maiden flight and also represented graphically in figure 3.8 in a wing loading vs weight plot. The total weight is the airplane empty weight plus the pilot weight, in the case of manned airplane, or the payload. Airplanes that stayed or still are at the design phase and were never built so far are not included.

Nr.	Name	Year	Designer	Wing span [m]	Mean Chord [m]	Length [m]	Wing Area [m²]	Aspect Ratio [-]	Empty Weight [kg]	Total Weight [kg]
1	Sunrise	1974	R.J. Boucher from Astro Flight, USA	9.75	0.86	4.38	8.36	11.4	12.25	
2	Sunrise II	1975	R.J. Boucher from Astro Flight, USA	9.75	0.86	4.38	8.36	11.4	10.21	
3	Solaris	1976	Fred Militky, Germany	2.06	0.20		0.41	10.3	0.61	
4	Ra	1977	Prof. Dr. V. Kupciks	1.37	0.12	0.84	0.16	11.9	0.19	
5	Utopie	1977	Dr. Roland Stuck, France	2.53	0.20	1.32	0.51	12.6	0.97	
6	Solar-Student	1978	Prof. Dr. V. Kupciks	1.96	0.22	1.04	0.43	8.91	0.93	
7	Solar One	1978	David Williams and Fred To	20.72	1.17	6.70	24.15	17.8	104.32	
8	Solar-X4	1979	H. Schenk	2.50	0.17	1.13	0.42	14.8	0.85	
9	Solar Silberfuchs	1979	Günter Rochelt	4.00	0.25	1.52	1.00	16.0	2.10	
10	Solar Riser*	1979	Larry Mauro	9.14	1.04	2.44	9.52	8.8	55.80	124.7
11	Solar-HB79	1980	Helmut Bruss	2.80	0.24	1.45	0.67	11.7	1.51	
12	Solair I*	1980	Günter Rochelt	16.00	1.38	5.40	22.00	14.0	120.00	200.0
13	Gossamer Penguin*	1980	Dr. Paul B. MacCready from Aerovironment	21.64	2.63		57.00	8.2	30.84	67.7
14	Solar-HB80	1981	Helmut Bruss	2.84	0.23	1.48	0.65	12.5	1.72	
15	Solar Challenger*	1981	Dr. Paul B. MacCready from Aerovironment	14.80	1.48	9.22	21.83	9.0	99.79	153.0
16	Solus Solar	1984	Helmut Bruss, F.W. Biesterfeld	3.20	0.29	0.88	0.93	11.0	2.20	
17	Poly	1986	Helmut Bruss	3.24	0.29	0.88	0.97	10.8	2.48	
18	Combi	1987	Peter Hartwig	2.96	0.26	0.85	0.77	11.4	2.29	
19	Solariane	1987	Franz Weissgerber, Ernst Schöberl	3.08	0.28	1.72	0.85	11.2	1.80	
20	Helios (model)	1989	Erich Töpfer	2.14	0.18		0.39	11.8	1.40	
21	Bloch	1989	Edwin Bloch	2.90	0.24		0.70	12.0	1.25	
22	Grosholz	1989	Rainer Grosholz	3.07	0.19		0.60	15.8	1.85	
23	Combi 2	1989	Helmut Bruss	2.95	0.28	1.54	0.77	11.3	1.70	
24	Ikaros	1989	Franz Weissgerber	2.50	0.23		0.58	10.8	1.80	
25	Bleher	1989	Wolfgang Bleher	2.00	0.24		0.49	8.18	1.37	
26	Romarino	1989	Urs Schaller	2.00	0.20		0.40	10.0	1.80	
27	Sol-e-moi	1989	Alfred Hitzler	3.00	0.17		0.50	18.0	2.10	
28	Wolf	1989	Josef Wolf	3.00	0.21		0.63	14.3	1.60	
29	WS-Solar	1989	Wener Schleidt	2.50	0.22		0.55	11.3	1.55	
30	Ariane Ultra	1989	Franz Weissgerber	1.98	0.21	1.14	0.41	11.0	3.02	
31	Solar Voyager	1990	Volker Klein	3.20	0.25		0.79	13.0	1.30	
32	Mardini	1990	Hans-Jakob Sommerauer	2.40	0.25		0.60	9.6	2.50	
33	Sollisolar	1990	Edwin Bloch	2.98	0.23		0.69	12.9	1.23	
34	PB 26-FL	1990	Marco Buholzer	2.60	0.22		0.58	11.8	2.30	
35	Solarbaby	1990	Werner Dettweiler	1.70	0.16		0.28	10.4	1.25	
36	Bleher	1990	Wolfgang Bleher	2.00	0.22		0.44	9.03	1.55	
37	Uccello	1990	Josef Kapfer	2.70	0.23		0.63	11.5	1.90	
38	Sole Florentino	1990	Franz Weissgerber	2.50	0.17		0.43	14.6	1.20	
39	Soli	1990	Ernst Schöberl	2.08	0.18		0.38	11.5	1.50	
40	Playboy	1990	Thomas Bley	2.40	0.19		0.45	12.8	1.35	
41	WS12 (then WS16)	1990	Dr. Wolfgang Schaeper	2.50	0.16	1.10	0.41	15.2	0.84	
42	Solar Flyer	1990	Peter Hartwig	2.64	0.23	1.48	0.61	11.5	1.60	
43	Blue Chip	1990	Hans W. Müller	2.20	0.23	1.25	0.50	9.66	0.75	
44	Solarmax	1990	Erich Töpfer	3.48	0.30	1.59	1.04	11.6	2.54	
45	Sollisolar 89-2	1990	Edwin Bloch	2.98	0.23	1.34	0.68	13.1	1.24	

* Denotes manned solar airplanes

Nr.	Name	Year	Designer	Wing span [m]	Mean Chord [m]	Length [m]	Wing Area [m²]	Aspect Ratio [-]	Empty Weight [kg]	Total Weight [kg]
46	Phönix	1990	Jens Stattler	2.62	0.21	1.29	0.56	12.2	1.18	
47	Sunseeker	1990	Eric Raymond							
48	Solar UHU	1991	Graupner (Ref. 4274)	2.30	0.23	1.20	0.53	10.0	1.45	
49	Blue-Wing	1991	Norbert Ladenburger, Germany	2.34	0.18	1.05	0.42	13.0	0.75	
50	Solar Schilti 1	1991	Jean-Pierre Schiltknecht	1.74	0.19	1.16	0.34	9.0	0.70	
51	Solar Schilti 2	1991	Jean-Pierre Schiltknecht	1.99	0.18	1.05	0.36	11.1	0.82	
52	Silizi Solar	1991	Horst Groner	2.25	0.21	1.30	0.47	10.7	1.08	
53	Solix	1991	Ernst Schöberl	2.37	0.20	1.30	0.48	11.7	1.05	
54	Solar mini challenger	1992	Astro Flight	1.55	0.18		0.28	8.5	0.94	
55	Rival-8 Solaris	1992	Palo Lishak, Slovakia	1.96	0.22	1.13	0.43	8.9	0.66	
56	Pathfinder	1994	AeroVironment, NASA	29.50	2.40	3.60	70.80	12.3	207.00	252.0
57	MikroSol	1995	Sieghard Dienlin	1.13					0.19	
58	Solair II*	1996	Günter Rochelt	20.00	0.86	6.12	17.00	23.5	140.00	230.0
59	Icaré II*	1996	UNI Stuttgart, Rudolf Voit-Nitschmann	25.00	1.03	7.70	25.70	24.3	270.00	360.0
60	Lo 120 Solar	1996	Hugo Post	15.46	1.03		16.00	14.9		
61	Solarflugzeug*	1996	Uwe Heinemann	18.00	1.50		27.00	12.0	190.00	280.0
62	O sole mio*)	1996	Dr. Antonio Bubbico	20.00	1.23		24.50	16.3	130.00	220.0
63	Solar Solitude	1996	Dave Beck	2.70	0.20		0.55	13.3	2.00	
64	NanoSol	1996	Sieghard Dienlin	1.11					0.16	
65	Centurion	1997	AeroVironment, NASA	61.80	2.40	3.60	148.32	25.8	533.00	862.0
66	Trosollmuffel	1997	Bernd Bossmann	2.50	0.25		0.62	10.1	1.14	
67	Global Flyer	1997	Helmut Bruss	2.50	0.23	1.20	0.57	11.0	1.04	
68	Pathfinder Plus	1998	AeroVironment, NASA	36.30	2.40	3.60	87.12	15.1	247.50	315.0
69	Solar Excel	1998	Wolfgang Schaeper	2.10	0.16	1.02	0.35	12.8	0.72	
70	Solitair	1998	DLR Institute of Flight Systems	5.20						
71	PicoSol	1998	Sieghard Dienlin	0.99					0.13	
72	LFMA	1998	Louis Fourdan, Michel Astier, France	1.90	0.25	1.15	0.47	7.75	1.20	
73	Helios	1999	AeroVironment, NASA	75.30	2.48	3.60	186.60	30.4	600.00	930.0
74	Sunrazor (Sunriser)	2000	Patrick Berry	2.70	0.30		0.81	9.06	1.10	
75	Goldcap 2	2001	Helmut Bruss							
76	Solarus	2001	Jonas Romblad	2.30	0.19		0.44	12.0	0.48	
77	FlyG	2002	Royal Institute of Technology, KTH	6.00	0.60	2.70	3.60	10.0	10.00	
78	Solar Pleaser	2003	Unknown	1.04	0.15	1.01	0.15	7.0	0.25	
79	No Name	2003	Matt Keennon	0.14	0.015	0.12	0.00	9.3	0.0017	
80	Solar Splinter	2003	Paul Breed	4.27	0.35	2.13	1.50	12.2	4.50	
81	Sol-Mite	2004	Ralph Bradley	0.81	0.12		0.10	6.5	0.13	
82	Sky-Sailor	2005	André Noth, Walter Engel, Roland Siegwart, EPFL	3.20	0.24	1.82	0.78	13.2	2.50	
83	Zephyr	2005	QinetiQ	18.00	1.55		27.90	11.6	30.00	
84	Solong	2005	Alan Cocconi from AcPropulsion	4.75	0.32		1.50	15.0	12.60	
85	NanSun	2006	Troy Tegeder	3.20	0.40	2.60	1.28	8.0	4.10	
86	Howie Mark	2006	Louis Dube, Joshua Alves, Corey Ohnstad	2.43	0.20		0.49	12.2	0.45	
87	SunSailor	2006	Technion IIT, Haifa, Israel	4.20	0.32	2.20	1.35	13.1	3.60	
88	Aphelion	2006	Carl Engel and Adam Woodworth from MIT	3.13	0.22		0.70	14.0		
89	2.765 g Solar MAV	2007	Brian Daniels	0.14	0.04	0.15	0.0057	3.4	0.0022	
90	SolFly	2007	Helmut Schweig	0.07					<0.001	
91	Micro-Mite	2007	Ralph Bradley	0.20	0.05		0.01	4.0	0.0095	

* Denotes manned solar airplanes

Appendix B

Matlab$^{®}$ Code of the Design Methodology

The following code contains the algorithm that solves the loop of figure 3.17 representing the solar airplane conceptual design methodology. Taking the 25 technological and 5 mission parameters as input, it calculates and plots graphically the potential solutions, as it was done in chapters 4 and 6. The program is divided in three parts :

- **InitParameters** that initializes the 30 parameters. This function is called only once at the beginning of the program
- **EvaluateSolution** that evaluates the feasibility of one single solution, the wingspan b and the aspect ratio AR being fixed
- **Main** that first calls InitParameters, then tries different combination of wingspan and aspect ratio using the EvaluationSolution routine to determine if the solution is feasible or not, and finally plots the results to show the solution space in a graphical manner.
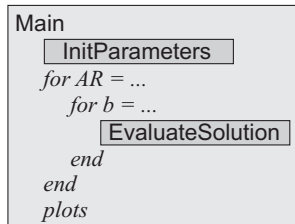
```
Main
    InitParameters
    for AR = ...
        for b = ...
            EvaluateSolution
        end
    end
    plots
```

Figure B.1: Schematic view of the conceptual design program

B.1   File InitParameters.m

```
%=========================================================================
%===            Global Design of Sky-Sailor Airplane
%===               - Initialization of Parameters -
%===                       A. Noth, 2008
%===
%=== This code initialize parameters for the design program of Sky-Sailor
%=== (or other solar airplane in general). Please read "Design of Solar
%=== Powered Airplanes for Continuous Flight" for more information about
%=== the calculations and for equations reference.
%=========================================================================


g               =   9.81;                   % Gravitational acceleration [m/s^2]
alt             =   500;                     % Initial altitude [m]
alt_array       =   [0, 1000, 2000, 4000, 6000, 10000, 15000, 20000, 25000, 30000];
rho_array       =   [1.224, 1.11, 1.006, 0.819, 0.659, 0.413, 0.192, 0.087, 0.039, 0.017];
rho             =   spline(alt_array,rho_array,500); % Airdensity at 500m [kg/m^3]

%=========== Irradiance conditions ==============
I_max           =   950;                     % Maximum irradiance [W/m^2]
T_day           =   13.2*3600;               % Duration of the day [s]
n_wthr          =   0.7;                     % Margin factor <1 take clouds into account [-]

%================ Aerodynamics ==================
C_L             =   0.8;                     % Airfoil lift coefficient [-]
C_D_afl         =   0.0126;                  % Airfoil drag coefficient [-]
C_D_par         =   0.0065;                  % Fuselage drag coefficient [-]
e               =   0.9;                     % Constant depending on wing shape [-]

%======= Wing & fuselage Structure ==============
k_af            =   0.44/9.81;               % Constant [~Kg/m3]
x1              =   3.1;                      % Scaling exponent for b  [-]
x2              =   -0.25;                    % Scaling exponent for AR [-]

%============= Propulsion group =================
n_ctrl          =   0.95;                    % Efficiency of motor controller [-]
n_mot           =   0.85;                    % Efficiency of motor [-]
n_grb           =   0.97;                    % Efficiency of gearbox [-]
n_plr           =   0.85;                    % Efficiency of propeller [-]
k_prop          =   0.008;                   % Mass/Power ration of propulsion group [kg/W]

%======= Battery and Stepdown converter =========
n_chrg          =   0.95;                    % Efficiency of charge process [-]
n_dchrg         =   0.95;                    % Efficiency of discharge process [-]
n_bec           =   0.65;                    % Efficiency of bec (5V stepdown) [-]
k_bat           =   190*3600;                % Energy density of LiPo [J/Kg]

%================ Solar cells ===================
k_sc            =   0.32;                    % Mass density of solar cells [Kg/m2]
k_enc           =   0.26;                    % Mass density of encapsulation [Kg/m2]
k_mppt          =   1/2368;                  % Mass/Power ratio of mppt [kg/W]
n_sc            =   0.169;                   % Efficiency of solar cells [-]
n_cbr           =   0.9;                     % Efficiency of cambered configuration [-]
n_mppt          =   0.97;                    % Efficiency of mppt [-]

%============== Avionics & Payload ==============
m_av            =   0.15;                    % Mass of controler and electronics [kg]
m_pld           =   0.05;                    % Mass of payload [kg]
p_av            =   1.5;                     % Power required for control [W]
p_pld           =   0.5;                     % Power required for payload [W]
```

B.2   File EvaluateSolution.m

```
%=========================================================================
%===              Global Design of Sky-Sailor Airplane
%===                   - Evaluation of the solution -
%===                         A. Noth, 2008
%===
%=== This code evaluates, based on given parameters, the feasibility of a
%=== certain configuration of solar airplane. In one sentence, the main
%=== problem is to balance weight/lift and obtained/required power. Please
%=== read "Design of Solar Powered Airplanes for Continuous Flight" for
%=== more information about the calculations and for equations reference.
%=========================================================================

C_D_ind             = C_L^2 / (e*pi*AR);              % Induced drag coefficient [-]
C_D                 = C_D_afl+C_D_ind+C_D_par;        % Total drag coefficient [-]

a0      =   C_D/(C_L^1.5)*sqrt(2*AR*(g^3)/rho);       % Eq 3.5
a1      =   1/(n_ctrl * n_mot * n_grb * n_plr);       % Eq 3.6
a2      =   1/(n_bec)*(p_av+p_pld);                   % Eq 3.6
a3      =   m_av + m_pld;                             % Eq 3.10
a4      =   k_af*AR^x2;                               % Eq 3.25
a5      =   k_sc + k_enc;                             % Eq 3.27
a6      =   k_mppt * I_max * n_sc * n_cbr * n_mppt;   % Eq 3.28
a7      =   T_night/(n_dchrg * k_bat);                % Eq 3.30
a8      =   k_prop;                                   % Eq 3.32
a9      =   pi/(2*n_sc* n_cbr*n_mppt*n_wthr) * ...    % Eq 3.26
            (1+T_night/(T_day*n_chrg*n_dchrg))*1/I_max;
a10     =   a0 * a1*(a7 + a8 + a9*(a5+a6));           % Eq 3.34
a11     =   a2 * (a7+a9*(a5+a6))+a3;                  % Eq 3.34
a12     =   a10 * 1/b;                                % Eq 3.35
a13     =   a11+a4*b^x1;                              % Eq 3.35

z       = roots([a12 -1 0 a13]);                     % Solving equation to find mass
Sol_m   = MinimumPositive(z)^2;                      % It can be 2 masses, we take the smallest one

if (isnan(Sol_m)==0)                                 % If a solution is found, we compute ...
    Sol_P_level      = a0*Sol_m^1.5/b;               % Eq 3.5   level flight power
    Sol_m_af         = a4*b^x1;                      % Eq 3.25  airframe mass
    Sol_P_elec_tot   = a1*Sol_P_level+a2;            % Eq 3.6   total electric power (level flight)
    Sol_m_bat        = a7*Sol_P_elec_tot;            % Eq 3.30  battery mass
    Sol_A_sc         = a9*Sol_P_elec_tot;            % Eq 3.26  solar panels area
    Sol_m_sc         = a5*Sol_A_sc;                  % Eq 3.27  solar panels mass
    Sol_m_mppt       = a6*Sol_A_sc;                  % Eq 3.28  mppt mass
    Sol_P_sc         = a6*Sol_A_sc/k_mppt;           % Eq 3.28  solar electrical power max
    Sol_m_prop       = a8*a1*Sol_P_level;            % Eq 3.32  propulsion group mass
    Sol_v            = sqrt(2*Sol_m*g/(C_L*rho*b*b/AR)); % Eq 3.3   level flight speed
    Sol_D            = Sol_m*g/C_L*C_D;              % Eq 3.1-2 total drag
    Sol_A            = b^2/AR;                        %          wing surface
end

if ((isnan(Sol_m)==1) || (Sol_A_sc > b*b/AR))        % If no solution, Nan is returned
    Sol_m            = NaN;
    Sol_P_level      = NaN;
    Sol_m_af         = NaN;
    Sol_P_elec_tot   = NaN;
    Sol_m_bat        = NaN;
    Sol_A_sc         = NaN;
    Sol_m_sc         = NaN;
    Sol_m_mppt       = NaN;
    Sol_P_sc         = NaN;
    Sol_m_prop       = NaN;
    Sol_v            = NaN;
    Sol_D            = NaN;
    Sol_A            = NaN;
end
```

B.3   File Main.m

```
%===========================================================================
%===              Global Design of Sky-Sailor Airplane
%===            - Plot Example for Unmanned Aerial Vehicle -
%===                    A. Noth, ASL, ETHZ, 2008
%===
%=== This code tries different combinations of wingspan and aspect ratio
%=== and then evaluates the feasibility or not of the solution. It uses the
%=== technological & mission parameters from Initparameters. The results
%=== are plotted on graph where one can also see the mass distribution.
%=== SCENARIO: Solar Unmanned Aerial Vehicle for 24h Flight
%===========================================================================

clc;clear;clf;
cmap        = colormap(gray(100));
j           = 0;

InitParameters;                                     % Parameters are initialized
T_night     = 24*3600-T_day;                        % Duration of the night [s]

for AR = [8,9,10,11,12,13,14,16,18,20]              % For different aspect ratios...
    j       = j+1;
    col     = cmap(floor(((100-20)-0)/(20-8)*(AR-8))+1,:);

    %================================================
    %===                CALCULATION
    %================================================

    i       = 0;
    b_max   = 6;
    b_step  = .1;

    for b=b_step:b_step:b_max                       % And different wingspans...
        EvaluateSolution;                           % ... the solution feasibiliy is computed
        i               = i+1;
        m(i)            = Sol_m;
        P_level(i)      = Sol_P_level;
        m_af(i)         = Sol_m_af;
        P_elec_tot(i)   = Sol_P_elec_tot;
        m_bat(i)        = Sol_m_bat;
        A_sc(i)         = Sol_A_sc;
        m_sc(i)         = Sol_m_sc;
        m_mppt(i)       = Sol_m_mppt;
        P_sc(i)         = Sol_P_sc;
        m_prop(i)       = Sol_m_prop;
        v(i)            = Sol_v;
        D(i)            = Sol_D;
        A(i)            = Sol_A;
    end

    %================================================
    %===                PLOTS
    %================================================

    width = 2;
    b=b_step:b_step:b_max;

    figure(1);set(gcf,'Position',[1056 204 560 420]);
    hold on;
        plot(b,m,'Color',col,'LineWidth',width);    % Plot total mass wrt to AR and b
        [m_min.m(j),index] = min(m);
         m_min.b(j)=b(index);
        grid on;
```

```matlab
        xlabel('Wingspan [m]');
        ylabel('Total Mass of Solar Airplane [Kg]');

    figure(2);set(gcf,'Position',[487 704 800 420]);
    subplot(2,2,1);hold on;
        plot(b,v,'Color',col,'LineWidth',width);        % Plot speed wrt to AR and b
        [v_min.v(j),index] = min(v);
         v_min.b(j)=b(index);
        grid on;
        ylabel('Speed [m/s]')
    subplot(2,2,3);hold on;
        plot(b,P_level,'Color',col,'LineWidth',width);  % Plot the propeller power wrt to AR and b
        grid on;
        ylabel('Power at propeller [W]');
        xlabel('Wingspan [m]');
    subplot(2,2,2);hold on;
        plot(b,A,'Color',col,'LineWidth',width);        % Plot wing area wrt to AR and b
        grid on;
        ylabel('Wing Area [m^2]');
    subplot(2,2,4);hold on;
        plot(b,A_sc./A*100,'Color',col,'LineWidth',width);% Plot solar area wrt to AR and b
        [ratio_area_min.ratio_area(j),index] = min(A_sc./(b.^2/AR)*100);
        ratio_area_min.b(j)=b(index);
        grid on;
        xlabel('Wingspan [m]');
        ylabel('Solar Area Ratio [%]');

    if (AR == 13)                                       % Plot mass distribution (AR given)
        figure(3);set(gcf,'Position',[487 204 560 420]);
        area(b,[m./m*m_pld;m./m*m_av;m_af;m_bat;m_sc;m_mppt;m_prop]');
        legend('Payload','Avionics','Airframe','Batteries','Solar Panels','Mppt',...
               'Propulsion group','Location','NorthWest');
        xlabel('Wingspan [m]');
        ylabel('Mass [kg]');
        colormap(gray(100));
    end
end

figure(1);
    plot(m_min.b,m_min.m,'xk','MarkerSize',4);
    legend('8','9','10','11','12','13','14','16','18','20','Location','NorthWest');

figure(2);
    subplot(2,2,1);
        plot(v_min.b,v_min.v,'xk','MarkerSize',4);
    subplot(2,2,4);
        plot(ratio_area_min.b,ratio_area_min.ratio_area,'xk','MarkerSize',4);
        legend('8','9','10','11','12','13','14','16','18','20','Location','NorthWest');
```

B.4   Function MinimumPositive.m

```matlab
function min_pos = MinimumPositive(z)
    min_pos = NaN;
    for j=1:1:length(z)
        if (isreal(z(j)) && z(j)>0)
            if isnan(min_pos)      min_pos = z(j);
            elseif z(j) < min_pos  min_pos = z(j);
            end
        end
    end
end
```

Appendix C

Sky-Sailor Airfoil

WE3.55/9.3 Coordinates

1	0	0.24534	0.07425	0.19566	-0.01856
0.99849	0.00118	0.22471	0.07235	0.21688	-0.01807
0.99404	0.00292	0.20477	0.07017	0.24069	-0.01734
0.98485	0.00553	0.18555	0.06773	0.26703	-0.01645
0.97357	0.00845	0.1671	0.06505	0.29392	-0.01543
0.9631	0.01107	0.14947	0.06213	0.31951	-0.0143
0.9527	0.01362	0.13268	0.05899	0.34442	-0.0131
0.94107	0.01642	0.11678	0.05565	0.3696	-0.01186
0.92812	0.01942	0.10179	0.05211	0.39491	-0.01065
0.91404	0.02248	0.08774	0.04841	0.42006	-0.00951
0.89889	0.02561	0.07466	0.04456	0.44541	-0.00831
0.88268	0.02882	0.06258	0.04059	0.47145	-0.00692
0.86547	0.03211	0.05152	0.03652	0.49864	-0.00547
0.84732	0.03544	0.04149	0.03236	0.52714	-0.0041
0.8283	0.03879	0.03252	0.02815	0.55596	-0.00274
0.80845	0.04213	0.02461	0.02391	0.58396	-0.00132
0.78784	0.04545	0.01777	0.01968	0.61055	0.0001
0.76653	0.04873	0.01203	0.01556	0.63554	0.00141
0.74458	0.05196	0.0074	0.01159	0.65968	0.00253
0.72205	0.05511	0.00382	0.00758	0.68373	0.00343
0.69901	0.05814	0.00128	0.00349	0.70744	0.00418
0.67551	0.06102	0	0	0.73038	0.00486
0.65162	0.06375	0.00023	-0.0023	0.75248	0.00547
0.6274	0.06634	0.00199	-0.00403	0.77381	0.006
0.60292	0.06876	0.00526	-0.00589	0.79479	0.00636
0.57824	0.07097	0.0099	-0.00784	0.81568	0.00649
0.55342	0.07295	0.01579	-0.00969	0.83573	0.00645
0.52852	0.0747	0.02291	-0.01139	0.85435	0.0063
0.50361	0.0762	0.03126	-0.01294	0.87258	0.00611
0.47875	0.07744	0.04083	-0.01433	0.89135	0.00591
0.45399	0.07841	0.05158	-0.01555	0.90943	0.00562
0.4294	0.0791	0.06351	-0.01659	0.92542	0.00515
0.40503	0.07951	0.0766	-0.01743	0.93945	0.00456
0.38094	0.07965	0.09078	-0.0108	0.95208	0.00392
0.35719	0.0795	0.10601	-0.01855	0.96402	0.00323
0.33383	0.07905	0.12243	-0.01882	0.97565	0.00249
0.31091	0.07829	0.14004	-0.01887	0.98586	0.0017
0.28849	0.07723	0.15821	-0.01882	0.99366	0.00086
0.26662	0.07588	0.17646	-0.01876	1	0
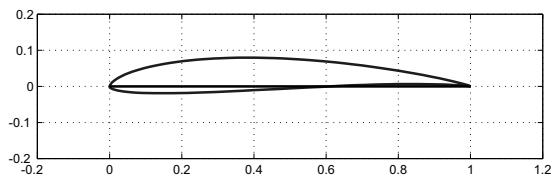
Bibliography

[1] Battery University.
http://www.batteryuniversity.com/.

[2] EPSON 2004 World's Lightest Micro-Flying Robot.
http://www.epson.co.jp/e/newsroom/news_2004_08_18.htm.

[3] Fliegen mit Sonnenkraft.
http://www.solarflugzeuge.de.

[4] History of Electric Flight.
http://www.iroquois.free-online.co.uk/hist.htm.

[5] History of Solar.
http://www1.eere.energy.gov/solar/pdfs/solar_timeline.pdf.

[6] History of the Berblinger Contest.
http://www.ifb.uni-stuttgart.de/icare/Englisch/flugberengl.html.

[7] Human-and Solar- Powered Aircraft Discovered New Frontiers, the
dryden x-press, wednesday, may 8, 2002.
*http://www.dfrc.nasa.gov/Newsroom/X-Press/stories/050802/res_
history.txt.html*.

[8] Icare at Uni Stuttgart.
http://www.ifb.uni-stuttgart.de/icare/Englisch/icare2eng.htm.

[9] Maxon motor catalogue. 07/08 Program, Maxon Motor AG, CH-6072
Sachseln/OW.

[10] NASA Vulture Project.
http://www.darpa.mil/ucar/programs/vulture.htm.

[11] Overview of Energy Storage Methods.
http://www.moraassociates.com/.

[12] Pathfinder and the Development of Solar Rechargeable Aircraft.
     http://www.llnl.gov/etr/pdfs/07_94.1.pdf.

[13] Pegasus Project.
     http://www.pegasus4europe.com.

[14] Sky-Sailor Website.
     http://sky-sailor.epfl.ch.

[15] Solar Flight of Wolfgang Schaeper.
     http://www.mfg-markdorf.de/rekorde/index.htm.

[16] Solar-Impulse Website.
     http://www.solar-impulse.com.

[17] Solar-Power Research at NASA Dryden.
     http://trc.dfrc.nasa.gov/Newsroom/FactSheets/PDF/FS-054-DFRC.pdf.

[18] Solar Solitude Official Website.
     http://personalpages.tds.net/~dbeck/.

[19] Solitair at DLR.
     http://www.dlr.de/ft/Desktopdefault.aspx/tabid-1388/1918_read-3385/.

[20] Sunseeker from eric raymond.
     hhttp://www.solar-flight.com/.

[21] The World Air Sports Federation.
     http://www.fai.org.

[22] World Smallest Solar Airplanes.
     http://home.main-rheiner.de/sieghard.dienlin.

[23] Zephyr from Qinetiq.
     http://www.qinetiq.com/home/products/zephyr.html.

[24] M. J. Allen and V. Lin. Guidance and Control of an Autonomous
     Soaring UAV. Technical report, NASA/TM-2007-214611, NASA Dry-
     den Flight Research Center, Edwards, California, April 2007.

[25] J. Alves, L. Dube, and C. Ohnstad. Solar Powered UAV Prototype Log
     and Results, MEG 498 Final Written Report. University of Nevada,
     Las Vegas, Howard R. Hughes College of Engineering, December 2006.

[26] A. Azuma. *The Biokinetics of Flying and Swimming*. Springer-Verlag,
     Tokyo, first edition, 1992.

[27] M. D. Bailey and M. V. Bower. High-Altitude Solar Power Platform. Technical report, NASA-TM-103578, George C. Marshall Space Flight Center Huntsville, AL, USA, April 1992.

[28] N. Baldock and M. R. Mokhtarzadeh-Dehghan. A Study of Solar-Powered, High-Altitude Unmanned Aerial Vehicles. *Aircraft Engineering and Aerospace Technology : An International Journal*, 78(3):187–193, 2006.

[29] F. Barbir, T. Molter, and D. Luke. Regenerative Fuel Cells for Energy Storage : Efficiency and Weight Trade-offs. In *Proc. International Energy Conversion Engineering Conference, AIAA-2003-5937*, Portsmouth, VA, Auguste 17-21 2003.

[30] F. Barnhart, M. Cuipa, D. Stefanik, and Z. Swick. Micro-Aerial Vehicle Design with Low Reynolds Number Airfoils. Brigham Yound University, Utah, March 2004.

[31] P. Berry. The Sunriser - A Design Study in Solar Powered Flight. In *Proc. of the World Aviation Conference*, San Diego, USA, Oct 10-12 2000.

[32] R. J. Boucher. Project Sunrise - A Flight Demonstration of Astro Flight Model 7404 Solar Powered Remotely Piloted Vehicle. In *Proc. of the 15th Joint Propulsion Conference, AIAA-79-1264*, Las Vegas, Nevada, June 18-20 1979.

[33] R. J. Boucher. History of Solar Flight. In *Proc. of the 20th Joint Propulsion Conference, AIAA-84-1429*, Cincinnati, Ohio, USA, June 1984.

[34] R. J. Boucher. Starduster - A Solar Powered High Altitude Airplane. In *Proc. of the 21st Joint Propulsion Conference, AIAA-1985-1449*, Monterey, CA, USA, July 1985.

[35] M. Boudellal. *La Pile à Combustible*. Dunod, Technique et Ingénierie, Paris, 2007.

[36] S. A. Brandt and F. T. Gilliam. Design Analysis Methodology for Solar-Powered Aircraft. *Journal of Aircraft*, 32(4):703–709, July-August 1995.

[37] J.-L. Brocard and L. Nguyen. Image Processing on Mars Aerial Pictures for Sky-Sailor. Bachelor Thesis, Autonomous Systems Lab, EPFL, Lausanne, June 2005.

[38] H. Bruss. *Solar Modellflug Grundlagen, Enwicklung, Praxis*. Verlag für Technik und Handwerk, Baden-Baden, Germany, 1991.

[39] D. Buccieri, P. Mullhaupt, Z. P. Jiang, and D. Bonvin. Velocity Scheduling Controller for a Nonholonomic Mobile Robot. In *Chinese Control Conference*, Harbin, 2006.

[40] G. Caprari. *Autonomous Micro-Robots : Applications and Limitations*. PhD thesis, Autonomous Systems Laboratory, Ecole Polytechnique Fédérale de Lausanne (EPFL), Lausanne, 2003.

[41] G. Caprari, T. Estier, and R. Siegwart. Fascination of Down Scaling - Alice the Sugar Cube Robot. *Journal of Micromechatronics*, 1:177–189(13), 1 July 2001.

[42] P. G. Carey, R. C. Aceves, N. J. Colella, K. A. Williams, R. A. Sinton, and G. S. Glenn. A Solar Module Fabrication Process for HALE Solar Electric UAVs. In *Proc of First World Conference On Photovoltaic Energy Conversion*, Waikoloa, Hawaii, USA, December 1994.

[43] A. Chan, K. Conley, C. T. Javorski, K.-H. Cheung, P. M. Crivelli, N. P. Torrey, and M. L. Traver. Nasa Advanced Design Program : Analysis, Design, and Construction of a Solar Powered Aircraft. Technical report, NASA-CR-192040, Worcester Polytechnic Institute, Mechanical Engineering Department, Worcester, MA, March 1992.

[44] D. F. Chichka and J. L. Speyer. Solar-Powered Formation-Enhanced Aerial Vehicle Systems for Sustained Endurance. In *Proc. of the IEEE American Control Conference*, volume 2, pages 684–688, Philadelphia, USA, June 1998.

[45] T. Chklovski. Pointed-Tip Wings at Low Reynolds Numbers. Department of Aerospace and Mechanical Engineering, University of Southern California, Los Angeles, September 2005. http://www-scf.usc.edu/%7Etchklovs/Proposal.htm.

[46] N. J. Colella and G. S. Wenneker. Pathfinder. Developing a Solar Rechargeable Aircraft. *Potentials, IEEE*, 15(1):18–23, February/March 1996.

[47] A. Colozza. Fly Like a Bird. *Spectrum, IEEE*, 44(5):38–43, May 2007.

[48] A. Colozza, M. Shahinpoor, P. Jenkins, C. Smith, K. Isaac, and T. Dal-Bello. Solid State Aircraft Concept Overview. *Proc. of the 2004*

NASA/DoD Conference on Evolution Hardware (EH'04), pages 318–324, 24-26 June 2004.

[49] A. J. Colozza. Preliminary Design of a Long-Endurance Mars Aircraft. In *Proc. of the 26th Joint Propulsion Conference, AIAA 90-2000*, Orlando, Florida, USA, July 16-18 1990.

[50] A. J. Colozza. Effect of Power System Technology and Mission Requirements on High Altitude Long Endurance Aircraft. Technical report, NASA CR 194455, Sverdrup Technology Incorporated, NASA Lewis Group, Brook Park, Ohio, November 1993.

[51] A. J. Colozza, D. A. Scheiman, and D. J. Brinker. GaAs/Ge Solar-Powered Aircraft. *SAE transactions*, 108(1):49–54, 1999.

[52] N. Diepeveen. The Sun-Surfer : Design and Construction of a Solar Powered MAV. Bachelor Thesis, Autonomous Systems Lab, ETH Zürich, Switzerland, March 2007.

[53] G. E. Dorrington. Performance of Battery-Powered Airships. *Proc. of the IMechE Part G Journal of Aerospace Engineering*, 221:91–104(14), 2007.

[54] J. A. Duffie and W. A. Beckman. *Solar Engineering of Thermal Processes*. Wiley-Interscience, New York, third edition, 1991.

[55] C. J. Engel, A. J. Woodworth, and M. Drela. Design and Testing of a Solar Powered High Endurance UAV. Massachusetts Institute of Technology, Cambridge, MA, 02139, March 2007.

[56] J. Fenner. Sky-Sailor : Exploiting Thermals. Bachelor Thesis, Automatic Control Laboratory, EPFL, Lausanne, March 2007.

[57] E. Fonseka. Modeling and Flying Thermal Tubes with an UAV. Bachelor Thesis, Autonomous Systems Lab, ETH Zürich, Switzerland, April 2007.

[58] B. Fuchs. Concept, Aerodynamic Optimisation and Construction of a Miniature Solar Aircraft. Bachelor Thesis, Autonomous Systems Lab, ETH Zürich, Switzerland, June 2007.

[59] J.-P. Fuchs. Solar Cell System for the Microglider. Bachelor Thesis, Laboratory of Intelligent Systems, EPFL, Lausanne, February 2008.

[60] S. Fux. Development of a Planar Low-cost Inertial Measurement Unit for UAVs and MAVs. Master thesis, Autonomous Systems Lab, ETH Zürich, Switzerland, April 2008.

[61] C. P. Garcia, B.-J. Chang, D. W. Johnson, D. J. Bents, V. J. Scullin, and I. J. Jakupca. Round Trip Energy Efficiency of NASA Glenn Regenerative Fuel Cell System. In *Proc. of the NHA Annual Hydrogen Conference 2006*, Long Beach, California, March 12-16 2006.

[62] J. Gedeon. Some Thoughts on the Feasibility of a Solar-Powered Plane. *Technical Soaring Magazine*, 6(1):11–17, September 1980.

[63] A. A. Gonzales, C. J. Corpus, D. W. Hall, and R. W. Parks. Development of a Useful Mars Airplane Exploration Concept at NASA / Ames Research Center. In *Proc. of the 6th Mars Society Conference*, August 2003.

[64] Z. X. Goraj, A. Frydrychiewicz, and J. Winiecki. Design Concept of a High-Altitude Long-Endurance Unmanned Aerial Vehicle. *Aircraft Design*, 2:19–44(26), March 1999.

[65] J. M. Grasmeyer and M. T. Keennon. Development of the Black Widow Micro Air Vehicle. In *Proc. of the 39th AIAA Aerospace Sciences Meeting and Exhibit, AIAA-2001-0127*, Reno, NV, USA, January 2001.

[66] G. Guglieri and F. Quagliotti. Performance Analysis of a Solar Powered Tail Less Motor Glider. *Technical Soaring Magazine*, 20(2):47–53, April 1996.

[67] M. D. Guynn, M. A. Croom, S. C. Smith, R. W. Parks, and P. A. Gelhausen. Evolution of a Mars Airplane Concept for the ARES Mars Scout Mission. In *2nd AIAA Unmanned Unlimited Systems, Technologies, and Operations, AIAA 2003-6578*, San Diego, California, September 2003.

[68] D. W. Hall, C. D. Fortenbach, E. V. Dimiceli, and R. W. Parks. A Preliminary Study of Solar Powered Aircraft and Associated Power Trains. Technical report, NASA CR 3699, December 1983.

[69] D. W. Hall and S. A. Hall. Structural Sizing of a Solar Powered Aircraft. Technical report, NASA CR 172313.

[70] F. G. Irving and D. Morgan. The Feasibility of an Aircraft Propelled by Solar Energy. In *Proc. of the 2nd International Symposium on the Technology and Science of Low Speed and Motorless Flight, AIAA-1974-1042*, Cambridge, Massachusetts, September 11-13 1974.

[71] B. Keidel. *Auslegung und Simulation von Hochfliegenden, Dauerhaft Stationierbaren Solardrohnen.* PhD thesis, Lehrstuhl für Flugmechanik und Flugregelung, Technische Universität München, 2000.

[72] K. Kotwani, N. Prabhu, and Y. Bhumkar. Micro/Mini Aerial Vehicle Propulsion System Studies. In *Proc. of All India Seminar on Mini and Micro Aerial Vehicles, The Institution of Engineers*, Pune, India, February 2004.

[73] M. Kovac, A. Guignard, J.-D. Nicoud, J.-C. Zufferey, and D. Floreano. A 1.5g SMA-Actuated Microglider Looking for the Light. *2007 IEEE International Conference on Robotics and Automation*, pages 367–372, 10-14 April 2007.

[74] G. A. Landis. Exploring Venus by Solar Airplane. In *Proc. of the STAIF Conference on Space Exploration Technology*, Albuquerque, NM, USA, February 2001.

[75] P. B. S. Lissaman. Low-Reynolds Number Airfoils. *Annual Review of Fluid Mechanics*, 15:223–239, 1983.

[76] V. Livshits, A. Ulus, and E. Peled. High-Power H2/Br2 Fuel Cell. *Electrochemistry Communications*, 8(8):1358–1362, August 2006.

[77] P. B. MacCready, P. B. S. Lissaman, W. R. Morgan, and J. D. Burke. Sun-Powered Aircraft Designs. *Journal of Aircraft*, 20(6):487–493, June 1983.

[78] T. Markvart and L. Castañer. *Practical Handbook of Photovoltaics : Fundamentals and Applications.* Elsevier, Oxford, UK, 2003.

[79] A. Mattio. Modeling and Control of the UAV Sky-Sailor. Master's project, Ecole Polytechnique Fédérale de Lausanne, Autonomous Systems Laboratory, Lausanne, June 2006.

[80] B. W. McCormick. *Aerodynamics, Aeronautics, and Flight Mechanics.* John Wiley, New-York, 1995.

[81] J. H. McMasters and M. L. Henderson. Low Speed Single Element Airfoil Synthesis. *Technical Soaring*, 6(2):1–21, 1980.

[82] R. W. Miles, K. M. Hynes, and I. Forbes. Photovoltaic Solar Cells : An Overview of State-of-the-Art Cell Development and Environmental Issues. *Progress in Crystal Growth and Characterization of Materials*, 51(1-3):1–42, January 2005.

[83] J. T. J. Miller. Literature Review of Low Speed Aerodynamics for Fixed and Rotary Wings. Mechanical Engineering & Engineering Science, University of North Carolina at Charlotte, September 2005. http://www.coe.uncc.edu/%7Erkeanini/lowreyn/LitRev.htm.

[84] F. Mitlitsky, N. J. Colella, and B. Myers. Unitized Regenerative Fuel Cells for Solar Rechargeable Aircraft and Zero Emission Vehicles, UCRL-JC-117130. In *Proc. of the 1994 Fuel Cell Seminar*, San Diego, California, November 1994.

[85] F. Mitlitsky, A. H. Myers, Weisberg, and Blake. Vehicular Hydrogen Storage Using Lightweight Tanks (Regenerative Fuel Cell Systems), UCRL-JC-134540. In *Proc. of the U.S. DOE Hydrogen Program 1999 Annual Review Meeting*, Lakewood, Colorado, May 1999.

[86] F. Mitlitsky, B. Myers, and A. H. Weisberg. Lightweight Pressure Vessels and Unitized Regenerative Fuel Cells, UCRL-JC-125220. In *Proc. of the 1994 Fuel Cell Seminar*, San Diego, California, November 1996.

[87] B. A. Moffitt, T. H. Bradley, D. E. Parekh, and D. Mavris. Design and Performance Validation of a Fuel Cell Unmanned Aerial Vehicle. In *Proc of the 44th AIAA Aerospace Sciences Meeting and Exhibit, AIAA 2006-0823*, Reno, Nevada, January 2006.

[88] T. J. Mueller and J. D. Delaurier. Aerodynamics of Small Vehicles. *Annual Review of Fluid Mechanics*, 35(1):89–111, 2003.

[89] L. M. Nicolai. *Fundamentals of Aircraft Design*. School of Engineering, University of Dayton, Dayton, Ohio, 1975.

[90] A. Noth. Design of a Lightweight & High Efficiency MPPT for Sky-Sailor Airplane. Internal Technical Report, Autonomous Systems Lab, ETH Zürich, Switzerland, Feb 2006.

[91] A. Noth, S. Bouabdallah, S. Michaud, R. Siegwart, and W. Engel. Sky-Sailor Design of an Autonomous Solar Powered Martian Airplane. In *Proc. of the 8th ESA Workshop on Advanced Space Technologies for Robotics*, Noordwick, Netherlands, 2004.

[92] A. Noth, S. Bouabdallah, and R. Siegwart. Dynamic Modeling of Fixed-Wing UAVs. Master Course in Mechanical Department, Autonomous Systems Lab, ETH Zürich, Switzerland, December 2006.

[93] A. Noth, W. Engel, and R. Siegwart. Design of an Ultra-Lightweight Autonomous Solar Airplane for Continuous Flight. In *Proc. of the Field and Service Robotics Conference*, Port Douglas, Australia, 2005.

[94] A. Noth, W. Engel, and R. Siegwart. Design of an Ultra-lightweight Autonomous Solar Airplane for Continuous Flight. In P. Corke and S. Sukkarieh, editors, *Field and Service Robotics : Results of the 5th International Conference*, volume 25, pages 441–452. Springer Berlin / Heidelberg, 2006.

[95] A. Noth, W. Engel, and R. Siegwart. Flying Solo and Solar to Mars - Global Design of a Solar Autonomous Airplane for Sustainable Flight. *IEEE Robotics and Automation Magazine*, 13(3):44–52, September 2006.

[96] A. Noth, R. Siegwart, and W. Engel. Autonomous Solar UAV for Sustainable Flight. In K. P. Valavanis, editor, *Advances in Unmanned Aerial Vehicles, State of the Art and the Road to Autonomy*, volume 33 of *Intelligent Systems, Control and Automation : Science and Engineering*, pages 377–405. Springer Verlag, 2007.

[97] P. H. L. Notten. Rechargeable Batteries : Efficient Energy Storage Devices for Wireless Electronics. In S. Mukherjee and et al., editors, *AmIware Hardware Technology Drivers of Ambient Intelligence*, Philips Research, part 5, pages 315–345. Springer Netherlands, 2006.

[98] C. Patel. The Design and Fabrication of a Solar Powered Model Aircraft. Bachelor Thesis, Dept. of Aerospace Engineering, IIT Bombay, March 2002.

[99] C. Patel, H. Arya, and K. Sudhakar. Design, Build & Fly a Solar Powered Aircraft. In *Proc. of the 53rd Annual General Meeting, The Aeronautical Society of India,*, Goa, India, January 2002.

[100] W. H. Phillips. Some Design Considerations for Solar-Powered Aircraft. Technical report, NASA TP 1675, NASA Langley Research Center, Hampton, VA, USA, June 1980.

[101] D. J. Pines and F. Bohorquez. Challenges Facing Future Micro-Air-Vehicle Development. *Journal of aircraft*, 43(2):290–305, 2006.

[102] M. S. Pressnell. The Structural Design and Construction of Man Powered Aircraft. In *Proc. of the Royal Aeronautical Society Symposium on "Man Powered Flight - The Way Ahead"*, London, UK, February 1977.

[103] D. P. Raymer. *Aircraft Design : a Conceptual Approach*. AIAA Education Series. American Institute of Aeronautics and Astronautics, Washington, D.C., third edition, 1999.

[104] M. A. Rehmet. Development of a Self Launching Solar Powered Sailplane. *Technical Soaring Magazine*, 19(1):23–28, January 1995.

[105] M. A. Rehmet, W. Scholz, and R. Voit-Nitschmann. Das Solarflugzeug Icaré, Vorläufer für eine Kategorie Elektrisch Getriebener Flugzeuge. Technical report, DGLR-JT95-009, Universität Stuttgart, Germany, 1995.

[106] M. A. Rehmet, R. Voit-Nitschmann, and B. Kröplin. Eine Methode zur Auslegung von Solarflugzeugen. Technical report, DGLR-JT97-031, Universität Stuttgart, Germany, 1997.

[107] K. C. Reinhardt, T. R. Lamp, J. W. Geis, and A. J. Colozza. Solar Powered Unmanned Aerial Vehicles. In *Proc. of the 31st Intersociety Energy Conversion Engineering Conference*, volume 1, pages 41–46, Washington D. C., USA, August 1996.

[108] L. Retzbach. *DMFV-Brushless-Fibel II*. Deutscher Modellflieger-Verband, 53123 Bonn, Germany, second edition.

[109] J. Rion. *Ultra-Light Photovoltaic Composite Sandwich Structures*. PhD thesis, Laboratoire de Technologie des Composites et Polymères, Ecole Polytechnique Fédérale de Lausanne (EPFL), Lausanne, 2008.

[110] E. Rizzo and A. Frediani. A Model for Solar Powered Aircraft Preliminary Design. In *Proc. of International Conference on Computational & Experimental Engineering & Sciences 04*, volume 1, pages 39–54, Madeira, Portugal, July 2004.

[111] C. Roberts, M. Vaughan, and W. J. Bowman. Development of a Solar Powered Micro Air Vehicle. In *Proc. of the 40th Aerospace Sciences Meeting and Exhibit, AIAA 2002-0703*, Reno, Nevada, USA, January 2002.

[112] G. Romeo and G. Frulla. Heliplat : High Altitude Very-Long Endurance Solar Powered UAV for Telecommunication and Earth Observation Applications. *The Aeronautical Journal*, 108:277–293, 2004.

[113] G. Romeo, G. Frulla, E. Cestino, and G. Corsino. Heliplat : Design, Aerodynamic, Structural Analysis of Long-Endurance Solar-Powered Stratospheric Platform. *Journal of Aircraft*, 41(6):1505–1520, November 2004.

[114] H. Ross and P. Frei. Solarangetriebene Flugzeuge = The True All Electric Aircraft. Eine Übersicht. Deutscher Luft- und Raumfahrtkongress 2006, DGLR-2006-150, November 2006.

[115] E. Schöberl. Solar-Powered Aircraft Design. *Technical Soaring Magazine*, 15(2):38–47, April 1991.

[116] E. Schöberl. Possibilities and Requirements for Long Endurance High Flying Solar Powered Platforms. *Technical Soaring Magazine*, 23(3):66–70, July 1999.

[117] W. Shyy, M. Berg, and D. Ljungqvist. Flapping and Flexible Wings for Biological and Micro Air Vehicles. *Progress in Aerospace Sciences*, 35:455–505, July 1999.

[118] C. S. Spiegel. *Designing & Building Fuel Cells*. McGraw-Hill Professionale, New York, first edition, May 2007.

[119] Stadt Ulm, Autorengruppe. *Fliegen mit Licht, Dokumentation über solares Fliegen und den Solarflugzeugwettbewerb Berblinger 1996 der Stadt Ulm*. Süddeutsche Verlagsgesellschaft Ulm, Ulm, 1996.

[120] W. Stender. *Sailplane Weight Estimation*. Organisation Scientifique et Technique Internationale du Vol à Voile (OSITIV), 1969.

[121] D. Stinton. *The Design of the Aeroplane*. Blackwell Science, Oxford, UK, second edition, 2001.

[122] T. Tegeder. Development of an Efficient Solar Powered Unmanned Aerial Vehicle with an Onboard Solar Tracker. Master's project, Brigham YoungC University, Department of Mechanical Engineering, April 2007.

[123] H. Tennekes. *The Simple Science of Flight - From Insects to Jumbo Jets*. MIT Press, Cambridge, Massachusetts, USA, 1992.

[124] T. C. Tozer, D. Grace, J. Thompson, and P. Baynham. UAVs and HAPs - Potential Convergence for Military Communications. In *Proc. of the IEEE Colloquium on Military Satellite Communications*, London, UK, July 2000.

[125] K. Uchino. Piezoelectric Actuators 2006. *Journal of Electroceramics, in collection Chemistry and Materials Science*, July 2007.

[126] R. Voit-Nitschmann. Solar- und Elektroflugzeuge - Geschichte und Zukunft. In *Jahrbuch aus Lehre und Forschung der Universität Stuttgart*, Universität Stuttgart, Germany, 2001.

[127] A. Weider, H. Levy, I. Regev, L. Ankri, T. Goldenberg, Y. Ehrlich, A. Vladimirsky, Z. Yosef, and M. Cohen. SunSailor : Solar Powered UAV. Technical report, Students Project Report, Faculty of Aerospace Engineering, Technion IIT, Haifa, Israel, 2006.

[128] C. Wilson, J. Nutbean, and I. Bond. Aerodynamic and Structural Design of a Solar-Powered Micro Unmanned Air Vehicle. *Proc. of the IMechE, Part G : Journal of Aerospace Engineering*, 214:97–106(10), 10 April 2000.

[129] R. J. Wood, S. Avadhanula, E. Steltz, M. Seeman, J. Entwistle, A. Bachrach, G. Barrows, S. Sanders, and R. S. Fearing. Design, Fabrication and Initial Results of a 2g Autonomous Glider. *Industrial Electronics Society, 2005. IECON 2005. 31st Annual Conference of IEEE*, 6-10 Nov. 2005.

[130] J. W. Youngblood and T. A. Talay. Solar-Powered Airplane Design for Long-Endurance, High-Altitude Flight. In *Proc. of the 2nd AIAA International Very Large Vehicles Conference, AIAA-82-0811*, Washington, DC, May 1982.

[131] J. W. Youngblood, T. A. Talay, and R. J. Pegg. Design of Long-Endurance Unmanned Airplanes Incorporating Solar and Fuel Cell Propulsion. In *Proc. of the 20th Joint Propulsion Conference, AIAA-84-1430*, Cincinnati, Ohio, USA, June 1984.

[132] J.-C. Zufferey, A. Klaptocz, A. Beyeler, J.-D. Nicoud, and D. Floreano. A 10-gram Microflyer for Vision-based Indoor Navigation. In *Proc. of the IEEE/RSJ International Conference on Intelligent Robots and Systems (IROS'2006)*, pages 3267–3272, Beijing, China, 2006.

Curriculum Vitæ

André Noth was born in Fribourg, Switzerland on February 10th 1980. He received his M.Sc. in Micro-Engineering in 2004 from the Ecole Polytechnique Fédérale de Lausanne (EPFL). His master thesis was the synthesis and implementation of a controller on a four rotors micro helicopter. Early 2004, he started his doctoral thesis in the field of design and control of solar powered airplanes at the Autonomous Systems Laboratory of EPFL on the Sky-Sailor project. In 2006, he moved with the laboratory of Prof. R. Siegwart to ETHZ where he continued his work. On the educational side, André supervised more than twenty student projects and was lecturer for the courses "Dynamic Systems Modeling" and "Aircraft and Spacecraft Systems : Design, Modeling and Control". He is author of several conference and journal papers and two book chapters on aerial robotics. His current research interests include multidisciplinary design, solar powered robots, and mecatronics systems development.

The reader is warmly welcome to submit questions, comments and remarks to the author (email: andre.noth@a3.epfl.ch).

Awards

1. Portescap Prize (Excellence in Micro-engineering) in March 2004 for the Master Thesis entitled "Design and Implementation of a Controller on a Quadrotor Helicopter" at EPFL, Switzerland
2. Best Paper Award at the Field and Service Robotics Conference FSR05 in August 2005 for the paper entitled "Design of an Ultra-Lightweight Autonomous Solar Airplane for Continuous Flight" in Port Douglas, Australia.

List of Publications

Book Chapters

- Noth, A., Siegwart, R. and Engel, W. "Autonomous Solar UAV for Sustainable Flight" in : *Advances in Unmanned Aerial Vehicles, State of the Art and the Road to Autonomy*, edited by Kimon P. Valavanis, Springer Verlag, 2007

- Noth, A., Engel, W. and Siegwart, R. "Design of an Ultra-Lightweight Autonomous Solar Airplane for Continuous Flight" in : *Field and Service Robotics : Results of the 5th International Conference*, edited by P. Corke, S. Sukkariah, Springer Berlin / Heidelberg, 2006, vol. 25

Journals

- Noth, A., Engel, W. and Siegwart, R. "Flying Solo and Solar to Mars - Global Design of a Solar Autonomous Airplane for Sustainable Flight", IEEE Robotics & Automation Magazine, vol. 13, no. 3, pp. 44-52, Sept. 2006

Peer-reviewed Proceedings

- Noth A., Engel W., Siegwart R. "Recent Progresses on the Martian Solar Airplane Project Sky-Sailor" in *Proc. of the 9th ESA Workshop on Advanced Space Technologies for Robotics (ASTRA 2006)*, Noordwick, Netherland, 2006

- Noth, A., Engel, W. and Siegwart, R. "Design of an Ultra-Lightweight Autonomous Solar Airplane for Continuous Flight" in *Proc. of Field and Service Robotics Conference FSR05*, Port Douglas, Australia, 2005

- Noth, A., Bouabdallah, S., Michaud, S., Siegwart, R. and Engel, W. "SKY-SAILOR Design of an autonomous solar powered martian airplane" in *Proc. of the 8th ESA Workshop on Advanced Space Technologies for Robotics, (ASTRA 2004)*, Noordwick, Netherland, 2004